AD_____

Award Number: DAMD17-99-1-9022

TITLE: Periscopic Spine Surgery: Anatomical Motion Tracking During Radiation Treatment

PRINCIPAL INVESTIGATOR: Kevin Cleary, Ph.D.

CONTRACTING ORGANIZATION: Georgetown University
Washington, DC 20057

REPORT DATE: February 2003

TYPE OF REPORT: Annual

PREPARED FOR: U.S. Army Medical Research and Materiel Command
Fort Detrick, Maryland 21702-5012

REPORT DOCUMENTATION PAGE

Form Approved
OMB No. 074-0188

1. AGENCY USE ONLY (Leave blank)	2. REPORT DATE	3. REPORT TYPE AND DATES COVERED
	February 2003	Annual (15 Jan 02 - 14 Jan 03)

4. TITLE AND SUBTITLE
Periscopic Spine Surgery: Anatomical Motion Tracking During Radiation Treatment

5. FUNDING NUMBERS
DAMD17-99-1-9022

6. AUTHOR(S) :
Kevin Cleary, Ph.D.

7. PERFORMING ORGANIZATION NAME(S) AND ADDRESS(ES)
Georgetown University
Washington, DC 20057

E-Mail: cleary@georgetown.edu

8. PERFORMING ORGANIZATION REPORT NUMBER

9. SPONSORING / MONITORING AGENCY NAME(S) AND ADDRESS(ES)
U.S. Army Medical Research and Materiel Command
Fort Detrick, Maryland 21702-5012

10. SPONSORING / MONITORING AGENCY REPORT NUMBER

11. SUPPLEMENTARY NOTES
Original contains color plates: All DTIC reproductions will be in black and white.

12a. DISTRIBUTION / AVAILABILITY STATEMENT
Approved for Public Release; Distribution Unlimited

12b. DISTRIBUTION CODE

13. ABSTRACT (Maximum 200 Words)
This project is aimed at improving the state of the art of image-guided and minimally invasive procedures by developing a new generation of clinical techniques along with the computer-based hardware and software needed for their implementation.

Key research accomplishments for this year are:

- Completed the first 20 patients in an FDA approved clinical trial of a joystick controlled robot for nerve and facet blocks in the spine under fluoroscopy guidance
- Received a research grant from NCI/NIH to develop a similar lung biopsy under CT Fluoroscopy in conjunction with Johns Hopkins URobotics Research Laboratory
- Completed phantom studies on a fully robotic biopsy testbed that showed high accuracy (better than 2 mm) could be obtained
- Completed studies with a liver respiratory motion simulator to demonstrate the feasibility of using magnetic tracking for minimally invasive liver interventions
- Began a new study of skin motion versus internal organ motion for stereotactic radiosurgery in cooperation with the Department of Radiation Medicine at Georgetown

14. SUBJECT TERMS:
medical robotics, tracking, image-guided, minimally invasive, spine procedures, technology development, visualization

15. NUMBER OF PAGES
117

16. PRICE CODE

17. SECURITY CLASSIFICATION OF REPORT	18. SECURITY CLASSIFICATION OF THIS PAGE	19. SECURITY CLASSIFICATION OF ABSTRACT	20. LIMITATION OF ABSTRACT
Unclassified	Unclassified	Unclassified	Unlimited

3 Table of Contents

4 Introduction

This project is aimed at improving the state of the art of image-guided and minimally invasive procedures by developing a new generation of clinical techniques along with the computer-based hardware and software needed for their implementation. The current focus of the project is on physician assist systems incorporating robotics, tracking, and visualization to improve the precision of instrument placement and manipulation in minimally invasive procedures. The project is led by the Imaging Sciences and Information Systems (ISIS) Center of the Department of Radiology at Georgetown University. Project collaborators include the Department of Radiation Medicine at Georgetown, the Urology Robotics Group at Johns Hopkins Medical Institutions, the NSF sponsored Engineering Research Center for Computer Integrated Surgical Systems and Technology at Johns Hopkins University, and the Engineering School at the Catholic University of America.

5 Report Body

This section describes the research accomplishments associated with each task in the statement of work. This is the fourth year report and includes research performed from 15 January 2002 to 14 January 2003. The award number is DAMD17-99-1-9022.

5.1 Task 1: Program Planning and Management

Program planning and management continues to focus on the direction of the project as well as relationships with project collaborators. Project planning and review meetings are held monthly at the ISIS Center, and it is the consensus that the current focus on physician assist systems for the next generation interventional suite is an appropriate direction. In the 2002 calendar year major progress was made on our hardware testbeds including completion of the first stage of the robot clinical trial and completion of phantom experiments using our liver respiratory motion simulator. The focus is now on evaluating these testbeds in the clinical environment, namely the interventional suite at Georgetown.

We have continued our very close cooperation with both the Urology Robotics Group at Johns Hopkins Medical Institutions (lab director Dan Stoianovici, PhD) and the NSF sponsored Engineering Research Center for Computer Integrated Surgical Systems and Technology at Johns Hopkins University (center director Russell Taylor, PhD). The collaboration with the Urology Robotics Group has led to our being awarded a grant from NIH/NCI to further development the system for robotically assisted lung biopsy. In addition, Johns Hopkins has spun off a small business (ImageGuide, Inc.) to commercialize the robot and Dr. Cleary has been named to the Board of Scientific Advisors.

With the Engineering Research Center at Johns Hopkins, we completed our studies of a robot biopsy testbed to demonstrate the concept of fully automated biopsy. Dr. Cleary also attended their strategic planning meeting in Boston this fall and we are continuing our financial support of one of their PhD students. Since there is no Engineering School

at Georgetown University, this provides the project with a graduate student to help develop the algorithms and software for this testbed. It also allows us to leverage off the extensive medical robotics program at Johns Hopkins University.

During this reporting period, we also completed our collaboration efforts with two local research groups. We completed our collaboration with the National Capital Area Medical Simulation Center of the Uniform Services University of the Health Sciences. The visiting researcher, Daigo Tanaka, MS, who had worked part-time at the Simulation Center, completed his project there and entered the PhD program in Biomedical Engineering at Carnegie Mellon University. We also completed our collaboration with the Department of Radiology at Walter Reed Army Medical Center. As an outgrowth of this collaboration, Walter Reed has been continuing to work with a consultant, Sharyn Greberman, Sc.D., to assist with ongoing studies in "Postmenopausal Coronary Artery Disease and Osteoporosis".

The group continues to be very active in presenting their work at national and international conferences. Dr. Cleary is on the program committee for the Computer Assisted Radiology and Surgery conference. He is organizing a medical robotics workshop for this year's meeting in June 2003. The group had three papers accepted at the February 2003 SPIE Medical Imaging Conference. The group has also participated in the Society of Interventional Radiology annual meeting, as part of our efforts to bridge the gap between scientific and clinical personnel.

5.2 Task 2: Spinal Robotics

One of the key research outcomes of this reporting period has been the completion of the first phase of a clinical trial incorporating the "needle driver" robot developed by the Urology Robotics Laboratory at Johns Hopkins Medical Institutions. The objective of this trial is to demonstrate that a physician controlled robotic needle driver is equivalent in safety and effectiveness to the standard manual technique for needle placement in nerve and facet blocks in the perispinal region. This is a single center, randomized feasibility study that has been approved by the Georgetown Institutional Review Board, the U.S. Army Human Subjects Board, and the Food and Drug Administration. The initial approval is for 20 patients, with the potential for 100 patients after the initial trial has been reviewed.

The initial trial of 20 patients was conducted at Georgetown University from August 2002 to December 2002. The results are shown in Table 1 on the next page. The trial was completed successfully with no adverse events. The data is currently being analyzed by the statistician and a report for the FDA is being prepared. Pending FDA and IRB approval, we plan to ask permission to continue the trial with an additional 80 patients.

Table 1: Results for the Twenty Patients

Patient	Age	Sex	Tech-nique	Block	Level	Pain before	Pain after	Pain 1 week	Accuracy (mm) AP/Lat
1	70	M	Manual	Facet	L-4-5	1	0	1	0.66mm/0.94mm
2	59	F	Manual	Nerve	L-5	1	0	0	0.41mm/0.23mm
3	60	M	Manual	Nerve	L-4	8	0	3	0.96mm/0.57mm
4	30	M	Manual	Nerve	L-4	9	1	2	0.69mm/0.81mm
5	55	F	Robot	Nerve	L-4	8	4	4	1.92mm/1.45mm
6	78	F	Robot	Nerve	S-1	4	3	4	0.23mm./0.18mm
7	74	F	Robot	Nerve	L-5	3	0	1	0.34mm/0.17mm
8	74	F	Robot	Nerve	L-4	4	1	2	2.00mm/1.44mm
9	60	F	Manual	Nerve	L-5	8	1	2	0.41mm/1.22mm
10	60	M	Robot	Nerve	L-4	8	0	1	0.66mm/0.10mm
11@	66	F	Robot	Facet	L-5	9	4	5	0.28mm/0.68mm
12	65	F	Manual	Facet	L-5	7	0	3	0.22mm/1.39mm
13	42	M	Manual	Facet	L-4	2	0	2	0.92mm/038mm
14	62	F	Robot	Nerve	L-4	5	1	2	0.40mm/1.01mm
15	69	M	Manual	Facet	L-4	8	3	7	0.53mm/ 0.57mm
16	70	M	Robot	Facet	L-3	8	2	7	0.90mm/0.97mm
17	65	F	Robot	Facet	L-3	6	0	0	0.63mm/0.42mm
18	42	M	Manual	Nerve	L-5	8	4	5	1.09mm/1.30mm
19	65	F	Manual	Facet	L-5	8	0	0	0.00mm/2.40mm
20	42	M	Robot	Nerve	L-5	8	3	7	0.75mm/0.55mm

@Patient 11: The needle driver kept slipping when trying to drive the needle. The procedure had to be completed by hand. No adverse event occurred.

A picture of the robotic device is shown in Figure 1[1]. The device consists of:

1) A mechanical arm that can be positioned at any location above the patient's spine.
2) A touch screen and joystick through which the operator can control the device.
3) A mounting base that attaches the device to the interventional table.

A picture of one of the patients from the clinical trial is shown in Figure 2. The physician uses the touch screen and joystick to control the robot. The robot then holds and directs the needle. Some preliminary results from the clinical trial are given in the poster in the appendix [Cleary 2003b][2] on page 96.

Several related papers and poster incorporating the robot were also published or presented during this reporting period. Papers included:

1) A paper at the *Computer Assisted Radiology and Surgery* meeting in June 2002 describing our work in developing a software architecture for robotically assisted and image-guided interventions [Cleary 2002a]
2) A paper that will be presented at the *SPIE Medical Imaging* meeting in February 2003 describing our work in fluoroscopy seroving and efforts to further automate the needle orientation and placement process [Mocanu 2003]

[1] All figures are in Section 10.1 which starts on page 14.

[2] All references are indicated by square brackets and listed in the reference section which starts on page 12. Copies of papers and posters are in the appendices.

Posters included:

1) A poster at the American Society of Neuroradiology in May 2002 describing the cadaver studies with the robot for spinal nerve and facet blocks [Watson 2002]
2) A poster at the *Computer Assisted Radiology and Surgery* meeting in June 2002 describing cadaver studies with the robot for manual versus robotically assisted needle placement [Cleary 2002b]
3) A poster presented at the *Biomedical Imaging Research Opportunities Workshop* in January 2003 describing the initial clinical trial and future plans for robotically assisted lung biopsy [Cleary 2003b]

5.3 Task 3: Robot Biopsy Testbed

In addition to the clinical protocol described in Task 2, we have also been developing a robot biopsy testbed. The goals of this testbed are 1) to compare robotically assisted biopsy to the current practice and 2) serve as a testbed for investigating software architectures for integrating robotics, tracking, and visualization. A system diagram is shown in Figure 3.

The initial feasibility study was completed on the testbed during this report period. A paper [Xu 2003] describing the study has been submitted to a special issue on Medical Robotics of the journal *IEEE Transactions on Robotics and Automation*. The testbed setup and components are shown in Figure 4. The intra-operative scenario for robotically assisted biopsy or therapy is as follows:

1. The patient is positioned on the table
2. The robot is mounted and calibrated
3. The patient is scanned
4. CT scans are sent to the physician's workstation
5. The physician selects the entry and target locations
6. The robot moves the needle to the entry point
7. The robot orients the needle to the target point
8. The robot inserts the needle to the predefined depth
9. Another CT scan is done for verification
10. The physician injects the therapeutic agent or takes the biopsy sample
11. The robot retracts the needle

The scenario was tested using the mobile CT scanner and an interventional abdominal phantom. Three sets of tests were done: 1) translation accuracy; 2) orientation accuracy; and 3) overall system accuracy. The results are shown in the paper in the appendix [Xu 2003], but the overall system accuracy was good at 1.66 mm with a standard deviation of 0.38 mm.

While these experiments showed the feasibility of this method, at the moment we have decided not to pursue this concept further as we believe it would be difficult to get clinical approval for a fully-automated biopsy system. Therefore, we plan to concentrate on joystick controlled robotic systems and our new work on robotically assisted lung biopsy for the next reporting period.

5.4 Task 4: Organ Tracking for Minimally Invasive Abdominal Interventional Procedures

The goal of this task is to investigate the use of magnetic tracking for precisely locating internal organs during interventional procedures. This is a collaboration with Northern Digital (Waterloo, Canada) and Traxtal Technologies (Houston, Texas). Northern Digital has been developing the AURORA™ magnetic tracking system, which enables instruments retrofitted with a sensing coil to be tracked and overlaid on an image of the anatomy. Our research group at Georgetown is serving as a beta test site and is one of the first research groups worldwide to receive this equipment. We have been developing an image-guided system for minimally invasive procedures that incorporates this technology. While image guidance using bony landmarks for procedures like pedicle screw insertion is now standard, a future challenge for the research community is to develop image guidance for internal organs.

The system is shown in Figure 5 and consists of a control unit, sensor interface device, and field generator as shown in the photograph on the left. The sensors (middle photograph) plug into the sensor interface unit and can be as small as 0.9 mm in diameter and 8 mm in length. For comparison, the sensor coil is shown next to a match with the leads protruding from the coil. According to a Northern Digital data sheet, the sensors have a positional accuracy of 1-2 mm and angular accuracy of 0.5-1 degree. The measurement volume (right photograph) is based on the reference coordinate system of the field generator. The distance along the x-axis is 280 to 640 mm, along the y-axis from –300 to 300 mm, and along the z-axis from –300 to 300 mm. This volume is sufficient to cover the area of interest for abdominal interventions.

To evaluate magnetic tracking for minimally invasive abdominal interventions, the Georgetown team has developed a liver respiratory motion simulator. The simulator includes a synthetic liver mounted on a one degree of freedom motion platform. Since most hepatic respiratory motion occurs in the cranio-caudal direction we felt this was a reasonable approximation. The linear motion platform is computer controlled, allowing physiologic respiratory patterns to be simulated. The simulator was first demonstrated at the Computer Aided Radiology and Surgery (CARS) Conference in Berlin, Germany, in June 2001. An improved version of the simulator was demonstrated at the Society of Interventional Radiology Annual Meeting in Baltimore, Maryland, in April 2002. A block diagram of the simulator is shown in Figure 6. The simulator consists of a dummy torso, a synthetic liver model, a motion platform, a graphical user interface, the AURORA magnetic tracker system, and a magnetically tracked probe and catheter.

To test the system, a simulated transjugular intrahepatic portosystemic shunt (TIPS) procedure was carried out using a foam liver phantom and the respiratory motion simulator. A foam liver was cast with two barium coated straws and mounted to the one degree of freedom motion platform. A rib cage was taken from an anatomical model and placed over the moving liver. Fiducials were mounted on the rib cage (multi-modality radiographic markers, IZI Medical, Baltimore, MD). A special catheter, containing a magnetically tracked sensor coil, was inserted into the liver simulating the insertion of a

coaxial catheter into the hepatic vein during the TIPS procedure. A pre-procedure CT scan was done (5 mm collimation with 1 mm reconstruction, 219 slices total). The scan was transferred to the image guidance software using the DICOM protocol. The desired path was then planned on the user interface by the interventional radiologist by selecting the skin entry and target points. The magnetic tracking system was then used to track the probe and provide image guidance. The system concepts and experiments are described in a paper [Levy 2002a] and poster [Levy 2002b]. Related work on the project is described in another paper [Banovac 2002a] and poster [Banovac 2002a,b].

The clinical lead on this project is Elliot Levy, MD, an interventional radiologist at Georgetown. Dr. Levy had previously been awarded a CIRREF Academic Transition grant for his work (CIRREF is the Cardiovascular and Interventional Radiology Research and Education Foundation). He recently also received a Ring Academic Development Grant from the same organization.

The project has also been greatly helped by a Radiology resident, Filip Banovac, MD, who recently finished a two-year research rotation at the ISIS Center. Dr. Banovac has received an NIH training grant and a research grant from the Radiology Society of North America (RSNA).

In addition, our work on magnetic tracking has led to a new collaboration with Brad Wood, MD, of the Department of Radiology at the NIH Clinical Center. Dr. Wood is interested in using magnetic tracking to aid in precision positioning for radiofrequency ablation of metastatic disease and related procedures. We have begun developing a volumetric treatment planning system to aid in this procedure and our preliminary work is shown in [Cleary 2003a]. The user interface for this system is shown in Figure 7.

Finally, several related initiatives have emerged from this task. First, we have had a medical student, David Boyd, work with us over the summer as a research intern. His project was to investigate skin motion over the liver for interventional procedures. This data would be valuable for determining the accuracy of our registration schemes for incorporating magnetic tracking for internal organ motion. Mr. Boyd completed several studies in the interventional suite and his paper was accepted for presentation at the SPIE Medical Imaging Conference in February 2003 and publication in the proceedings [Boyd 2003].

We also wrote a survey paper reviewing the published studies on liver motion. This survey paper was published in the journal *Computer Aided Surgery* [Clifford 2002]. The survey showed that liver motion is primarily cranial-caudal (head to foot), but that there may also be significant side to side and front to back motion that cannot be ignored.

5.5 Task 5: Stereotactic Radiosurgery

We have begun a new project this year in conjunction with the Radiation Medicine Department at Georgetown. A new system for precision radiation therapy (the CyberKnife) was installed at Georgetown in Spring 2002. The system includes a robotic arm which is capable of precisely positioning the radiation beam and moving it in real-

time to compensate for organ motion due to respiration. Our joint research project is to investigate the use of skin motion as a predictor of internal organ motion to enhance the precision of these treatments. A protocol to collect this data during ongoing patient treatments have been approved by the Georgetown Institutional Review Board and the Army Human Subjects Research Review Board. A picture of the test setup is shown in Figure 8 and a copy of the protocol is included in the appendix. We began enrolling patients in this study in December and have completed 5 patients to date, but the study data is not available yet.

This is part of our overall plan to characterize respiratory motion for minimally invasive interventions. As a related effort, we did a feasibility study of electromagnetic tracking in the stereotactic radiosurgery suite as shown in Figure 9 [Cleary 2002c]. The study showed that is may be possible to use electromagnetic tracking to sense internal organ motion and that further studies are desirable.

5.6 Year 5 Plans

In year 5, we plan to continue our research in three major areas:

1) robotic assistance for needle placement in the spine and lung
2) electromagnetic position sensing for abdominal interventions
3) skin motion tracking for stereotactic radiosurgery and correspondence to internal organ motion

Our overall goal remains the same: technology development to provide assistance to the physician during minimally invasive interventions. One of our project themes has been the characterization of respiratory motion and we will continue to do studies in this area. We will also continue to look for new funding opportunities and synergistic collaborations.

6 Key Research Outcomes

This section provides a bulleted list of key research accomplishments:

- Completed the first 20 patients in an FDA approved randomized clinical trial of using a joystick controlled robot for nerve and facet blocks in the spine under fluoroscopy guidance
- Received a research grant from NCI/NIH to develop a similar robotic system for robotically assisted lung biopsy under CT Fluoroscopy in conjunction with Johns Hopkins URobotics Research Laboratory
- Completed phantom studies on a fully robotic biopsy testbed and showed that high accuracy (better than 2 mm) could be obtained
- Completed studies with a liver respiratory motion simulator to demonstrate the feasibility of using magnetic tracking for precision minimally invasive liver interventions

- Began a new study of skin motion versus internal organ motion for stereotactic radiosurgery in cooperation with the Department of Radiation Medicine at Georgetown
- Received a research contract from the NLM/NIH to integrate and evaluation a segmentation and research toolkit (Insight ITK) for segmentation of tumors in the liver

7 Reportable Outcomes

This section provides a list of reportable outcomes.

The major product of this year is the list of manuscripts and posters given in Section 10, References. Six conference papers were published or submitted, seven poster presentations were made, and two journal articles were published or submitted. A protocol for skin motion tracking during CyberKnife treatment was approved. Copies of these documents are provided in the appendix.

In addition, several grant applications to the National Institutes of Health were submitted based on this work. Two of these grant applications have now been funded. A graduate student from Catholic University and a graduate student from Johns Hopkins University were supported during the year to assist in software development for the robotic biopsy testbed. The research group at Georgetown continued to take a lead in the Washington Area Computer Aided Surgery Society (www.washcas.org), which was formed in 2000 to promote research in the field.

8 Conclusions

The fourth year of work on the Periscopic Spine Surgery has continued to lay the groundwork for developing the physician assist systems of the future. These systems will incorporate robotics, tracking, and visualization to improve the precision of instrument placement and manipulation in minimally invasive procedures. A clinical trial of the robot needle driver system was completed. Studies were completed with a robotic biopsy testbed and using a liver respiratory motion simulator for investigating electromagnetic position sensing. The focus of the next year will continue to be on technology improvements and moving this technology to clinical practice to improve patient care.

9 References

[Banovac 2002a] Banovac F, Glossop N, Lindisch D, Tanaka D, Levy E, and Cleary, K, "Liver tumor biopsy in a respiring phantom with the assistance of a novel electromagnetic navigation device," *Medical Image Computing and Computer-Assisted Intervention (MICCAI 2002)*, Springer, pages 200-207 (both the paper and poster are included in this report).

[Banovac 2002b] Banovac F, Glossop N, Jay M, Lindisch D, Cleary K, "Feasibility of image-guided abdominal interventions using a novel magnetic position sensing device in an interventional radiology suite," poster presented at *Computer Assisted Radiology and Surgery (CARS)*, Paris, June 2002.

[Boyd 2003] Boyd D, Tang J, Banovac F, Tanaka D, Dieterich S, Lindisch D, Levy E, Cleary K, "Quantification of skin motion over the liver using optical tracking," *SPIE Medical Imaging 2003: Visualization, Image-Guided Procedures, and Display*, San Diego, California, February 15-20, 2003.

[Cleary 2003a] Cleary K, Tanaka D, Stewart D, Wood B, Mocanu M, Levy E, Banovac F, Lindisch D, Roderick S, Tang J, Chung H, "Volumetric treatment planning and image guidance for radiofrequency ablation of hepatic tumors," *SPIE Medical Imaging 2003: Visualization, Image-Guided Procedures, and Display*, San Diego, California, February 15-20, 2003.

[Cleary 2003b] Cleary K, Watson V, Lindisch D, Patriciu A, Mazilu D, Stoianovici D, "Robotically assisted interventions in the spine and lung," poster presented at *Biomedical Imaging Research Opportunities Workshop*, Bethesda, MD, January 2003.

[Cleary 2002a] Cleary K, Patriciu A, Xu S, Mocanu M, Stoianovici D, "Software architecture for robotically assisted and image-guided interventions," *Computer Assisted Radiology and Surgery (CARS)*, Springer, 2002, pages 218-223.

[Cleary 2002b] Cleary K, Ruitort K, Watson V, Stoianovici D, "A cadaveric study of robotically assisted needle placement versus manual placement," poster presented at *Computer Assisted Radiology and Surgery (CARS)*, Paris, June 2002.

[Cleary 2002c] Cleary K, Gange C, Boyd D, Dieterich S, "Feasibility of electromagnetic position sensing in the CyberKnife stereotactic radiosurgery suite," poster prepared for in-house review, September 2002.

[Clifford 2002] Clifford M, Banovac F, Levy E, Cleary K, "Assessment of hepatic motion secondary to respiration for computer assisted interventions," *Computer Aided Surgery,* Volume 7, Issue 5, pages 291-299, 2002.

[Levy 2002a] Levy E, Cleary K, Banovac F, Tanaka D, Xu S, Lindisch D, Glossop N, "Evaluation of a magnetic tracking-guided needle placement system featuring respiratory gating in an in vitro liver model," *Computer Assisted Radiology and Surgery (CARS),* Springer, 2002, pages 329-334.

[Levy 2002b] Levy E, Cleary K, Banovac F, Glossop N, Tanaka D, Xu S, Lindisch D, "Implementation of a magnetic tracking system for accurate puncture needle guidance," poster presented at *Society of Interventional Radiology Annual Meeting*, Baltimore, MD, April 2002.

[Mocanu 2003] Mocanu M, Patriciu A, Stoianovici D, Mazilu D, Lindisch D, Corral G, Gruionu G, Cleary K, "Fluroscopy servoing using translation/rotation decoupling in an A/P view," *SPIE Medical Imaging 2003: Visualization, Image-Guided Procedures, and Display*, San Diego, California, February 15-20, 2003.

[Xu 2003] Xu S, Cleary K, Stoianovici D, and Fichtinger G, "Registration and tracking of a needle placement robot for CT-guided spinal procedures," paper under review for special issue of *IEEE Transactions on Robotics and Automation.*

[Watson 2002] Watson V, Cleary K, and Lindisch D, "Robotically assisted perispinal selective nerve and facet blocks: cadaver studies," poster presented at *American Society of Neuroradiology Annual Meeting*, Vancouver, May 2002.

10 Appendices

10.1 Figures

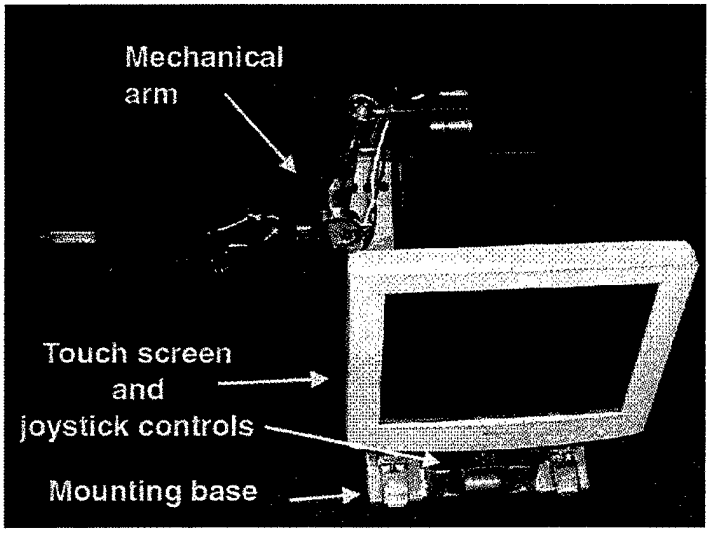

Figure 1: Robotic device showing mechanical arm and joystick control
(courtesy of Dan Stoianovici, PhD, Johns Hopkins Urology Robotics)

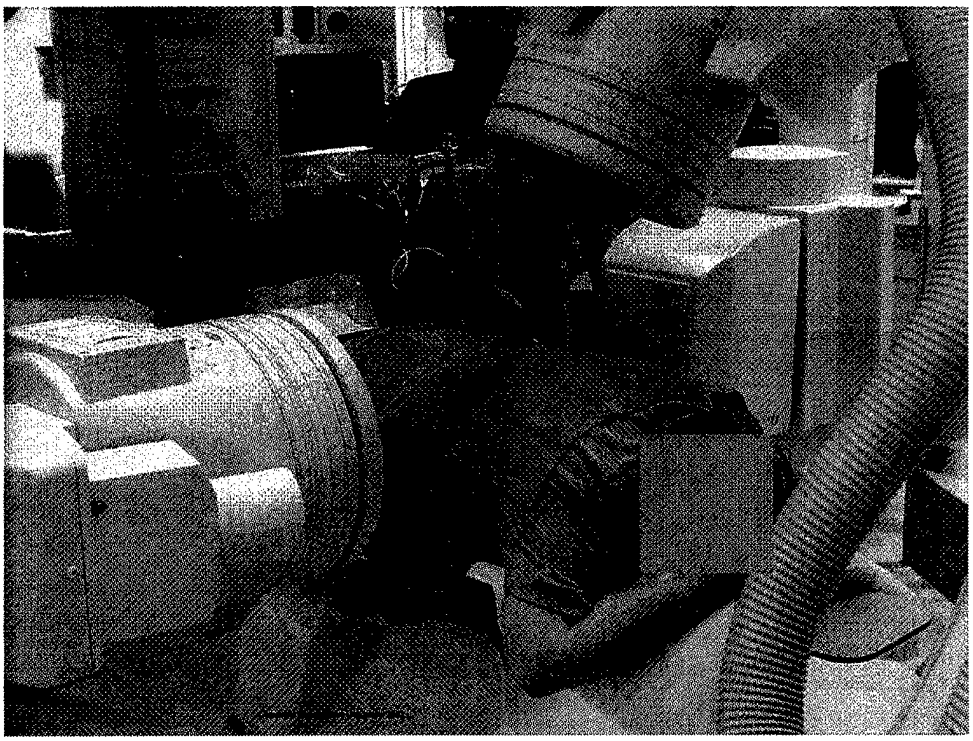

Figure 2: Clinical trial of robotic device for nerve and facet blocks at Georgetown University (interventional radiologist is Vance Watson, MD)

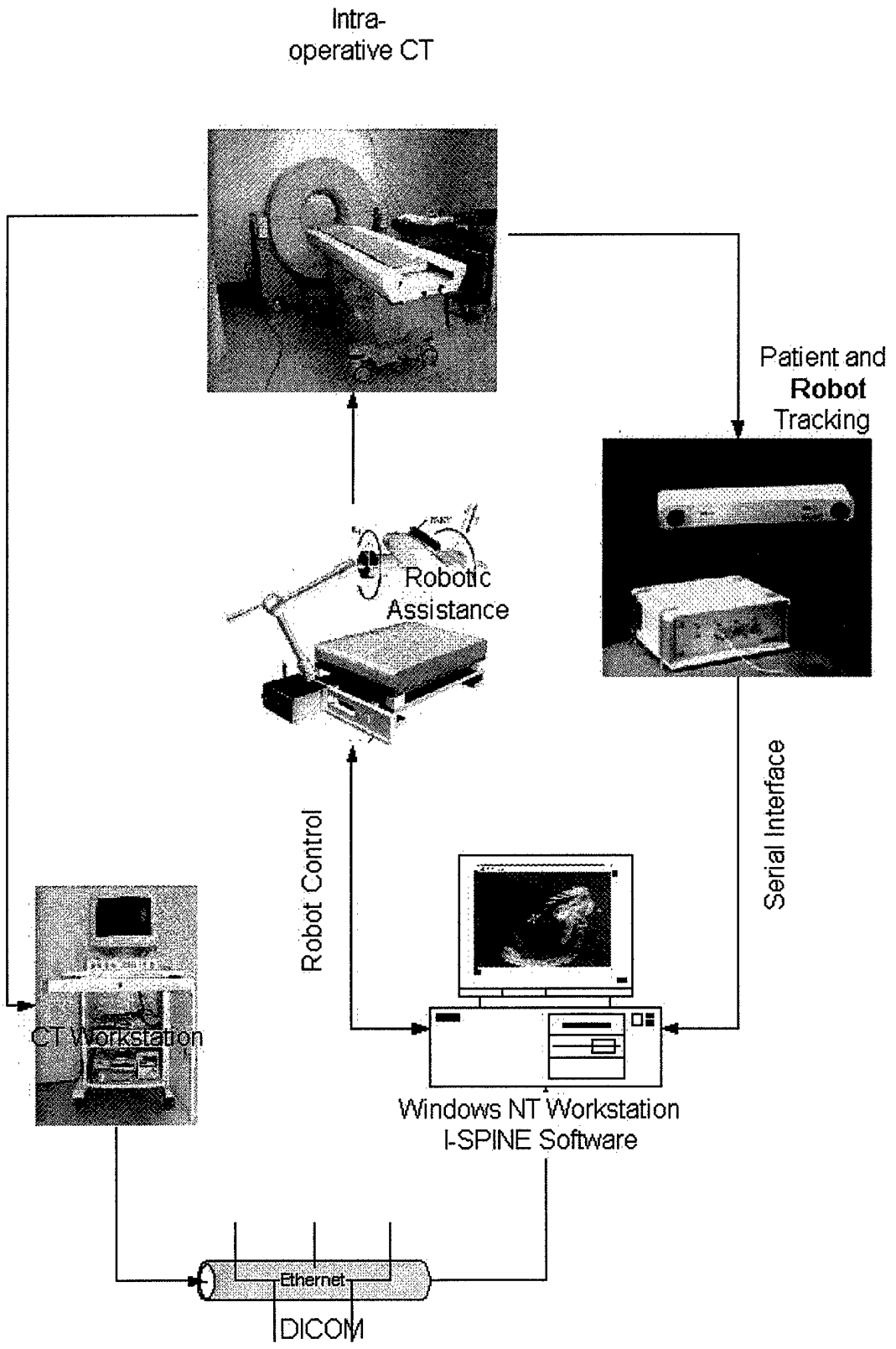

Figure 3: Robot biopsy testbed architecture

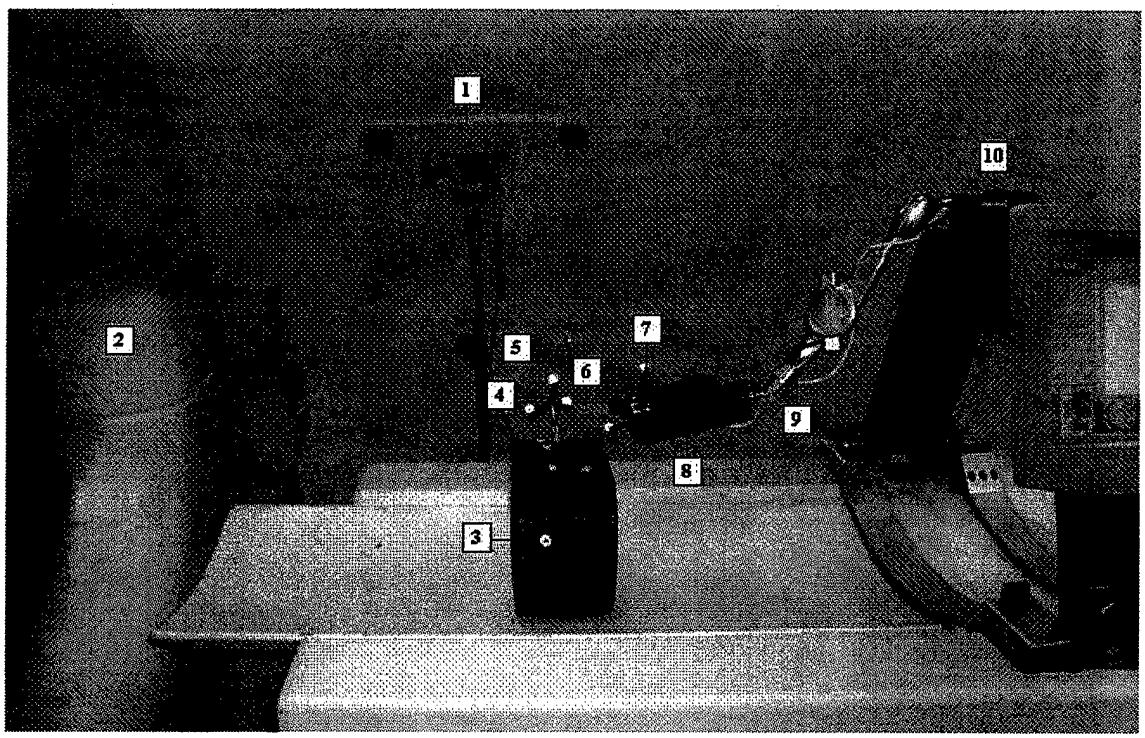

Figure 4: Robot Biopsy Testbed Components
(1) Polaris Optical Tracker (2) CT Gantry (3) Abdominal Phantom (4) Fiducial Carrier (5) Needle (6) Needle Driver (7) Robot Tracker (8) RCM Stage (9) Passive Arm (10) Cartesian Bridge

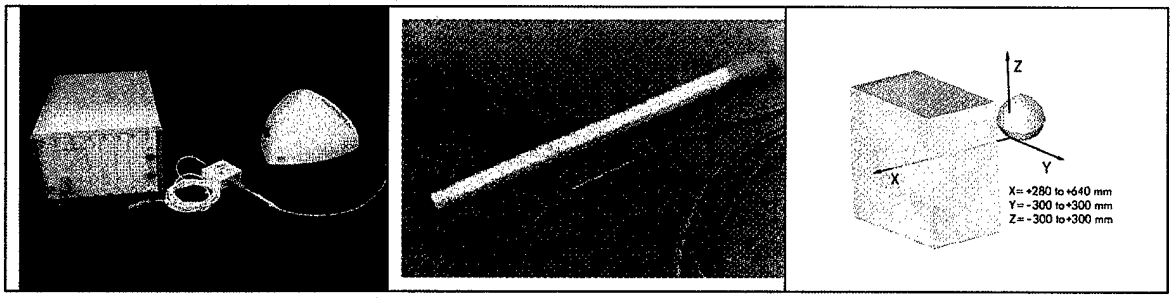

Figure 5: AURORA™ sensors, magnetic tracking system components, and measurement volume
The left picture shows (from left to right) the control unit, sensor interface device, and magnetic field generator. The middle picture shows the sensor coils along with the electrical wires protruding from the coil, compared to a match. The right picture shows the measurement volume in mm relative to the location of the field generator. (Photos courtesy of Northern Digital, Inc.)

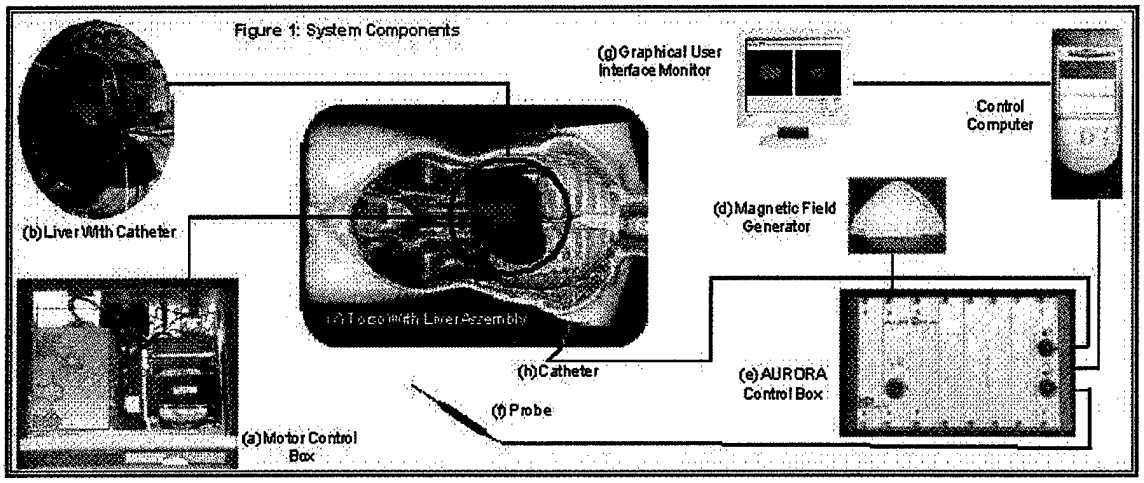

Figure 6: Liver respiratory motion simulator and system components

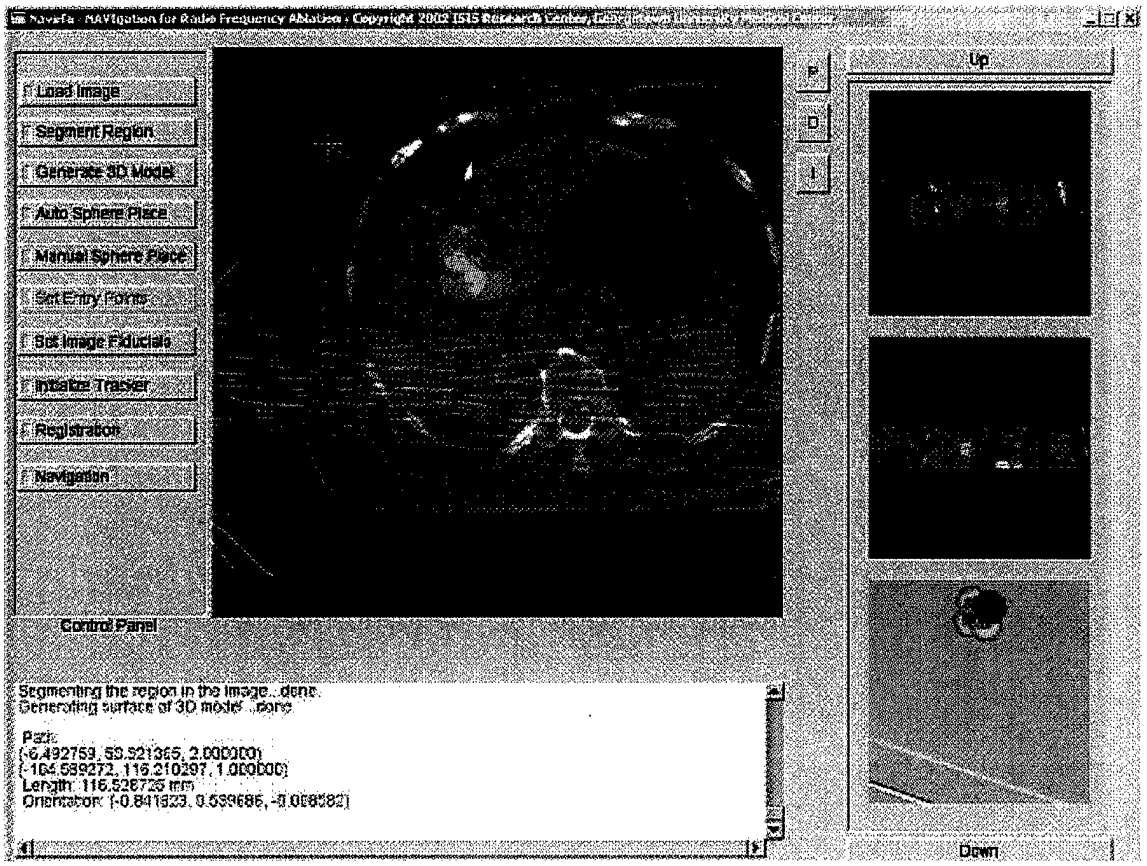

Figure 7: User interface for radiofrequency ablation volumetric treatment planning

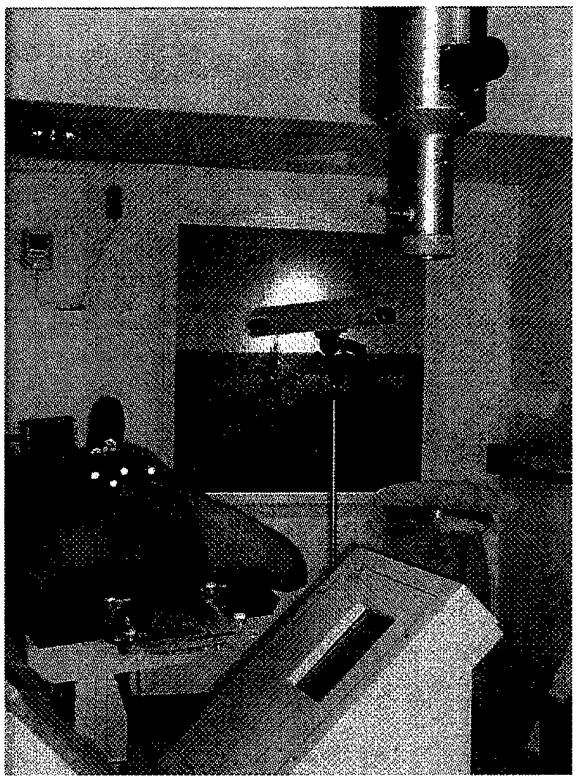

Figure 8: Test setup for collecting skin motion data during CyberKnife stereotactic radiosurgery treatment

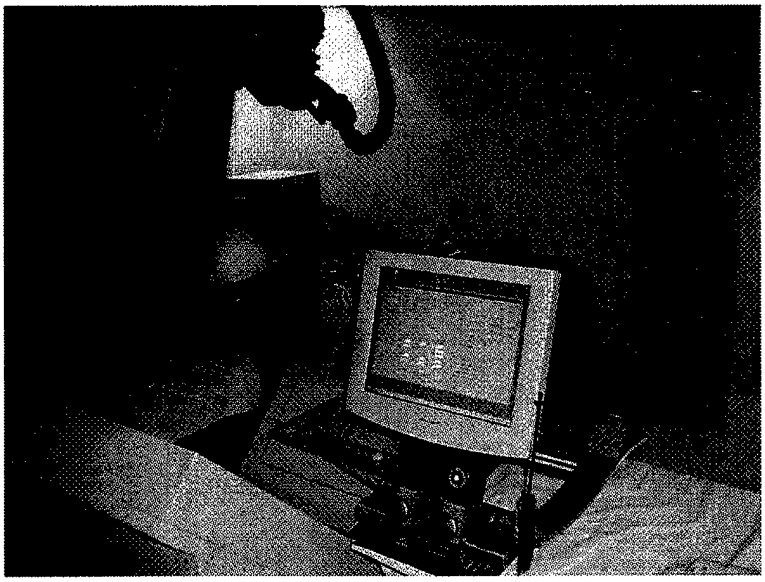

Figure 9: Electromagnetic position sensing experiments in the CyberKnife suite (robotic device is used to hold an electromagnetically tracked needle)

10.2 Papers

Copies of the two journal papers submitted or published and six conference papers published are reproduced in this section.

10.2.1 Banovac 2002a: Liver Tumor Biopsy

Reprint begins on the next page and is 8 pages.

Published in MICCAI 2002

Liver Tumor Biopsy in a Respiring Phantom with the Assistance of a Novel Electromagnetic Navigation Device

Filip Banovac[1,2], Neil Glossop[3], David Lindisch[1],
Daigo Tanaka[1], Elliot Levy[1,2], and Kevin Cleary[1]

[1]Imaging Sciences and Information Systems Center (ISIS), Department of Radiology,
Georgetown University, 2115 Wisconsin Avenue, Suite 603
Washington, DC, U.S.A.
[2]Georgetown University Hospital, 3800 Reservoir Road, N.W., Washington, DC, U.S.A.
{Banovac, Lindisch, Tanaka, Levy, Cleary}
@isis.imac.georgetown.edu
[3]Traxtal Technologies LLC, 5116 Bissonnet, Bellaire, TX 77401

Abstract. The purpose of this study was to evaluate our ability to insert magnetically tracked needles into liver phantom tumors which move simulating physiologic respiration. First, a novel image-guided platform based on a new magnetic tracking device (AURORA™) was constructed. Second, an accuracy evaluation of a compatible magnetically tracked needle (MagTrax) was performed. Finally, 16 liver tumor punctures were attempted using only the image-guided platform for guidance. The inherent MagTrax needle positional error was 0.71±0.43 mm in the non-surgical laboratory setting. Successful puncture of liver tumors was achieved in 14 of 16 attempts (87.5%) by two users. The average time of each procedure was short (163±57 seconds.) The system adequately displayed the moving liver allowing for tumor target visualization and targeting. The AURORA based navigation platform and the compatible MagTrax needle appear promising for more rigorous phantom accuracy studies and *in vivo* tumor puncture testing in a respiring animal.

1 Introduction

Image-guided systems for intervention in the thorax and abdomen have not been developed, in part because of problems related to organ motion induced by respiration. The internal organs are not rigid nor directly accessible and therefore difficult to track and register for purposes of image guidance. This is in contrast to intracranial and musculoskeletal interventions where image-guided systems based on bony landmarks have been developed by many researchers and commercial systems are available.

In particular, the need for organ tracking and precision instrument placement in liver procedures has multiple clinical justifications. Tumor biopsy, radiofrequency ablation of tumors, portal and hepatic venous access for intrahepatic shunts, and billiary access for drainage all require precision for procedural success. The liver predominately moves in a cranio-caudal direction during quiescent physiologic breathing exhibiting displacements from 10 to 25 mm [1, 2]. For open surgery, Herline et al. explored the feasibility of surface based registration methods for intraoperative liver tracking [3]. They also showed the feasibility of liver tracking in open and laparoscopic procedures [4]. However, for percutaneous minimally invasive

procedures, the only clinically accepted methods are direct visualization with fluoroscopy or ultrasound, each of which has its own shortcomings.

Several image-guided surgical systems based on magnetic position tracking are currently commercially available. BioSense Webster, a Johnson and Johnson company, offers two navigational systems for cardiac catheterization and mapping, the NOGA™ and CARTO™ systems. This product has been used in early clinical studies showing feasibility for intracranial neuro-navigation [5] and cardiac mapping in treatment of arrhythmias [6]. Solomon et al. used the Biosense system to assist in placement of a transjugular intrahepatic portosystemic shunt (TIPS) in swine [7]. For endoscopic sinus surgery, Visualization Technologies Inc. a subsidiary of General Electric (Lawrence, MA) sells the InstaTrack 3000® image-guided surgery system.

A magnetic positioning guidance system that is targeted at intra-abdominal interventions is the UltraGuide1000 (UltraGuide, Tirat Hacarmel, Israel). The UltraGuide device was introduced to complement currently used sonographic guidance techniques, especially to enhance the freehand techniques. The device uses small magnetic sensors attached to the hub or the shaft of the needle to help the user navigate the needle to the target. Howard et al. and Krombach et al. independently reported the successful use of UltraGuide to perform liver and kidney percutaneous procedures respectively [8, 9]. Wood et al. reported the use of the same device in RF ablation of renal cell carcinoma [10].

The purpose of this study was to evaluate the usefulness of magnetic tracking and image guidance for precision biopsy of simulated lesions in a moving liver phantom. This study was based on a liver respiratory motion simulator developed by our group and the AURORA magnetic tracking system under development by Northern Digital Inc., Ontario, Canada. An accuracy evaluation of a newly developed, commercially available and AURORA compatible needle was also performed.

2 Materials and Methods

2.1 Liver Respiratory Motion Simulator

To evaluate magnetic tracking for minimally invasive abdominal interventions, the Georgetown group has developed a liver respiratory motion simulator. The simulator includes a synthetic liver mounted on a motion platform. The simulator consists of a dummy torso, a synthetic liver model, a motion platform, a graphical user interface, the AURORA magnetic tracking system, and a magnetically tracked needle and catheter as previously described [11, 12].

2.2 Liver Phantom

A human torso model containing a liver phantom was modified from our previously described prototype [12]. The liver phantom was made from a two part flexible foam (FlexFoam III, Smooth-On, Easton, PA) which was cast from a custom made mold. The foam material was cured to approximately simulate liver tissue resistance to needle puncture. Two spiculated, silicone, elliptical tumors (maximum diameters of 3.1 and 2.2 cm) containing radio-opaque CT contrast were incorporated into the liver model prior to curing to serve as tumor targets. The liver was attached to

a linear motion platform at the base of the torso's right abdomen (Figure 1).

The platform can be programmed to simulate physiologic cranio-caudal motion of the liver with options for respiratory rate control, breath depth, and breath pause (breath hold). A ribcage and single layer latex skin material (Limbs and Things, Bristol, UK) were added for aesthetic and physical reality.

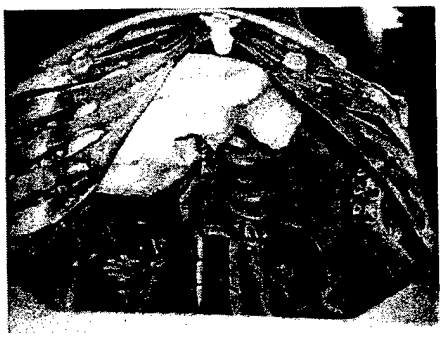

Fig. 1. A foam liver model (white) mounted on a linear platform inside the torso model.

2.3 Magnetic Tracking Device and Sensors

A prototype of a new magnetic field based tracking system, the AURORA, was used in the experiments. The system consists of a control unit, sensor interface device, and field generator as shown in Figure 2.

The AURORA uses cylindrically shaped sensors that are extremely small (0.9 mm in diameter and 8 mm in length). This enables the sensors to be embedded into surgical instruments. We used two magnetically tracked instruments in these experiments: 1) A prototype 5-French catheter with an embedded sensor coil was provided by the manufacturer; and 2) A needle/probe combination (MagTrax) as shown in Figure 3.

The MagTrax (Traxtal Technologies, Houston, Texas) needle/probe consists of a 15 cm stylette with a magnetic sensor at its tip and an 18-gauge trocar. This instrument was used in the study to puncture the tumors.

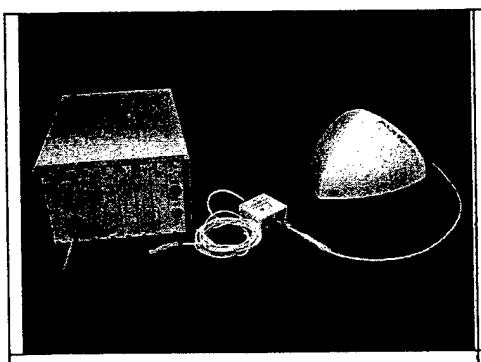

Fig. 2. AURORA control unit and field generator (courtesy of Northern Digital Inc.)

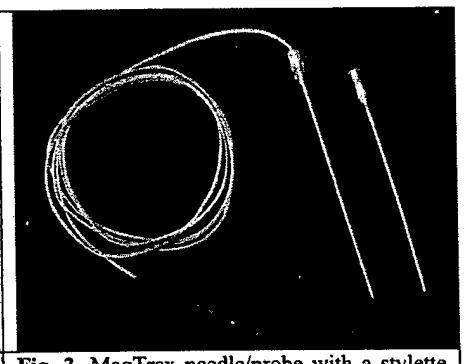

Fig. 3. MagTrax needle/probe with a stylette containing a magnetic sensor in its tip and leads exiting the hub. An 18-gauge trocar is seen on the right.

2.4 Guidance System and Software

A PC-based software application called ROGS (Respiring Organ Guidance System) was developed to assist the physician in performing the puncture of the liver parenchyma and needle guidance into the liver tumors. The system incorporates a graphical user interface [13] shown in Figure 4. The ROGS software allows for the loading of serial axial CT images, pre-procedural planning to the target of interest, tracking of respiratory motion, and real-time display of the biopsy needle as it approaches the target tumor. The sequence of steps in path planning and needle placement is shown in Figure 5.

2.5 MagTrax Needle/Probe Accuracy Evaluation

A MagTrax needle/probe containing a single five degree of freedom magnetically tracked sensor was solidly fixed to two passive optically tracked rigid bodies (small 50 x 50 mm and large 95 x 95 mm). The sensor assembly was moved randomly through 101 positions in a volume of 36 mm x 36 mm x 47 mm. At each location the sensor assembly was clamped and 10 samples from each of the targets were collected by the POLARIS optical system (Northern Digital Inc, Ontario, Canada) and AURORA magnetic system. The data sets were aligned by mathematical transformations and the difference in position and orientation of the two POLARIS sensors (control) versus the larger POLARIS sensor and MagTrax probe were calculated over the 101 positions. The experiment was performed in the absence of ferromagnetic interference.

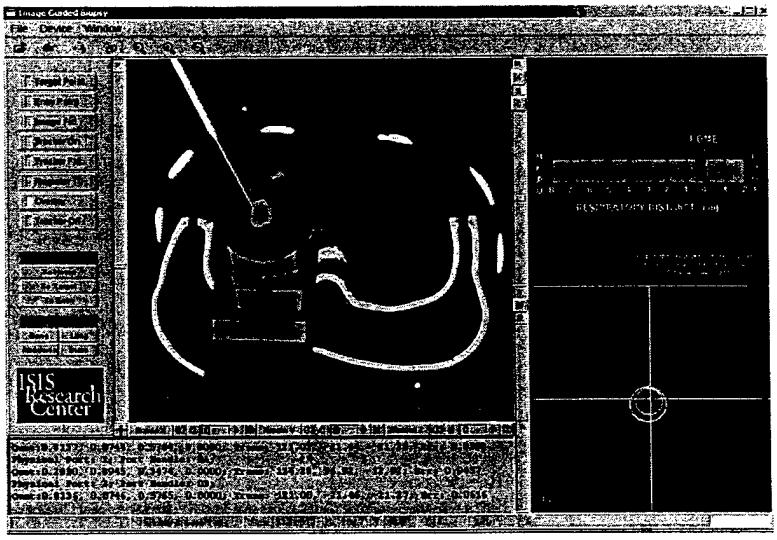

Fig. 4. Graphical user interface (center window shows probe overlaid on image, respiratory tracking in upper right, targeting window in lower right, *patent pending 2001-2002*)

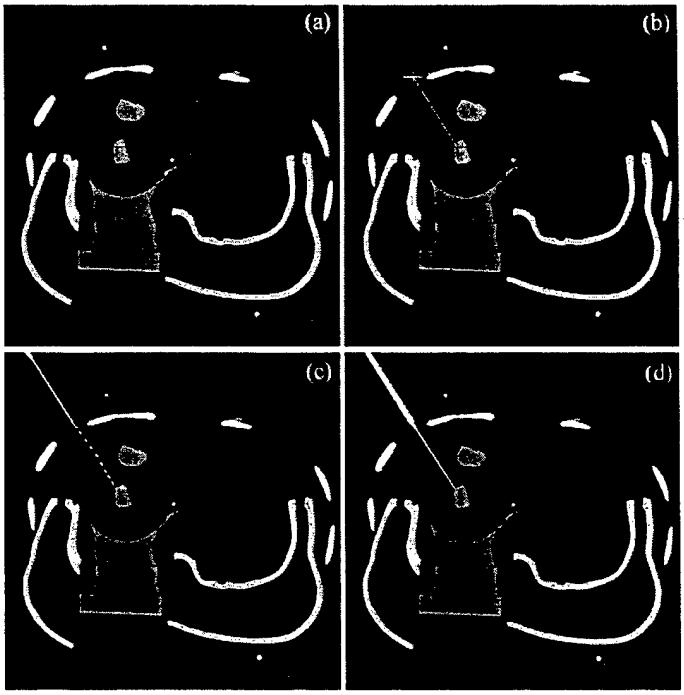

Fig. 5. Target tumor on an axial image of the phantom torso is selected by the radiologist (a); subsequently, the radiologist selects the skin entry point (b) and a planned path appears on the reconstructed image; the needle/probe is placed at the skin entry point (c) using cross hairs targeting window (Fig 4. lower right); finally, the needle is driven into the tumor (d) along the planned path indicated by the dotted line.

2.6 Real-Time Tumor Biopsy Evaluation

A series of tumor targeting experiments were performed to test the usefulness of the system in accurately guiding a user to a target while the phantom resumes physiologic respiration. Two users (F.B. and D.L) independently performed 8 punctures each. The experimental design was divided into three stages as follows:

Stage 1: CT Scanning and Registration

1. A magnetically tracked catheter was wedged in the hepatic vein of the liver. Several skin fiducials (multimodality markers, IZI Medical, Baltimore, Maryland) were placed on the rib cage.
2. A series of 3 mm axial slices with 1 mm axial reconstructions were obtained on CT VolumeZoom (Siemens, Erlangen, Germany) from the base of the lungs through the liver while the liver was kept in end-inspiration (simulating the breath-hold technique used in clinical practice).
3. The images were transferred to the ROGS using the DICOM standard.

4. The tracking catheter was left in the hepatic vein and the simulator was moved to the interventional radiology suite. The magnetic field generator was positioned near the phantom above the chest.
5. The position of the wedged catheter was read in the magnetic coordinate system. The position of the skin fiducials were read in the magnetic coordinate system by touching each fiducial with the MagTrax needle.
6. The position of the catheter and fiducials was determined in CT coordinate space by prompting the user to select these same points on the CT images.
7. A least-squares fit registration algorithm was invoked to determine the transformation matrix from magnetic space to CT space.

Stage 2: Biopsy Path Planning Phase

8. Each user was allowed one practice "planning phase" and "puncture (biopsy) phase" to get familiarized with the ROGS.
9. The user selected the target and a suitable skin entry point by scrolling through the axial images (figure 5a and 5b) thus selecting a biopsy path.
10. Simulated respirations were initiated at 12 breaths per minute with 2 cm cranio-caudal liver excursion.

Stage 3: Biopsy Phase

11. The MagTrax needle/probe was positioned on the skin entry point as determined in the "planning phase" and displayed by the ROGS overlay.
12. A real-time display of the current liver position was displayed by the ROGS system based on the position of the magnetically tracked catheter.
13. The MagTrax needle was tracked in real-time and the transformation matrix computed in step 7 was used to compute the overlay of the probe on the CT images which were reconstructed so to show the planned path of the needle.
14. When satisfied with the target position relative to the planned path, the user would initiate temporary cessation of respiration (simulating a 20 second breath hold in clinical practice). If the allotted time was exceeded, the phantom would continue spontaneous respirations for a minimum of 20 seconds (hyperventilation in clinical practice). Any partially inserted needle would be left in place as is frequently done during biopsy procedures.
15. Repeating step 14 the user would keep making minor adjustments to the needle until satisfied with the needle position as displayed on ROGS.
16. The time for each "planning phase" and "biopsy phase" were recorded. Multi-projection fluoroscopic images were taken at the end of each needle placement to ascertain whether the target tumor was successfully punctured.

3 Results

3.1 Accuracy evaluation of the MagTrax Needle

Using the optical passive tracking system as the gold standard as described in the methods in Section 2.5, the mean measurement error and standard deviation of the MagTrax needle/probe using the AURORA system was 0.71±0.43 mm (n=101) in a non-surgical environment. The maximum error noted was 2.96 mm.

3.2 Tumor Biopsy Evaluation

The targeted tumor was successfully punctured in 14 out of 16 biopsy attempts (87.5%). This was done without any additional real-time imaging guidance such as fluoroscopy. Instead, fluoroscopy was used to confirm the final location of the needle and evaluate accuracy.

Each user missed the target tumor once. In those instances, the maximal tangential distance from the lesion to the needle was 3.98 mm. On most occasions, the user was able to reach the tumor in a single continuous puncture after the needle was positioned on the skin entry point. This was done within a single 20 second breath hold (pause in liver motion) in end-inspiratory liver position. More than two breath hold cycles with intervening period of hyperventilation were needed on only 1 out of 16 experimental trials. The time needed for registration ranged from 173-254 seconds. The planning time, needle manipulation time, and total procedure times for the 16 trials are presented in Table 1.

Table 1. Planning, needle manipulation and total procedure times for ROGS assisted biopsy of tumors in a respiring liver phantom

	Mean Planning Time (s) ± SD	Needle Manipulation Biopsy Time (s) ± SD	Total Procedure Time (s) ± SD
User 1	72 ± 35	79 ± 40	151 ± 59
User 2	61 ± 31	111 ± 41	172 ± 43
Overall	71 ± 36	93 ± 43	163 ± 57

4. Discussion

Image-guided surgery is now an established practice for brain, ENT, and spinal procedures. These systems are based on optical tracking and bony landmarks. The introduction of a new magnetic tracking system with sensor coils small enough to be embedded into instruments may enable the development of image-guidance for abdominal and thoracic internal organs.

The overall goal of the research described here is to develop magnetic tracking for internal organs, including methods of compensating for respiratory motion. The initial results presented here show the feasibility of magnetic tracking, but much work remains to be done before this technology can implemented in clinical practice.

The accuracy of the MagTrax needle/probe used with the AURORA was measured as 0.71 mm. This should be sufficient for clinical practice. Additionally, the location of the magnetic sensor in the tip of the needle/probe means the instrument is not subject to errors introduced by needle bending unlike those used in the UltraGuide system where the proximal end of the needle is tracked [8].

The ROGS interface allowed a high success rate (87.5%) for needle puncture of the two small to medium sized simulated tumors. Most notably, the procedure was done while actively tracking the physiologic motion of the liver. To our knowledge, ROGS is the first system that allows real-time compensation for the moving intra-abdominal

target and subsequent compensated guidance for the needle puncture. The system was easy to use requiring only a single practice attempt to attain a satisfactory comfort level. The entire average procedure time lasted less than three minutes which is shorter than the time needed to perform this task during a conventional CT guided biopsy. These initial results are promising towards the development of a clinically useful system. Further experiments and animal studies are planned.

Acknowledgements

This work was funded by U.S. Army grant DAMD17-99-1-9022, an NIH National Research Service Award Fellowship (F32HL68394-01), and a CIRREF Academic Transition Award.. The content of this manuscript does not necessarily reflect the position or policy of the U.S. Government. The authors would like to thank Northern Digital, Inc., for the loan of the magnetic tracking system. The software was developed by Daigo Tanaka of Georgetown University and Sheng Xu, a graduate student in the NSF-funded Center for Computer Integrated Surgical Systems and Technologies at Johns Hopkins University.

References

1. Davies, S.C., et al., *Ultrasound quantitation of respiratory organ motion in the upper abdomen.* Br J Radiol, 1994. **67**(803): p. 1096-102.
2. Suramo, I., M. Paivansalo, and V. Myllyla, *Cranio-caudal movements of the liver, pancreas and kidneys in respiration.* Acta Radiol Diagn (Stockh), 1984. **25**(2): p. 129-31.
3. Herline, A.J., et al., *Surface registration for use in interactive, image-guided liver surgery.* Comput Aided Surg, 2000. **5**(1): p. 11-7.
4. Herline, A.J., et al., *Image-guided surgery: preliminary feasibility studies of frameless stereotactic liver surgery.* Arch Surg, 1999. **134**(6): p. 644-9; discussion 649-50.
5. Zaaroor, M., et al., *Novel magnetic technology for intraoperative intracranial frameless navigation: in vivo and in vitro results.* Neurosurgery, 2001. **48**(5): p. 1100-7
6. Gepstein, L., G. Hayam, and S.A. Ben-Haim, *A novel method for nonfluoroscopic catheter-based electroanatomical mapping of the heart. In vitro and in vivo accuracy results.* Circulation, 1997. **95**(6): p. 1611-22.
7. Solomon, S.B., et al., *TIPS placement in swine, guided by electromagnetic real-time needle tip localization displayed on previously acquired 3-D CT.* Cardiovasc Intervent Radiol, 1999. **22**(5): p. 411-4.
8. Howard, M.H., et al., *An electronic device for needle placement during sonographically guided percutaneous intervention.* Radiology, 2001. **218**(3): p. 905-11.
9. Krombach, G.A., et al., *US-guided nephrostomy with the aid of a magnetic field-based navigation device in the porcine pelvicaliceal system.* J Vasc Interv Radiol, 2001. **12**(5): p. 623-8.
10. Wood, B.J., et al., *Percutaneous radiofrequency ablation with three-dimensional position sensor guidance.* Cardiovasc Intervent Radiol, 2001(in print).
11. Cleary, K., et al. *Development of a Liver Respiratory Motion Simulator to Investigate Magnetic Tracking for Abdominal Interventions.* in *SPIE Medical Imaging.* 2002. San Diego, CA.
12. Banovac, F., et al. *Design and Construction of a Liver Phantom for CT Imaging and Interventions that Simulates Liver Motion Seen During Respiration.* in *Radiologic Society of North America.* 2001. Chicago, IL.
13. Cleary, K., et al. *Feasibility of Magnetic Tracking for Image-Guided Abdominal Interventions Based on a Liver Respiratory Motion Simulator.* submitted to *IEEE International Symposium on Biomedical Imaging.* 2002. Washington, DC.

10.2.2 Boyd 2003: Quantification of Skin Motion

Reprint begins on the next page and is 12 pages.

To be presented at SPIE Medical Imaging 2003 and published in the proceedings

Quantification of Skin Motion over the Liver Using Optical Tracking

David Boyd[a,b], Jonathan Tang[a], Filip Banovac[a,b], Daigo Tanaka[a], Sonja Dieterich[a,b], David Lindisch[a,b], Elliot Levy[a.b], Kevin Cleary*[a]

[a]Imaging Sciences and Information Systems (ISIS) Center, Department of Radiology, Georgetown University, Washington, DC
[b]Georgetown University Hospital/MedStar Health, Washington, DC

ABSTRACT

The purpose of this study was to quantify skin motion over the liver when patients are repositioned during image-guided interventions. Four human subjects with different body habitus lay supine on the interventional radiology table. The subjects held their arms up over their heads and down at their sides for 13 repositioning trials. Precise 3-D locations of the four skin fiducials permitted deformable skin motion to be quantified. For the first two occasions, the average skin motion was 1.00 ± 0.82 mm in the arms-up position and 0.94 ± 0.56 mm in the arms-down position, a small, but not statistically significant difference. Three out of the four subjects exhibited increased skin motion in the arms-up position, suggesting that patient-positioning technique during CT imaging may have an effect on the skin-motion component of registration error in image-guided interventions. The average skin motion was 0.65 ± 0.39 mm for Subject 1 and 1.32 ± 0.78 mm for Subject 2, a significant difference. Subjects 3 and 4 demonstrated a similar amount of skin motion (0.86 ± 0.55mm and 0.89 ± 0.59mm, respectively). The subject with the largest body habitus demonstrated significantly less skin motion, an observation that is difficult to explain. The skin fiducial on the xiphoid process exhibited significantly less skin motion than the other fiducials, suggesting that certain anatomic locations could influence motion of the fiducial, and subsequently, the introduced error.

Keywords: skin motion, liver, image-guided interventions, interventional radiology, repositioning, fiducials, deformable, patient-positioning, registration, xiphoid process

1. INTRODUCTION

Thanks to the development of new interventional techniques and the desire of clinicians and patients to decrease procedure-related morbidity and trauma, minimally invasive abdominal interventional procedures are rapidly increasing in popularity. Such interventions are performed using catheters, needles, or other instruments, that are introduced, targeted, and maneuvered without the benefit of direct visualization afforded by the normal surgical exposure. This greatly minimizes trauma to the patient, but severely limits the physician's view of the underlying anatomy. Image-guided surgical procedures, however, circumvents this hindrance. It utilizes magnetic resonance imaging (MRI) or computed tomography (CT) scans to guide interventional procedures.

Image-guided systems for intervention in the abdomen have not been developed, in part, because of complexities related to intra-abdominal organ motion induced by respiration. Intra-abdominal organs are not rigid or directly accessible and are thus difficult to track and register for image-guided purposes. This is in contrast to intracranial and musculoskeletal interventions where image-guided, point-based, rigid-body registration systems based on bony anatomical landmarks and optical tracking have been developed by many researchers, and commercial systems are available.

* Correspondence: Kevin Cleary, PhD, ISIS Center, Department of Radiology, Georgetown University, 2115 Wisconsin Avenue, Suite 603, Washington, DC, 20007; telephone: 202-687-8253; fax: 202-784-3479; e-mail: cleary@georgetown.edu

Specifically, tracking of the liver for precise instrument placement in intrahepatic interventions could enhance the ease and accuracy of existing interventions and enable new interventions. Such tracking has several clinical uses, including tumor biopsy, radiofrequency ablation of tumors, portal and hepatic venous access for intrahepatic shunts, and biliary access for drainage, which all require precision for procedural success.

Tracking systems, based on magnetic field generation, have the major advantage in that they do not require that a direct line of sight be maintained. A magnetic positioning guidance system that uses small magnetic sensors attached to the hub or shaft of the needle to target intra-abdominal organs is the UltraGuide 100 (UltraGuide, Tirat Hacarmel, Israel). Howard, et al., independently reported the successful use of UltraGuide to perform liver percutaneous procedures[1].

Solomon, et al., have demonstrated the feasibility of using magnetic tracking with skin fiducials to accurately perform several percutaneous interventional radiology (IR) procedures, including a transjugular intrahepatic portosystemic shunt (TIPS) in swine[2]. In this procedure, the actual position of the needle instrument was registered with pre-operative images, permitting the operator to successfully perform the procedures without visualizing the target with a real-time imaging modality[2].

Our research has shown that the combination of an image-guided navigation platform based on the AURORA™ magnetic tracking system (Northern Digital, Inc., Ontario, Canada) and the compatible MagTrax needle/probe (Traxtal Technologies, Houston, Texas) that has small magnetic sensor coils embedded in its tip, can be used to accurately biopsy liver tumors in a liver phantom model[3]. Like the Solomon group's TIPS procedure in swine, these punctures were performed without visualizing the target with a real-time imaging modality, but instead using fluoroscopy only to confirm instrument placement[2,3]. Implementing such an image-guided system with magnetic tracking of organ motion could also permit respiratory-gated needle placement[4].

All image-guided surgical navigation systems use registration, a process in which computer software aligns defined points in the preoperative imaging data set with their corresponding points in the operating field volume. The Georgetown group is currently testing a surface fiducial registration approach, which, in addition to an intrahepatic magnetically tracked needle being inserted into the liver, entails several radio-opaque fiducial markers being placed on bony landmarks on the skin overlying the liver. Pre-operative CT images with fiducial locations are taken, the images are reconstructed into 3-D space, and these images are then transferred to computer software. Next, on the IR procedure table, registration is performed by touching the magnetically tracked probe at the tip of the needle to the centers of the skin fiducials, which allows determination of the positions of the fiducials in 3-D magnetic space. A least squares fit registration algorithm is invoked to determine the transformation matrix from magnetic space to CT image space. Once this is completed, the differences between the 3-D positions of the fiducials on the IR table and the pre-procedure 3-D positions determined by the CT scanner constitute registration error.

Such a surface fiducial registration system for the abdomen relies heavily on skin fiducial stability on a mobile skin surface. Skin fiducial stability with repositioning would thus seem to be important to enhance the accuracy of registration for precision placement of instruments during minimally invasive abdominal procedures. Even during breath hold, the skin is moving both in the CT scanner and on the IR table. Such deformable skin motion could introduce significant errors into the registration process.

Besides skin motion, liver motion and respiratory motion also contribute to registration error. In this study, given that only external skin fiducials were used and that only end-expiratory breath holding was utilized, the amount of liver motion and respiratory motion, respectively, were assumed to be inconsequential, leaving only skin motion to be determined. These experiments quantified the deformable skin motion that occurred between reference and comparison measurements, with the subjects repositioning onto the IR table in between the two measurements. We investigated the amount of deformable skin motion related to several different variables, including body position (arms up for both measurements, arms down for both measurements, and arms up for the reference measurement and down for the comparison measurement); body habitus (different for the four subjects); and skin marker location (Markers A, B, C, and D – See Section 2 below).

2. METHODOLOGY

The following skin motion study was performed on two separate occasions in the IR suite about one month apart: June 19, 2002 (Occasion 1) and July 16, 2002 (Occasion 2). An additional experiment was carried out on December 19, 2002 (Occasion 3) to increase the sample size and to enhance gender diversity in the study.

The protocol used was as follows:

In the IR suite, the POLARIS optical tracking system was set up and the Polytrax application software was opened on the laptop. The POLARIS system was set up approximately 1.5 m from the infrared sensors, the optimal distance according to Northern Digital, Inc.[5]

Two human subjects, Subject 1 and Subject 2 (both male), participated in the first two experiments. First, Subject 1 removed his shirt and positioned himself to lie supine on the IR procedure table. The four active infrared sensors (labeled A, B, C, and D) were attached with double sided tape onto the following bony anatomical landmarks on the skin in a diamond-like pattern (See Figures 1 and 2 below):

A: Xiphoid process.
B: Right fifth rib in semilunar line, also known as the right lateral rectus plane.
C: Right 7th rib in nipple line.
D: Right costal margin, halfway between the semilunar line and midline, where the medial part of the 8th rib meets the medial part of the 7th rib.

FIGURE 1

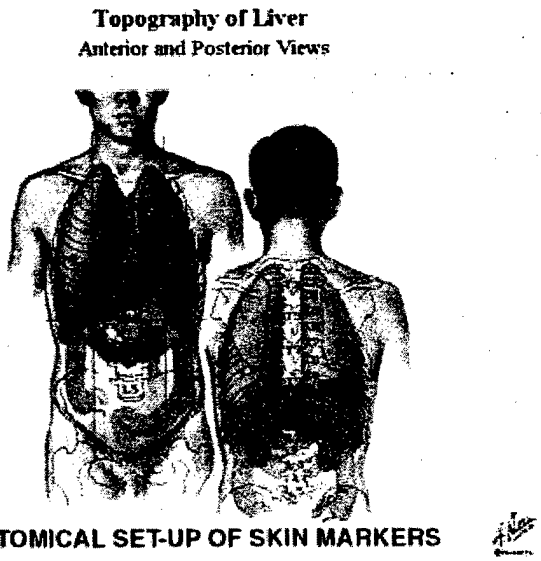

(Permission granted by Icon Learning Systems) [6]

FIGURE 2

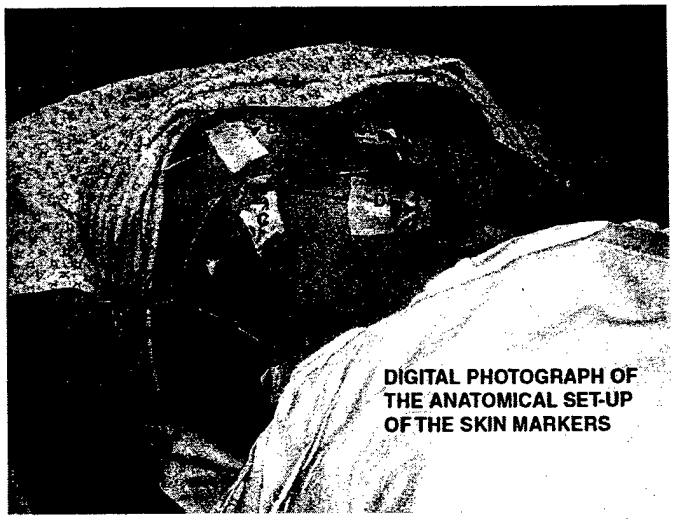

While continuing to lie in a supine position, Subject 1 proceeded to assume a position on the patient table with his "arms up," meaning that his arms were above his head, interlocked, and bent roughly ninety degrees at the elbows, consistent with the position that patients hold during CT scans (arms interlocked with right hand holding left elbow and vice-versa).

Subject 1 then held his breath on end-expiration, just as CT scans and IR procedures are performed in end-expiration, and the PolyTrax application was executed by pressing the ENTER key on the laptop. After the execution, which took approximately 1-2 seconds each time, Subject #1 was able to resume breathing normally. During these experiments, the laboratory technician ran the software and checked to make sure that the POLARIS camera picked up the 3-D positions of each of the four skin fiducials for each trial. The PolyTrax application created a "template.rig" file with x, y, and z coordinates for each marker (A, B, C, and D). The template.rig file was opened in Internet Explorer and saved as templateX.html, with X being the number of the trial (X=1, 2, 3,...13).

Before each of the 12 subsequent trials, Subject 1 would re-position himself by arising from a supine to a sitting position and move about the procedure table for several seconds before returning to the supine position with arms up. This re-positioning was utilized to simulate the fact that every time a patient (same or different) climbs onto the IR table, there will be a different amount of deformable skin motion overlying his abdomen (liver). Each trial was then executed by the method mentioned above. After each trial, the template. rig file was updated by pressing the F5 key and then the file was again saved in the aforementioned manner.

After the above arms-up regimen was completed, Subject 1 then positioned his "arms down," meaning that his arms were at his side and straight, consistent with the position that patients hold on the procedure table during an IR procedure. 13 trials were executed with Subject 1 via the aforementioned re-positioning protocol. These two positions were used to simulate the positional changes that patients undergo from the CT scan (arms up), which produces pre-procedure 3D intra-abdominal images, to the IR procedure table (arms down), where the registration process and ultimately, the procedure occur.

Subject 2 also underwent the arms up and arms down regimens in the same manner as Subject 1 did. A December 19, 2002 experiment (Occasion 3) introduced two new subjects, Subjects 3 (male) and 4 (female), who also underwent the typical re-positioning protocol [14, instead of 13 trials were performed to obtain a preferable even number of trials]. At the times of the experiments, the 6'3" Subject 1 weighed 250 pounds (body mass index [BMI] 31 kg/m^2), the 6'1" Subject 2 weighed 180 pounds (BMI 24 kg/m^2), the 6'2" Subject 3 weighed 230 pounds (BMI 30 kg/m^2), and the 5'5" Subject 4 weighed 135 pounds (BMI 23 kg/m^2). These BMI differences among the subjects introduced the additional variable of body habitus into this study. For the purposes of these experiments, Subjects 1 and 3 were considered to be

the subjects with larger body habitus and Subjects 2 and 4 were considered to be the subjects with thinner body habitus. Photographs of the anatomical set-up of the markers on Subject 2 were taken with a digital camera (See Figure 2 above). After the experiments were completed, all of the 3-D data of were copied to Microsoft Excel.

Measurements were grouped into pairs to calculate deformable skin movement. The first measurement in each pair provided the reference locations for the four markers, and the second measurement was utilized to compare to the reference to calculate skin movement. Each pair was chosen so that the subject repositioned himself between the reference and comparison measurements. Registration was performed between the two sets of readings to align the coordinate systems and account for any absolute movement of the body between measurements, leaving only deformable skin motion to be quantified. The Euclidean distances between corresponding markers were then calculated.

Measurement pairings were first made within arm position. That is, the first 12 of the 13 measurements taken in the arms-up position were paired together, and the first 12 of the 13 measurements taken in the arms-down position were paired together. This provided 12 independent observations for each combination of subject, arm position (up and down), and occasion (96 observations total). Each observation consisted of a set of four distances reflecting skin movement (one for each of the four markers.) Because the four skin movement distances within each observation were very likely to be correlated, the data were analyzed using a repeated measures analysis of variance (ANOVA), with marker location representing four repeated measurements for each independent observation.

Next, the 13 measurements taken in the arms-up position were paired together with the 13 measurements taken in the arms-down position. This provided 13 independent observations for each combination of subject and occasion (arm position was up for reference, down for comparison) for a total of 52 observations. These observations were not independent of the other arm-position observations, being obtained from the same measurements, and thus, they were analyzed separately. Again, a repeated measures ANOVA was used to account for correlation of skin movement distances among the four markers within observations.

3. RESULTS

A repeated measures ANOVA model was first fit to the entire collection of data observations from the first two experiment occasions. The main effect for occasion from this model was statistically significant [$f(1,40)=8.48$, $P=0.01$]. This signifies a difference in mean skin movement between the first two occasions, with lower mean skin movement on Occasion 2. This occasion difference may reflect subject and/or experimenter maturation over time. For example, subjects may have become more consistent in their breath holding and arm raising with practice, experimenters may have learned to place the markers more securely, and/or environmental conditions may have been slightly different between occasions, affecting experimental error (slightly higher humidity could have caused more marker slipping on the skin, slight temperature differences could have affected measurement precision, etc.).

Before using this model as a basis to test the main comparisons, the variability in skin movement measurements between the first two occasions was evaluated by fitting separate ANOVA models for each occasion and then comparing the resulting mean square errors. The second occasion had considerably smaller error variance than the first. Since homogeneity of error variances is needed for a combined analysis of the two occasions, each occasion was evaluated separately.

In the following four tables below, repeated measures ANOVA models were utilized to determine the statistical significance of any differences in mean distances. RMSE, mean distance, standard deviation, and maximum and minimum distances are reported, as well as the number of distances available for each estimate. All measurements are in millimeters (mm).

Table 1 below presents comparisons between arm positions. There was no evidence for arm-position/marker-location or arm-position/subject interaction on either of the first two occasions (i.e., the difference between arm positions was similar for each marker and for each subject). Therefore, the main effect for arm position is presented, combining information across marker location and subject. Unlike Occasions 1 and 2, on Occasion 3, the data exhibited a

statistically significant interaction between subject and arm position – the difference in skin movement between Subjects 3 & 4 depended on arm position, and the difference in skin movement between arm positions depended on subject. Thus, for Occasion 3, the data for both subjects were not combined with each other for statistical analysis purposes (no main effects presented in Table 1).

For the first two occasions, the average skin motion was 1.00 ± 0.82 mm in the arms-up position and 0.94 ± 0.56 mm in the arms-down position. For Occasion 3, thanks to a surprisingly low average amount of skin motion exhibited by Subject #4 in the arms-up position (0.59 ± 0.30 mm), the average skin motion was 0.81 ± 0.48 mm in the arms-up position and 0.94 ± 0.65 mm in the arms-down position. These results suggest that the arms-down position may be associated with smaller skin movements, however, the observed difference in means was not sufficient to claim statistical significance on any occasion.

Table 1 Skin Movement Comparisons between Arm Positions (Up vs. Down)

	Distance RMSE	Mean Distance ± Std. Dev.	Maximum	Minimum	N
Subjects #1 & #2					
06/19/02 Arms up	1.72	1.32 ± 1.11	5.09	0.26	48
06/19/02 Arms down	1.43	1.19 ± 0.80	3.28	0.03	48
Difference		0.13[(1)]			
07/16/02 Arms up	0.85	0.68 ± 0.52	2.27	0.07	40
07/16/02 Arms down	0.74	0.68 ± 0.31	1.41	0.13	44
Difference		0.00[(2)]			
Occasion 3 (12/19/02)					
Subject #3					
Arms up	1.15	1.03 ± 0.52	2.45	0.35	28
Arms down	0.87	0.69 ± 0.54	2.00	1.66	28
Difference		0.34[(3)]			
Subject #4					
Arms up	0.66	0.59 ± 0.30	1.17	0.22	28
Arms down	1.35	1.18 ± 0.66	3.35	0.34	28
Difference		-0.59[(4)]			

Notes: Statistical significance evaluated by repeated measures ANOVA

(1) $F_{1,21}$=0.17, P=0.68

(2) $F_{1,18}$=0.02, P=0.89

(3) $F_{1,12}$=4.45, P=0.06

(4) $F_{1,12}$=3.11, P=0.10

Occasion 3: Test for interaction between arm position and subject: $F_{1,24}$=7.16, P=0.01

Table 2 below reports comparisons between the subjects on the three occasions. For Occasions 1 and 2, since no interaction terms were evident, main effects are reported. In contrast, for Occasion 3, interaction terms were again evident, and hence, main effects are again not reported. For all three occasions, the average skin motion was 0.65 ± 0.39 mm for Subject 1, 1.32 ± 0.78 mm for Subject 2, 0.86 ± 0.55 mm for Subject 3, and 0.89 ± 0.59 mm for Subject 4. The subject with the largest body habitus (Subject 1 - BMI 31 kg/m^2) exhibited significantly less motion than the subject with a thinner body habitus (Subject 2 - BMI 24 kg/m^2). This is consistent for all of the measures (RMSE, mean, max and min) and for both of the first two occasions. Mean distance differences between Subjects 1 and 2 were found to be statistically significant on both Occasions 1 and 2.

Table 2 Skin Movement Comparisons between Subjects (Same Arm Position)

	Distance RMSE	Mean Distance ± Std. Dev.	Maximum	Minimum	N
06/19/02 Subj. #1	0.92	0.77 ± 0.50	2.27	0.03	48
06/19/02 Subj. #2	2.04	1.75 ± 1.07	5.09	0.33	48
Difference		-0.68(1)			
07/16/02 Subj. #1	0.60	0.53 ± 0.27	1.14	0.07	48
07/16/02 Subj. #2	1.00	0.88 ± 0.49	2.27	0.23	36
Difference		-0.35(2)			
Occasion 3 (12/19/02)					
Subject #3					
Arms up	1.15	1.03 + 0.52	2.45	0.35	28
Arms down	0.87	0.69 + 0.54	2.00	1.66	28
Difference		0.34(3)			
Subject #4					
Arms up	0.66	0.59 + 0.30	1.17	0.22	28
Arms down	1.35	1.18 + 0.66	3.35	0.34	28
Difference		-0.59(4)			

Notes: Statistical significance evaluated by repeated measures ANOVA

(1) $F_{1,21}=8.89$, P=0.01

(2) $F_{1,18}=5.18$, P=0.04

(3) $F_{1,12}=1.12$, P=0.23

(4) $F_{1,12}=6.99$, P=0.02

Occasion 3: Test for interaction between arm position and subject: $F_{1,24}=7.16$, P=0.01

Table 3 below reports comparisons among the four marker locations. The markers are listed in order of decreasing mean skin movement for each occasion. The hypothesis of no difference between marker locations was addressed using the repeated measures ANOVA model, and was rejected at the alpha=0.05 level of significance for all three occasions. Comparisons between individual markers were made using Tukey's honestly significant difference procedure for multiple comparisons using alpha=0.05. Superscripts are reported next to each marker to indicate which markers had statistically significant differences in mean skin movement. For example, on Occasion 1 (6/19/02), Marker B was found to have significantly more skin movement than the other three markers; however, there was no evidence for differences among the remaining three. On Occasions 2 and 3 (7/16/02 and 12/19/02), Marker A was found to be associated with a significantly smaller amount of skin movement, with no differences among the remaining three markers.

Table 3 Skin Movement Comparisons between Marker Locations (Same Arm Position)

	Distance RMSE	Mean Distance ± Std. Dev.	Maximum	Minimum	N
06/19/02:(1)					
Marker B(a)	1.85	1.46 ± 1.17	5.09	0.29	24
Marker D(b)	1.48	1.23 ± 0.84	3.61	0.12	24
Marker A(b)	1.51	1.18 ± 0.98	4.02	0.16	24
Marker C(b)	1.45	1.16 ± 0.89	4.23	0.03	24
07/16/02:(2)					
Marker B(a)	0.95	0.83 ± 0.46	2.27	0.13	24
Marker D(a)	0.80	0.68 ± 0.42	2.11	0.22	24
Marker C(a)	0.79	0.66 ± 0.44	1.99	0.07	24
Marker A(b)	0.62	0.55 ± 0.30	1.55	0.14	24
12/19/02:(3)					
Marker B(a)	1.23	1.02 ± 0.70	3.35	0.23	28
Marker C(a)	1.09	0.93 ± 0.58	2.45	0.22	28
Marker D(a)	1.05	0.90 ± 0.56	2.36	0.17	28
Marker A(b)	0.74	0.67 ± 0.34	1.55	0.18	28

Notes: Statistical significance evaluated by repeated measures ANOVA
(1) Main effect for marker location: $F_{3,63}=3.15$, $P=0.03$
(2) Main effect for marker location: $F_{3,54}=7.81$, $P<0.01$
(3) Main effect for marker location: $F_{3,81}=7.81$, $P<0.01$

Marker positions for the same date with the same superscripts are not statistically different when comparing mean distance (using Tukey's Honestly Significant Difference for multiple pair-wise comparisons at alpha=0.05.)

The analysis of the data of the arms-up vs. arms-down pairings paralleled that for the same arm-position pairings. The combined ANOVA model again resulted in a statistically significant occasion effect [$F(1,45)=248.7$, $P<0.01$], with smaller mean skin movement occurring on the second occasion (7/16/02). Individual models for the first two occasions showed significantly smaller error variance on Occasion 2, so data from the first two occasions were analyzed separately. The ANOVA models for each occasion demonstrated significant interaction between subject and marker location, indicating that differences between subjects were not consistent for all marker locations. Similarly, differences among marker locations depended upon the subject. Therefore, no tables for main effects are presented.

Instead, Table 4 below displays marker locations by subject on each of the three occasions, permitting the observed differences among subjects at each marker to be evaluated. Although the magnitudes of differences change, Subject 1 consistently displayed smaller skin movement than Subject 2 at each marker location on each of the first two occasions. The statistical significance of this result was determined using F-tests for the main effect due to subject. On Occasion 1, this statistic was $F(1,24)=447$, $P<0.01$. On Occasion 2, it was $F(1,21)=44.8$, $P<0.01$. One can conclude that generally, Subject 1 is associated with smaller mean skin movement than Subject 2 on both of the first two occasions. However, the magnitude of difference depends upon the specific marker location and occasion, with possibly small (or no) difference for some marker-location/occasion combinations.

Next, the marker locations for each subject were compared. Using Tukey's honestly significant difference procedure, Table 4 includes superscripts next to each marker location that indicate the significant marker-location differences. On Occasion 1 (6/19/02) and for Subject 1, Marker B was observed to have the highest mean skin movement, followed in decreasing order by Markers A, D, and C. The differences between Markers A and D, and D and C were not statistically significant, but the difference between A and C did reach statistical significance. For Subject 2, Marker B was observed to have the highest mean skin movement, followed by Marker D, with no evidence of a difference between Markers C and A. On Occasion 2 (7/16/02), Subject 1 was observed to have large mean skin movement at Markers B and C, while Marker A was associated with the smallest mean skin movement. Subject 2 exhibited large mean skin movement at Markers D and C, and Marker A again displayed the smallest mean skin movement. On Occasion 3 (12/19/02), Subject

3 exhibited the largest mean skin movement at Marker B, while Marker D was associated with the smallest mean skin movement. The results for Subject 4 are more consistent with those seen with Subjects 1 and 2 previously: The largest mean skin movement was seen at Marker B, and Marker A exhibited the least amount of mean skin movement.

Although differences in marker location are not consistent between subjects or occasion, it is observed that Marker A was generally associated with the smallest amount of skin movement, while Marker B was generally associated with the largest amount of skin movement. The skin movements at Markers D and C were similar for the most part.

Table 4 Skin Movement (Arms Up to Arms Down) Comparisons

	Distance RMSE	Mean Distance ± Std. Dev.	Maximum	Minimum	N
06/19/02:					
Subject #1					
Marker A[(b)]	4.97	4.93 ± 0.68	6.01	3.94	13
Marker B[(a)]	6.19	6.14 ± 0.82	7.30	5.02	13
Marker C[(c)]	4.24	4.19 ± 0.68	5.38	3.15	13
Marker D[(b) (c)]	4.67	4.54 ± 1.17	6.38	3.11	13
Subject #2					
Marker A[(c)]	9.72	9.62 ± 1.46	11.78	7.01	13
Marker B[(a)]	21.63	21.55 ± 1.92	24.31	17.68	13
Marker C[(c)]	9.97	9.88 ± 1.34	12.13	7.48	13
Marker D[(b)]	17.47	17.41 ± 1.47	19.79	14.66	13
07/16/02:					
Subject #1					
Marker A[(c)]	3.22	3.18 ± 0.53	4.18	2.59	13
Marker B[(a)]	4.82	4.78 ± 0.67	5.49	3.47	13
Marker C[(a) (b)]	4.41	4.38 ± 0.49	5.13	3.74	13
Marker D[(b)]	4.12	4.08 ± 0.60	4.85	2.96	13
Subject #2					
Marker A[(c)]	3.55	3.36 ± 1.19	6.59	2.10	10
Marker B[(b)]	6.87	6.84 ± 0.74	8.04	5.66	10
Marker C[(a)]	7.78	7.61 ± 1.70	10.52	5.56	10
Marker D[(a) (b)]	7.71	7.49 ± 1.92	10.58	5.30	10
12/19/02:					
Subject #3					
Marker A[(b)]	4.80	4.78 ± 0.51	5.97	4.13	14
Marker B[(c)]	6.11	6.06 ± 0.79	7.88	5.10	14
Marker C[(b)]	4.97	4.91 ± 0.81	6.72	3.66	14
Marker D[(a)]	3.89	3.82 ± 0.73	5.26	2.88	14
Subject #4					
Marker A[(a)]	3.76	3.69 ± 0.74	5.17	2.74	14
Marker B[(b)]	6.25	6.15 ± 1.17	7.83	3.92	14
Marker C[(b)]	5.91	5.89 ± 0.57	6.73	4.78	14
Marker D[(a)]	4.19	4.10 ± 0.93	5.84	2.71	14

Notes: Marker positions for the same date and subject with the same superscripts are not statistically different when comparing mean distance (using Tukey's Honestly Significant Difference for multiple pair wise comparisons at alpha=0.05.)

Five observations were excluded from the primary analysis. They originated from three measurements taken for Subject 2 on Occasion 2: Arms up measurements #1 and #2, and Arms down measurement #10. The observations were extreme

outliers and were thought to have resulted from one or more markers moving on the skin during the experiment. After the initial results were obtained, the analysis was repeated with these observations included. Although the magnitude of estimates changed, no substantive change in comparisons between factors was noted.

Using the MATLAB program, a 3-D graph representing the distribution of a sampling of the raw data was constructed and appears below. The tighter cluster of data at Skin Fiducial A on the xiphoid process demonstrates that this skin fiducial exhibited less skin motion variability compared to the other fiducials.

FIGURE 3

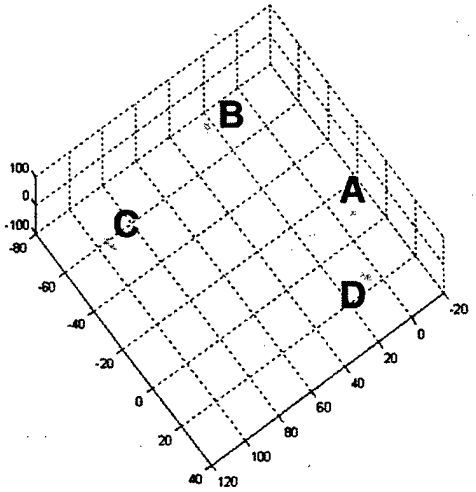

3D GRAPH OF THE DISTRIBUTION OF SKIN MARKER DATA

4. DISCUSSION

Deformable skin motion is a source of registration error in image-guided abdominal interventions. This skin deformation was quantified and analyzed in this study. The overall goal of this research is to enhance the accuracy of registration and thus, the clinical accuracy of minimally invasive intra-abdominal image-guided procedures.

The POLARIS 3-D optical tracker utilized in these experiments is used many commercial systems and has been found to be very reliable and precise[7]. According to Northern Digital, Inc., the RMS accuracy for the POLARIS tracker is 0.35 mm[5].

The smaller error variance on Occasion 2 vs. Occasion 1 can most likely be explained by a combination of both subject and experimenter maturation -- more consistent breath holding, arm raising, and better securing of the markers onto the skin. On Occasion 3, it is unclear why Subject 4 exhibited less skin motion in the arms-up position than in the arms-down position, resulting in a statistically significant interaction between subject and arm position. It is possible that gender (Subject 4) was a contributing factor to this result, although only one female replication does not allow us to draw any firm conclusions on the role of gender. More likely, this result demonstrates simple subject-to-subject variation.

Three out of the four subjects did exhibit increased skin motion in the arms-up position, suggesting that patient-positioning technique during CT imaging may have an effect on the skin motion component of registration error, with the arms up position (CT position) possibly increasing the amount of skin motion. This seems reasonable given that holding one's arms up is an active process, which likely entails increased skin tension and skin motion, whereas holding

one's arms at one's side is more of a passive process, probably involving less skin tension and skin motion. It seems therefore important to consider this when positioning the patient for CT imaging and in the operating environment.

Assuming all other variables to be equal, body habitus (the amount of skin) appeared to influence the degree of skin marker motion. It was expected that the subjects who weighed relatively more and thus had more skin would have greater skin motion than the subjects weighing relatively less, but counter intuitively, the opposite result occurred. The subject with the largest body habitus (Subject 2) demonstrated significantly less skin motion than the subject with a thinner body habitus (Subject 1). Variabilities in end-expiratory breath holding and arm raising by the subjects may account for this result. It is possible that Subject 2 had greater variability in end-expiratory breath holding than Subject 1, which might then explain the greater variability in skin motion. It is also possible that Subject 2 used a greater amount of skin tension in the arms up position than Subject 1 did, causing Subject 2 to exhibit more skin motion. Potentially, because of a comparatively increased "skin sag" (skin overlying abdomen was not as taut), Subject 1 may have exhibited less skin motion. Or some other factor differentiating Subjects 1 and 2 may have caused this outcome. Clearly, this result is difficult to explain in this limited study.

In general, the skin fiducial on the xiphoid process exhibited the least amount of skin motion, suggesting that this anatomical landmark is the most rigid of the four landmarks investigated. In contrast, the skin fiducial on the medial aspect of the 5th rib displayed the highest amount of skin motion, suggesting that this landmark is the least rigid of the four studied. The selection of specific anatomic locations for fiducial placement could influence motion of the fiducial and subsequently, the introduced error. It is well-established in the literature that using rigid bony points on the skin for fiducial placement reduces the amount of skin motion error in registration as compared with less rigid soft tissue points[8]. However, to our knowledge, this is the first study that quantifies the skin motion variability over specific bony landmarks that overlie the liver. Fiducial attachment to bony landmarks such as the xiphoid process and other rigid sites over the liver could reduce the amount of skin motion error and therefore, registration error in image-guided abdominal procedures.

In their TIPS study of anesthetized swine, Solomon's group reported a total registration error of 3 mm, an unspecified amount of which is skin motion error. Solomon's group glued and sewed into place 10-20 metallic markers on the abdomen and used most, but not all, of the markers for registration in their TIPS study. The exact locations of the skin fiducials on the abdomen were not specified. In contrast, our group used only four infrared markers and used all four markers for registration. Our subjects were not anesthetized and the skin fiducials were secured with tape, not glued or sewn into place, all of which likely caused our skin motion errors to be even higher than those in Solomon's experiments in swine[3]. Even so, our relatively small skin motion errors in the range of 1-2 mm may be acceptable for clinical practice, and they undoubtedly can be improved upon with additional anatomical studies. Given our results, we conclude that skin motion error is a significant source of registration error that may or may not be clinically important.

This initial skin motion study is limited by the small sample size (n = 4), the small number of experiments (3), the difference in error variance between the first two occasions, and the statistically significant interaction terms on Occasion 3. The observed differences in body position, body habitus, and skin marker location could be the result of simple subject-to-subject variation. In future experiments, a greater number of human subjects should be utilized. Also, a greater number of fiducials should be placed at an increased number of different bony anatomical points on the skin over the liver. This would permit further delineation of the optimal rigid anatomic locations, likely leading to reduced registration error and potentially, greater clinical accuracy in image-guided abdominal procedures. Additionally, more extensive skin motion studies, taking into account tidal volumes, anterior-posterior distances of the chest, and angular arm positions should be undertaken to investigate the potential clinical importance of these factors in image-guided abdominal interventions.

5. ACKNOWLEDGEMENTS

This work was funded by U.S. Army grant DAMD17-99-1-9022. The content of this manuscript does not necessarily reflect the position or policy of the U.S. Government. The authors very much appreciate the comprehensive statistical analysis done by Byron K. McKinney (Beta Statistics, San Diego, CA).

6. REFERENCES

1. MH Howard, RN Nelson, EK Paulson, MA Kliewer, DH Sheafor. "An Electronic Device for Needle Placement during Sonographically Guided Percutaneous Intervention." Radiology, **218**(3):905-11, 2001.
2. SB Solomon, C. Magee, DE Acker, AC Venbrux. "TIPS Placement in Swine, Guided by Electromagnetic Real-Time Needle Tip Localization Displayed on Previously Acquired 3-D CT." Cardiovasc Intervent Radiol, **22**:411-14, 1999.
3. F. Banovac, N. Glossop, D. Lindisch, D. Tanaka, E. Levy, K. Cleary. "Liver Tumor Biopsy in a Respiring Phantom with the Assistance of a Novel Electromagnetic Navigation Device." In: Medical Image Computing and Computer-Assisted Intervention (MICCAI). Tokyo, Japan. pp. 200-207, 2002.
4. K. Cleary, F. Banovac, E. Levy, D. Tanaka. "Development of a Liver Respiratory Motion Simulator to Investigate Magnetic Tracking for Abdominal Interventions." *Proc. SPIE*, SK Mun, Ed., 4681:25-29, Medical Imaging, San Diego, CA, 2002.
5. POLARIS Optical Tracking System. Application Programmer's Interface Guide. Northern Digital Inc., Ontario, Canada. 1998.
6. FH Netter. *Atlas of Human Anatomy*. 2nd ed. Plate 269a – Topography of Liver, 1999. Icon Learning Systems, LLC. A Subsidiary of MediMedia, USA, Inc.
7. R. Khadem, CC Yeh, M Sadeghi-Tehrani, MR Bax, JA Johnson, JN Welch, EP Wilkinson, R. Shahidi. "Comparative Tracking Error Analysis of Five Different Optical Tracking Systems." Comput Aided Surg, **5**(2):98-107, 2000.
8. CR Maurer Jr., T. Rohlfing, D. Dean, JB West, D. Rueckert, K. Mori, R. Shahidi, DP Martin, MP Heilbrun, RJ Maciunas. "Sources of Error in Image Registration for Cranial Image-Guided Surgery." In: *Advanced Techniques in Image-Guided Brain and Spine Surgery*, IM Germano, Ed., p. 10-36, Thieme, New York, 2002.

10.2.3 Cleary 2003a: Volumetric Treatment Planning

Reprint begins on the next page and is 7 pages.

To be presented at SPIE Medical Imaging 2003 and published in the proceedings

Volumetric treatment planning and image guidance for radiofrequency ablation of hepatic tumors

Kevin Cleary*[a], Daigo Tanaka[b], David Stewart[c], Brad Wood[d], Mihai Mocanu[e], Elliot Levy[c], Filip Banovac[c], David Lindisch[a], Stephen Roderick[a], John Tang[a], Ho Young Chung[f]

[a]Imaging Science and Information Systems (ISIS) Center, Department of Radiology, Georgetown University, Washington, DC, USA
[b]Carnegie Mellon University, Biomedical Engineering Department, Pittsburgh, PA, USA
[c]Georgetown University Hospital/MedStar Health, Washington, DC, USA
[d]Clinical Center, National Institutes of Health, Bethesda, Maryland, USA
[e]Department of Software Engineering, University of Craiova, Romania
[f]School of Medicine, Kyungpook National University, Taegu, Korea

ABSTRACT

This paper describes a computer program for volumetric treatment planning and image guidance during radiofrequency (RF) ablation of hepatic tumors. The procedure is performed by inserting an RF probe into the tumor under image guidance and generating heat to "cook" a spherical region. If the tumor is too large to be ablated in a single burn, then multiple overlapping spherical burns are needed to encompass the entire target area. The computer program is designed to assist the physician in planning the sphere placement, as well as provide guidance in placing the probe using a magnetic tracking device. A pre-operative CT scan is routinely obtained before the procedure. On a slice by slice basis, the tumor, along with a 1 cm margin, is traced by the physician using the computer mouse. Once all of the images are traced, the program provides a three-dimensional rendering of the tumor. The minimum number of spheres necessary to cover the target lesion and the 1 cm margin are then computed by the program and displayed on the screen.

Keywords: radiofrequency ablation, volumetric treatment planning, sphere packing, tumors

1. INTRODUCTION

Primary and secondary malignant hepatic tumors are among the most common tumors worldwide. Although radiofrequency ablation is becoming an alternative to surgical resection for unresectable hepatocellular carcinoma and liver metastases, the procedure has several technical limitations. These limitations are mostly related to the difficulty o precisely placing the RF probe to ablate the entire tumor and achieve adequate margins. To assist the interventional radiologist in treatment planning as well as provide image guidance during the procedure, we have developed a computer program and graphical user interface as described in this paper.

The increasing computer power and graphics capabilities available on desktop PCs now makes it possible to handle large medical image data sets with inexpensive computers. There has also been a growing interest in the mathematical modeling and pre-operative planning of minimally invasive procedures so that more predictable and consistent results might be obtained. While the treatment planning system described here is in its early stages of development, such systems may become common for radiofrequency ablation and other procedures. This will require a close partnership between physicians, engineers, and scientists to produce robust systems that are usable in the clinical environment.

The paper is organized as follows. In Section 2, both clinical and technical background relevant to our work are presented. The section begins with a description of the radiofrequency ablation procedure and a discussion of some of the relevant technical limitations. We then describe the software development process we have adopted in an attempt to

*cleary@georgetown.edu; phone (202) 687-8253, fax (202) 784-3479, www.visualization.georgetown.edu, Imaging Science and Information Systems (ISIS) Center, Department of Radiology, 2115 Wisconsin Avenue, Suite 603, Washington, DC, 20007.

develop robust and reusable code. Next, the user requirements and the software design for our prototype computer program is given, along with the details of how the spheres are placed. In Section 3, the user interface developed is shown. Conclusions are presented in Section 4.

2. METHODS

2.1 Radiofrequency Ablation

Radiofrequency ablation (RFA) is a minimally invasive procedure that is performed by placing a thin needle (approximately 17 or 18 gauge) in the tumor under imaging guidance (CT, ultrasound, or MRI). The needle has an uninsulated tip (electrode) which generates heat up to 100 degrees Celsius. After 10 to 30 minutes of continuous contact with the tumor tissue, the RF energy "cooks" a 3 to 7 cm sphere. Larger tumors can be treated by ablating overlapping spheres. The dead cells are not actually removed, but the tissue undergoes scar formation and eventually involutes. Typically, the procedure is done on an outpatient basis under light sedation. The patient can usually be discharged on the same day with adequate pain control.

Pre-treatment and post-treatment CT scans of a typical case are shown in Figure 1 and Figure 2. This 3 cm hepatocellular carcinoma is a recurrence of disease of a previously resected primary liver tumor. Repeat surgery was avoided by treating this tumor with percutaneous RFA. A needle was inserted through the skin and the tumor was ablated. Note that there is a clean margin of dark and devascularized, dead tissue including the tumor itself and a surrounding 1 cm margin of normal tissue.

Figure 1: Before treatment – note the low attenuation liver mass in the posterior segment of the right hepatic lobe abutting the liver capsule

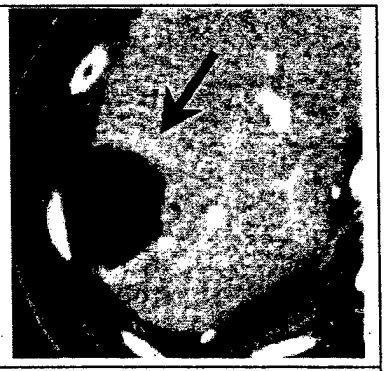

Figure 2: After treatment– note a clean margin of dark, devascularized, ablated tissue including the original tumor and the surrounding tissue

Although RF ablation has become a widely used modality in the primary treatment of HCC and liver metastases, the procedure has several technical limitations. These limitations are mostly related to the difficulty of precisely placing the probe to ablate the entire tumor and achieve adequate margins. The recurrence of disease has been shown to be associated with tumor size and thus the total volume of tumor ablated, with the largest tumors having the highest recurrence rates [1]. Inadequate volumetric coverage of tumors during a single needle insertion can require several probe repositionings during the procedure [1, 2]; this is essential to obtain adequate treatment margins but can be technically difficult.

Positioning the probe within the tumor to achieve overlapping spheres of treatment is difficult because geometric overlap of treatment spheres is hard to precisely accomplish. Using an early version of RF technology (a single electrode rather than the multi-pronged devices now available), Dodd et al. indicated that on the basis of a 3 cm thermal injury, tumors 2-3 cm in diameter are treated by six overlapping ablations (Figure 3) and tumors larger than 3 cm can require up to 14 overlapping ablations to treat the tumor volume with adequate margins [3]. The resultant area of combined spherical treatments does not correspond to the larger, usually spherical tumor.

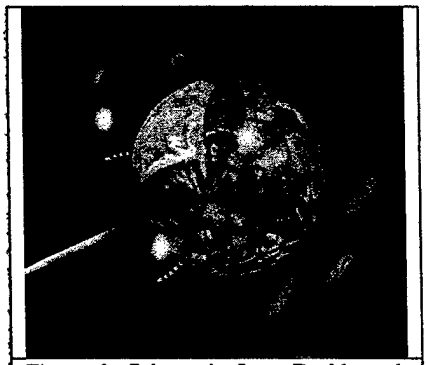

Figure 3: Schematic from Dodd et al. [3] shows how tumors 2-3 cm in diameter are treated by six overlapping ablations

While ultrasound is the primary modality for probe placement and treatment planning, the modality has some technical limitations. The hyperechogenicity of the ablated tissue that occurs during treatment can obscure the visualization of the deeper parts of the lesion and make ultrasound guided repositioning

technically difficult using manual methods [4]. An intense hyperechoic sonographic pattern caused by gas bubble formation can require 5-10 minutes after each ablation to decrease enough to visualize the needle repositioning.

In fact, all accepted modalities for RF probe guidance and monitoring are presently two dimensional (2D), while three dimensional (3D) visualization would be preferable to more precisely define the entire volume of tumor to be treated. Therefore, the goal of this work was to provide a 3D visualization and placement system that could assist the interventionalist in precisely carrying out these procedures.

2.2 Software Process for Robust Development

Over the past several years, our research group at Georgetown has developed software for a number of prototype systems in the computer assisted interventions field. Like many similar research groups, we have struggled with how to develop code that is reliable and sustainable. Typically, as new students and researchers come and go, it is difficult to build on previous software in developing new systems and enhancing existing systems. For these reasons, we have recently placed a high priority on the development of quality and robust software.

One of the fundamental assumptions we have made is that our software development process will have a lifecycle consisting of many iterations. This assumption has much in common with the current practices of agile software development [5] and extreme programming [6]. We envision an iterative or spiral development process where the cycle of requirements, design, implementation, and testing is repeated several times. The characteristics we are striving for include:

1) robustness: the underlying design should be solid and reliable
2) understandable: documentation should be built into the code
3) maintainable: the software should be modular and capable of being changed
4) reusable: common functionality should be identified

A model of our development process, based on use cases, is shown in Figure 4. The model starts with user stories, which are documented as use cases. The stories are then prioritized, with the goal of identifying essential functionality that can be eliminated in the near term first. The developer should then first create unit tests, then implement the software for the selected user scenario. One key to keeping the code maintainable is knowing when to refactor, i.e., knowing when the code base is starting to get ugly and taking the time to reorganize it. Reviews can be useful here, but experienced programming staff will also be required to correctly implement this process.

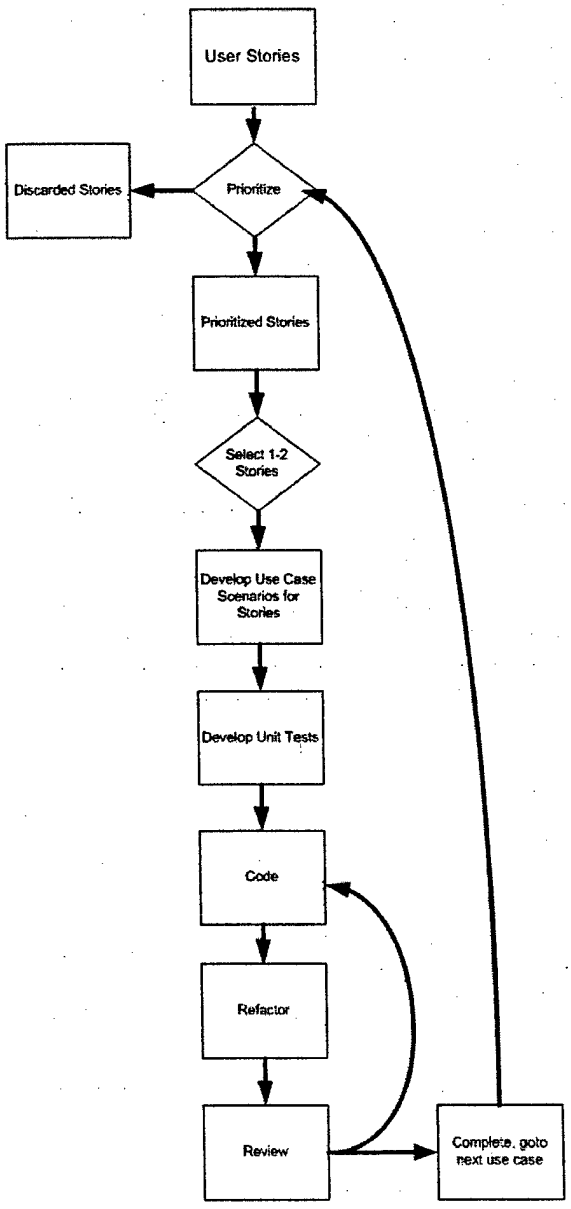

Figure 4: Georgetown software development process

2.3 User Requirements

Following the above model, a conscientious effort was made to elaborate the user requirements from our clinical partners during the early phases of this project. The RFA procedure was broken down into the following steps:

- CT or MRI scans are obtained

- The tumor region is segmented by the radiologist
- Overlapping spheres are placed to cover the tumor
- 3D visualization is provided and the radiologist re-arranges the spheres as desired
- Path planning for probe placement is the next step, followed by intraoperative navigation and image guidance

A strawman GUI was sketched and presented to the clinicians for feedback as shown in Figure 5. Based on this information, a project scheduled was developed which consisted of a short research phase to investigate the literature for possible sphere packing approaches, a development phase, a revision phase, and a documentation phase.

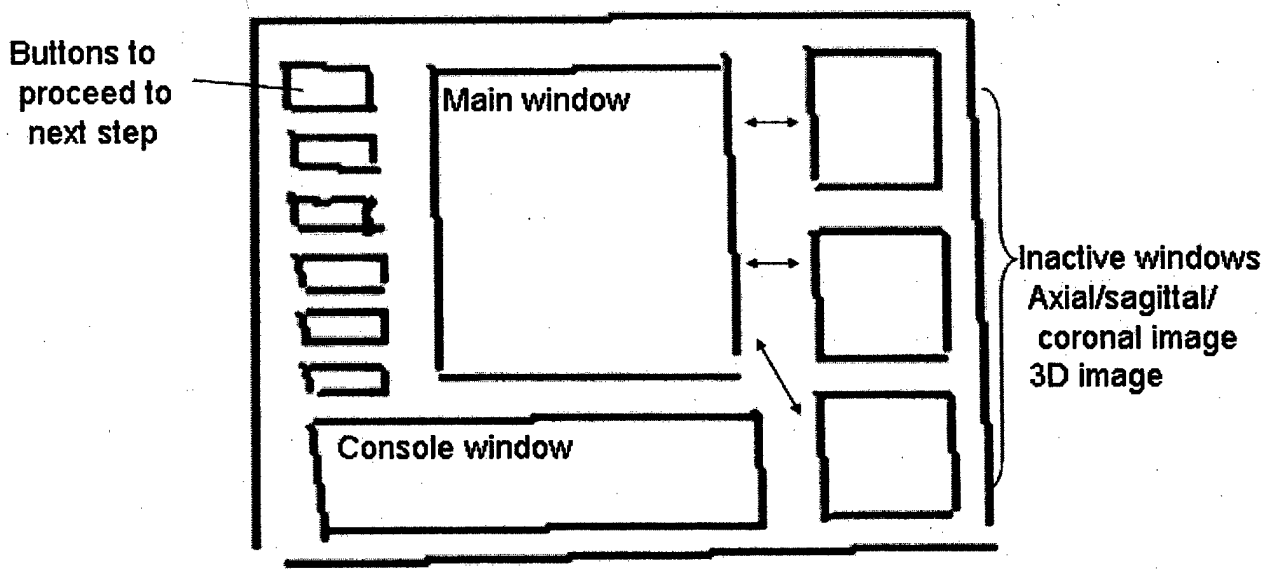

Figure 5: Sample GUI presented to clinicians during software design process.

2.4 Software Design

Once the user requirements were identified, the software design process was begun. One of the major goals of the software design was to re-use some existing software that had already been developed in our laboratory. Issues involved in re-using the existing software included:

- Each class must be designed to have the minimum variables and functions needed to accomplish its purpose. Additional objects should be implemented in a derived class in order for more specific functionality.
- Input/output parameters and other resources that the class requires should be clearly documented so that the class can be easily removed from an existing application and put in a tool kit.
- Coding standards should be followed so that multiple developers can work more efficiently.

The software design was documented using the Unified Model Language (UML) diagram as shown in Figure 6. The software is dependent on the Visualization Took Kit 4.0 (VTK) for the scene graph control [7]. It is also dependent on the Fast Light Tool Kit 1.10 (FLTK) for the graphical user interface control. The design uses several classes derived from the 3D Slicer for voxel data processing and displaying. The 3D Slicer is an open-source software package for visualization, registration, and quantification of medical data [8]. Development of the 3D Slicer is an ongoing collaboration between the MIT Artificial Intelligence Lab and the Surgical Planning Lab at Brigham & Women's Hospital, with sustained contribution from the CISST Center at Johns Hopkins. Among the classes developed by Georgetown are classes for the sensor device driver and a basic DICOM image reader. The classes for application control and image display are re-used from previous software development projects. The existing code is shown in the grey region in Figure 6.

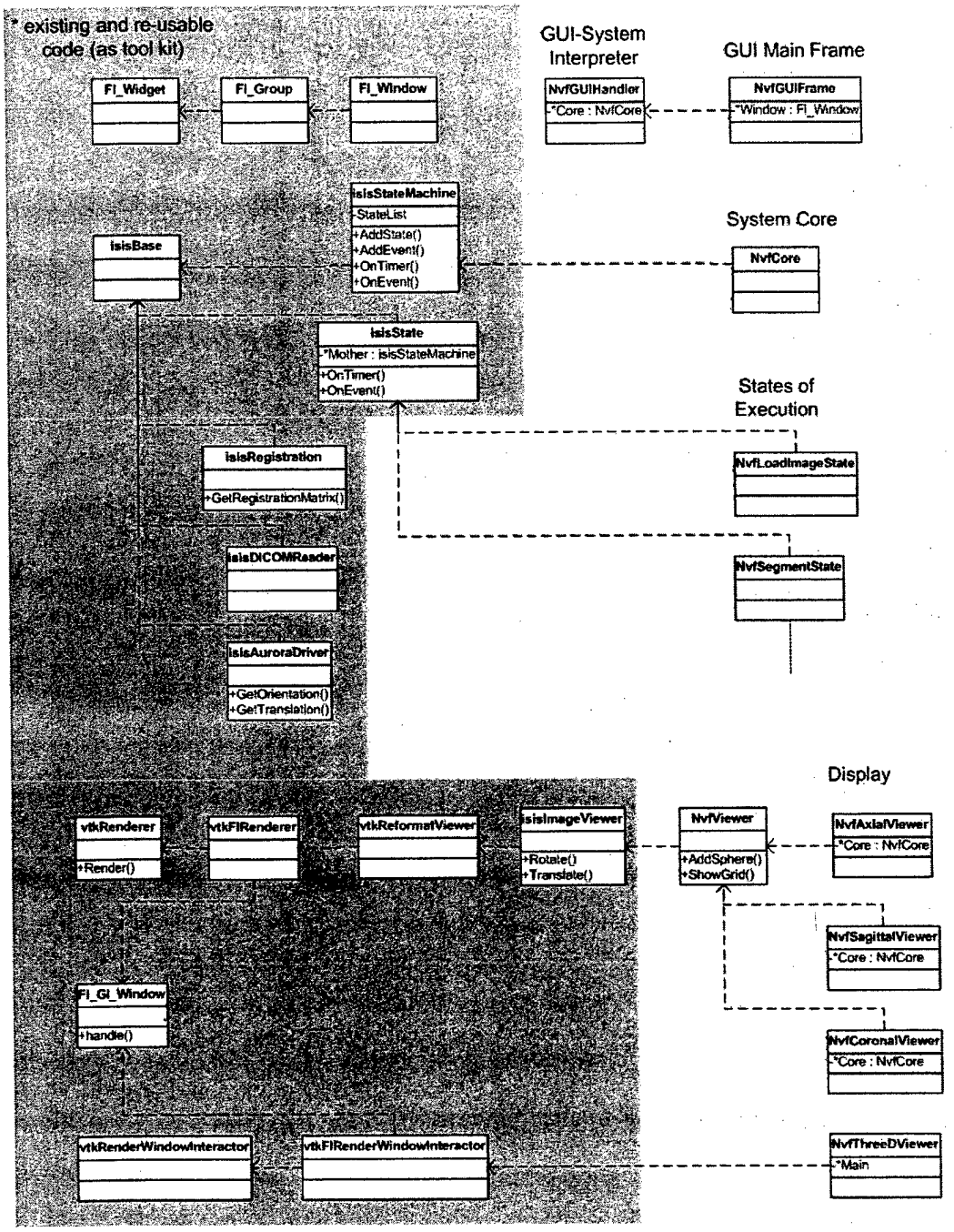

Figure 6: Software Design

2.4 Sphere Placement

The planning process for radiofrequency ablation includes specifying the tumor region plus a 1cm margin and placing the overlapped spheres. First, the DICOM images are loaded and displayed. Users can change the window and level of the image to enhance the tumor region. The region of the tumor is then manually contoured by the user with the mouse. The system generates a 3D surface model from the manually defined region to show a 3D model of the segemented tumor. The radius of the sphere of RFA can be specified by the user and then the system automatically places the

minimum number of the spheres to cover the tumor region. The spheres placed are graphically shown on the axial, sagittal and coronal images as well as on the 3D display. The location and the diameter of the sphere can then be manually adjusted by the user. After the sphere placement, the entry point of the RFA electrode is set by the user by clicking a point in the image. The paths to each sphere are shown with green lines. The system automatically re-slices the axial image to show the path if the entry point is not on the same slice as the center of the sphere.

3. RESULTS

The resulting GUI from the software development process is shown in Figure 7. The steps in the planning and treatment process are indicated by the pushbuttons on the left hand side of the screen. The center window shows the main view and currently shows axial CT slices of the liver. The tumor is difficult to see in this figure but the overlapping spheres can be seen in the center of the axial image and in the image in the lower right.

To date, the GUI has been qualitatively evaluated by two interventional radiologists and the general design has been found to be satisfactory. The pushbuttons are the left hand side of the screen were found to be useful in leading the radiologists through the envisioned workflow during the planning process. Several enhancements have been suggested and these will be implemented in future work.

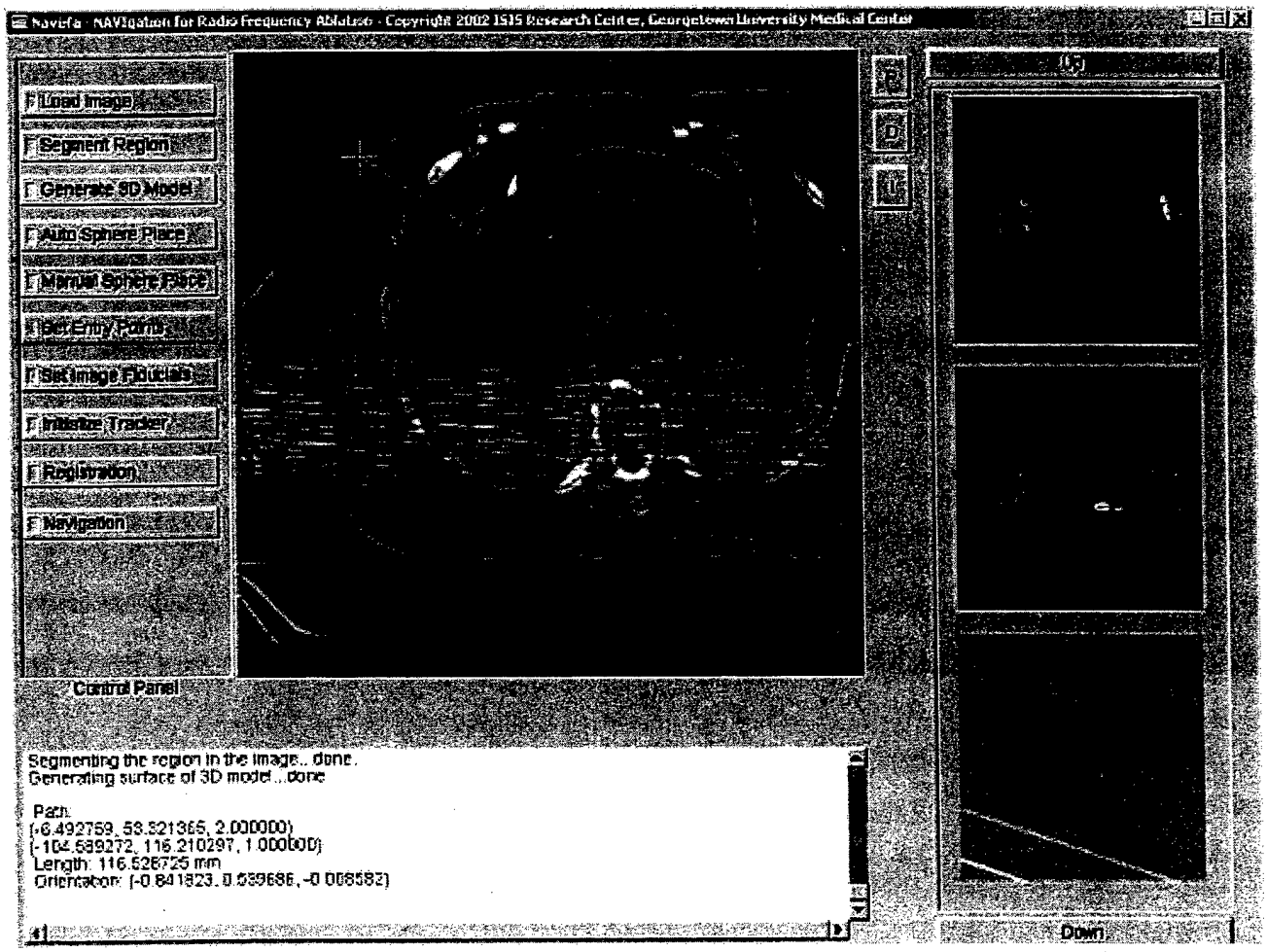

Figure 7: User Interface Showing Overlapping Spheres for Treatment Planning

4. CONCLUSIONS

This paper presented our work to date in developing a volumetric treatment planning and image guidance system for radiofrequency ablation of liver tumors. We believe that this type of system has broad applicability to other diseases and treatment methods and will become more common in the future to increase the precision and repeatability of interventional procedures. In the next phase of this project, we plan to add a electromagnetic tracking component to provide the physician assistance in carrying out the planned paths. This component would integrate our work with the AURORA™ from Northern Digital with the graphical user interface shown above. We are also working under an NLM/NIH contract on a related project to apply the Insight Registration and Segmentation Toolkit (ITK) to the segmentation of these liver tumors.

ACKNOWLEDGMENTS

This work was funded by U.S. Army grant DAMD17-99-1-9022. The content of this manuscript does not necessarily reflect the position or policy of the U.S. Government. The authors would like to thank Kevin Gary, PhD, for useful discussions on the software development process and for contributing Figure 4.

REFERENCES

[1] T. de Baere, D. Elias, C. Dromain, M. G. Din, V. Kuoch, M. Ducreux, V. Boige, N. Lassau, V. Marteau, P. Lasser, and A. Roche, "Radiofrequency ablation of 100 hepatic metastases with a mean follow-up of more than 1 year," *AJR Am J Roentgenol*, vol. 175, pp. 1619-2., 2000.

[2] H. Rhim and G. D. Dodd, 3rd, "Radiofrequency thermal ablation of liver tumors," *J Clin Ultrasound*, vol. 27, pp. 221-9, 1999.

[3] G. D. Dodd, 3rd, M. C. Soulen, R. A. Kane, T. Livraghi, W. R. Lees, Y. Yamashita, A. R. Gillams, O. I. Karahan, and H. Rhim, "Minimally invasive treatment of malignant hepatic tumors: at the threshold of a major breakthrough," *Radiographics*, vol. 20, pp. 9-27, 2000.

[4] T. Livraghi, S. N. Goldberg, S. Lazzaroni, F. Meloni, T. Ierace, L. Solbiati, and G. S. Gazelle, "Hepatocellular carcinoma: radio-frequency ablation of medium and large lesions," *Radiology*, vol. 214, pp. 761-8, 2000.

[5] A. Cockburn, *Agile Software Development*: Pearson Education, 2001.

[6] K. Beck, *Extreme Programming Explained: Embrace Change*: Pearson Education, 1999.

[7] W. Schroeder and B. Lorenson, *Visualization Toolkit*: Prentice Hall, 1996.

[8] D. T. Gering, A. Nabavi, R. Kikinis, N. Hata, L. J. O'Donnell, W. E. Grimson, F. A. Jolesz, P. M. Black, and W. M. Wells, 3rd, "An integrated visualization system for surgical planning and guidance using image fusion and an open MR," *J Magn Reson Imaging*, vol. 13, pp. 967-75, 2001.

10.2.4 Cleary 2002a: Software Architecture

Reprint begins on the next page and is 6 pages.

CARS 2002 – H.U. Lemke, M.W. Vannier; K. Inamura, A.G. Farman, K. Doi & J.H.C. Reiber (Editors)

Software Architecture for Robotically Assisted and Image-Guided Minimally Invasive Interventions

Kevin Cleary[a], Alexandru Patriciu[b,c], Sheng Xu[c],
Mihai Mocanu[a,d], Dan Stoianovici[b,c]

[a]Imaging Science and Information Systems (ISIS) Center, Radiology Department, 2115 Wisconsin Avenue, Suite 603, Georgetown University Medical Center, Washington, DC, USA

[b]URobotics Laboratory, Urology Department, Johns Hopkins Medical Institutions, Baltimore, MD, USA

[c]NSF-funded Center for Computer Integrated Surgical Systems andTechnologies, Johns Hopkins University, Baltimore, MD, USA

[d]Department of Software Engineering, University of Craiova, Romania

Abstract

Although more sophisticated software and hardware components are becoming available, technology for the operating room and interventional suite can be slow to change. The integration of vendor specific software and hardware components remains difficult, and the resulting systems are limited in reuse, flexibility, interoperability, and maintainability. One potential solution to this problem is to develop open software architectures as a platform for rapidly integrating new technologies into the operating room. In an ongoing effort to develop modular software architectures for systems designed to assist in minimally invasive interventions, two systems are outlined here: a "needle driver" robot and an image-guided surgery system based of magnetic tracking of internal organ motion. To date, the robot system has been used to complete a cadaver study of nerve and facet block placement under joystick control of the interventionalist. The image-guided surgery system has been used in phantom studies of liver needle placement. Potential future developments include fluoroscopy servoing in which the robot will automatically align the needle along the C-arm trajectory and the integration of the robot and tracking systems.

Keywords: Medical Robotics, Image-Guided Surgery, Minimally Invasive Interventions

1. Introduction

Minimally invasive procedures are rapidly growing in popularity, due to the substantially reduced trauma for the patient. As part of these procedures, there are many clinical situations where precise manipulation of instruments is important. Novel integrated systems incorporating tracking, visualization, and robotics, may enable the physician to more accurately target hard-to-reach anatomy as well as target the anatomy directly from the images themselves.

Image guidance has been used in one form or another in various medical procedures since the first applications of ionizing radiation. However, during the last decade there has been a continuous and marked increase in interest in this field, which can be largely attributed to developments in imaging algorithms and increased computer power [1]. Percutaneous needle and instrument placement has also become an essential part of diagnostic and therapeutic

modalities. However, software architectures for the integration of imaging, localization, and robotic instrumentation have not been investigated except in a very few research centers. For example, current surgical navigation systems usually employ proprietary software interfaces with fixed instrument types.

The goal of software architectures for these systems is to facilitate the development of applications for the interventional environment. The long-term goal of the research program at Georgetown is to develop an integrated system to enable the next generation of minimally invasive interventions. Within this project, a flexible, component-based software framework plays a central role. Since its development is a cooperation between medical imaging and robotics experts at Georgetown and Johns Hopkins Medical Centers, a systematic process for software development is needed. This includes software development based on formal specifications, advanced methods for software design (UML), source code control (SourceSafe), rapid application development in high-level object-oriented languages (C++), and use of documentation tools (Doxygen).

A related effort is the 3D Slicer for surgical planning and intraoperative visualization [4]. The 3D Slicer is freely available, open-source software for visualization, registration, segmentation, and quantification of medical data. The Slicer is an ongoing collaboration between the MIT Artificial Intelligence Lab and the Surgical Planning Lab at Brigham & Women's Hospital, an affiliate of Harvard Medical School. The Center for Computer Integrated Surgical Systems and Technologies at Johns Hopkins University has also been working to extend Slicer to include robot control, among other functionality.

2. Specifications and Methods

Large software applications are typically built in layers. At the lowest level, our architecture includes proprietary, vendor-specific software levels for individual hardware components such as a motion control card and watchdog timer. On top of this level, we build a higher level application programming interface (API). At the highest level is the user interface. Our application is built on C and C++ based libraries including the Motion Engineering Incorporated (MEI) DSP-Series Motion Control Library, the Matrox Imaging Library (MIL), and the Visualization ToolKit (VTK) from Kitware [2].

2.1. Robot Control Library

An object-oriented software library for robot control, denoted URoboticsLib, has been designed and implemented by the URobotics Laboratory at Johns Hopkins. This library was built on the MEI Motion Control Library and is meant for high-level control of a new generation of robots such as the one in Figure 1. The library was defined and tested as a API using object oriented methodologies including the uniform modelling language (UML) tool Visual Modeller for design and Visual C++ for coding. When developing this library, attention was paid to portability (the core part of the library does not use Microsoft Foundation Classes (MFC)), flexibility and ease of use (all functions are based on engineering units such as millimeters), ease of progress towards a wide range of applications, an efficient and simple user interface, and support for calibration and use in clinical studies.

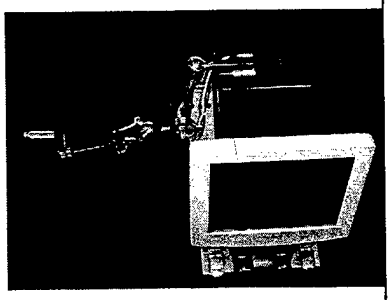

Figure 1. "Needle Driver" Robot

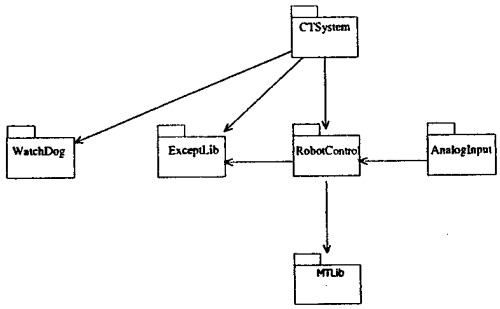

Figure 2. URoboticsLib Overall Architecture

The overall architecture of the URoboticsLib library is shown in Figure 2. Packages include classes for basic robot control, safety features (WatchDog), real-time control (CMEICard), support classes for error reporting and handling (ExceptLib) or for multithreading and access synchronization (MTLib). The overriding goals were that

1) the library must not be tied to a specific motion card; and
2) the library has to be easy to reconfigure and extend.

There were several other key requirements including platform independence, parallel execution speed achieved by multithreading, real-time monitoring accomplished through the use of specialized hardware, and the ability to specify a user-defined control loop.

A generic interface to a motion control card was developed as shown in Figure 3. This included generic "disconnected" interfaces such as CMotionControlCard, CAnalogInputCard, and CDigitalIOCard. While the Motion Engineering Inc. card was used in our application, the library is designed so that another card may be easily substitute

2.2. Imaging Libraries

The fact that C code can be combined seamlessly with new C++ code has been a major advantage. Migration from C to C++ has not required us to discard or rewrite functional C code. Many commercial frameworks, and even some components of the Standard Library itself, are built upon legacy C code that is wrapped in an object-oriented interface. We have chosen a similar approach, using both C and C++ libraries in object-oriented imaging applications [3].

The device-independent Matrox Imaging Library (MIL) is a high-level C library with an extensive set of optimized functions for image processing (point-to-point, statistics, filtering, morphology, geometric transforms), pattern matching, blob analysis, gauging, OCR, bar and matrix code recognition, and calibration. We are using MIL to accelerate the development of medical imaging and image analysis applications, such as fluoroscopy servoing for robot control.

The Visualization ToolKit (VTK) is an open source, freely available software system used as a graphics engine for image processing and visualization. VTK consists of a C++ class library, and several interpreted interface layers such as Tcl/Tk. VTK supports a wide variety of visualization algorithms including scalar, vector, tensor, texture, and

volumetric methods. Advanced modelling techniques such as implicit modelling, polygon reduction, mesh smoothing, cutting and contouring are also included.

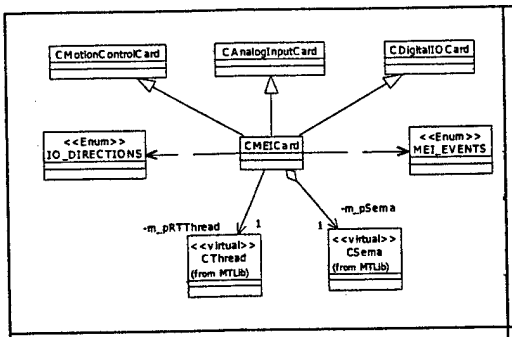

Figure 3. Robot Motion Control

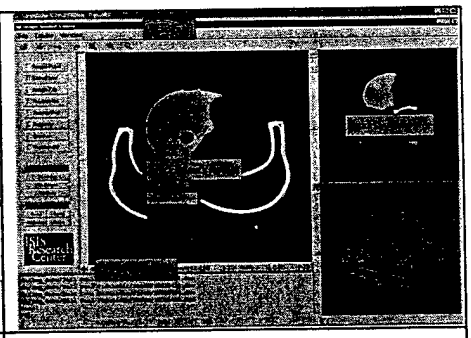

Figure 4. User Interface for IGBiopsy

3. Image-Guided System Architecture

IGBiopsy is a system developed at Georgetown incorporating magnetic tracking for image guidance during minimally invasive abdominal interventions. An image-guided surgery system typically provides a method for registration of pre-operative images to the physical space of the patient, a user interface that display images and the position of instruments, and a computer workstation that runs the application. Unlike image-guided surgical systems based on bony landmarks, the IGBiopsy system is designed to be applied to internal organs such as the liver that move with respiration. This means that some method of tracking and/or modelling respiratory motion is required, as well as a means for targeting the anatomy as it moves during respiration. The IGBiopsy system incorporates a magnetically tracked catheter that is part of the AURORA™ magnetic tracking system from Northern Digital, Inc. Preliminary results to date using a specially designed liver respiratory motion simulator show that this approach may be feasible for future image-guided liver interventions. In the long term, interfacing this tracking system with the robot software described previously could provide a system capable of compensating for respiratory motion and precisely placing a needle in a breathing subject.

The IGBiopsy user interface is shown in Figure 4 which also has labels indicating the major classes. The magnetically tracked catheter indicates the current position of the liver and can also provide the physician with a visual cue to indicate the right time for placing the needle. In the most recent version of the software, a targeting window was added to help the user align the needle based on the skin entry point and angle of approach. A depth control indicator was also added. This grouping of targeting window and depth indicator should help even an inexperienced physician to precisely drive the needle to the target.

Key software issues addressed in the design of the IGBiopsy system included portability, platform independence, and parallel execution speed achieved by pipelining. The class levels used in the development are shown in Figure 5.

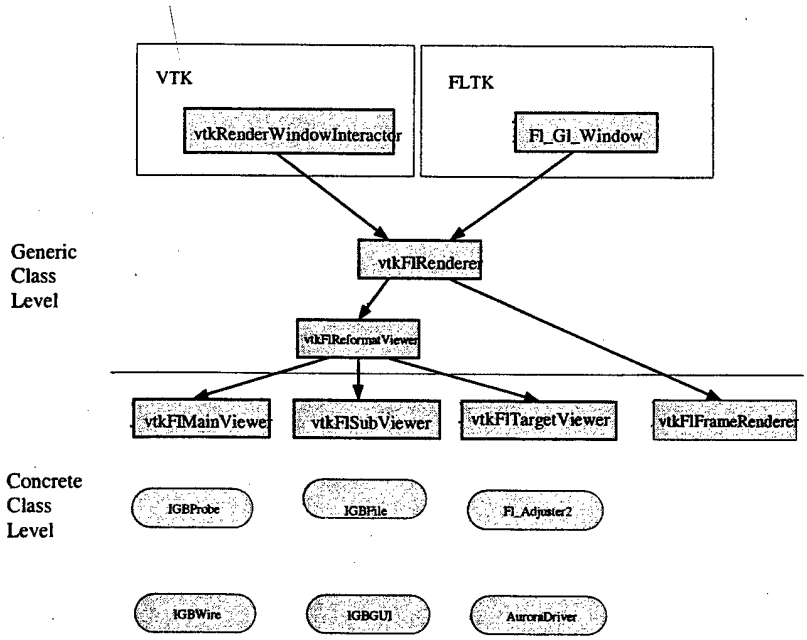

Figure 5. Hierarchy Chart for the Image-Guided Surgery System

The object-oriented design for the system is based on a formal and iterative process of decomposing requirements by objects rather than by functions through multiple design cycles. The generic steps performed are:

- Identification of main objects that describe entities and processes in the environment.
- Definition of views that will be used to present those objects to users.
- Determination of interactions between entity and process objects required to accomplish specific tasks.

This design process was applied from the initial development of the system. This led to a design decision to base the system on software libraries currently in widespread use: OpenGL, Visualization Toolkit (VTK), Fast Light Tool Kit (FLTK), in which:

- Upper entries form the VTK-FLTK (-OpenGL) "basement" of the system, i.e. vtkFlRenderWindowInteractor class used to attach and enable VTK to render to and interact with a FLTK window, or Fl_Gl_Window – the FLTK (-OpenGL) window group class.
- Intermediate entries indicate generic elements supported in an abstract manner in the system, i.e. vtkFlRenderer.
- Lower entries contain concrete elements, their role may be seen in "transforming" the view, i.e. vtkFlReformatViewer – which contains functions for "marching through" the volume, or in "selecting" a view or working with specialized views, i.e. vtkFlMainViewer, vtkFlSubViewer or vtkFlTargetViewer.
- Also at a lower level in the object-oriented design of Image-guided Biopsy System we placed classes like IGBFile (file input/output) and IGBProbe/IGBAurora (acquire probe/catheter data from the magnetic tracker).

4. Conclusion

Minimally invasive image-guided surgery is increasingly popular as it can considerably reduce trauma for the patient. Robotic systems may provide increased precision in performing surgical interventions, and may be integrated with image-guided surgery systems for targeting purposes. The integration of the software parts of such components, similar to those described in this paper, may lead to the development of novel interventional techniques. To date, software testing has shown good robustness and safety performance. Although some preliminary clinical experiments have been completed, more clinical studies are still required to further investigate the advantages and disadvantages of this system for interventional procedures.

The lifecycle of the software system described here is expected to include a short initial development phase (08/01 to 4/02), a longer phase of product support and refinement, and extensive testing from the customer (physician) perspective. A formal software development and change control process is also needed to ensure reliable and usable systems.

Acknowledgements

This work was funded by U.S. Army grant DAMD17-99-1-9022. The content of this manuscript does not necessarily reflect the position or policy of the U.S. Government.

References

[1] Viergever, M. A., "Image guidance of therapy", *IEEE Transactions on Medical Imaging*, **17**(5), 669-671, 1998.

[2] Schroeder W., Martin K., Lorensen B., *The Visualization Toolkit - An Object-Oriented Approach To 3D Graphics*, Prentice Hall, 1998.

[3] Elder, M. C., Knight, J. C. "Specifying User Interfaces for Safety-Critical Medical Systems," *Medical Robotics and Computer Assisted Surgery*, Wiley-Liss, 1995, pp. 148-155.

[4] Gering, D.T., et al. "An Integrated Visualization System for Surgical Planning and Guidance using Image Fusion and Interventional Imaging", *Medical Image Computing and Computer-Assisted Intervention-MICCAI* 1999, Springer, pp. 809-819.

10.2.5 Clifford 2002: Assessment of Hepatic Motion

Reprint begins on the next page and is 13 pages.

Published in Computer Aided Surgery 2002

Review Article

Assessment of Hepatic Motion Secondary to Respiration for Computer Assisted Interventions

Mark A. Clifford[1], MS; Filip Banovac[1,2], MD;
Elliot Levy[1,2], MD; and Kevin Cleary[1], PhD

[1]Imaging Science and Information Systems (ISIS) Center, Department of Radiology, Georgetown University Medical Center

[2]Georgetown University Hospital/MedStar Health, Department of Radiology

Washington, DC, 20007

Correspondence: cleary@georgetown.edu

Running Title: Assessing Hepatic Motion for Computer Assisted Interventions

ABSTRACT

This paper reviews the published efforts to characterize hepatic motion secondary to respiration with the specific goal of defining the limitations and potential applications for image-guided systems in percutaneous liver interventions (computer assisted interventions). Hepatic motion and deformation due to respiration remain obstacles to applying stereotactic localization techniques to the liver. Respiratory-associated hepatic motion is complex. Nine studies using diagnostic imaging or modeling are reviewed, and their findings are tabulated herein. The significant variation in their findings is discussed including cranio-caudal translation, anterior-posterior and lateral translation, movement secondary to tissue deformation, and motion with respect to surrounding tissue. Techniques for correcting for hepatic respiratory motion are then described, including gating techniques, modeling approaches, real-time liver tracking, and magnetic tracking technology.

Key words: image-guided surgery, computer assisted surgery, liver motion, hepatic motion, minimally invasive, percutaneous, respiration, registration

INTRODUCTION

Percutaneous, minimally invasive procedures offer significant advantages over traditional surgical alternatives, including lower significant complication rates, shortened hospital stays due to decreased recovery time, and decreased expense[1]. The liver is a frequent subject for a variety of medical interventions, and a rich assortment of percutaneous hepatic procedures has been developed. These procedures include percutaneous or endoscopic biliary drainage and cholecystostomy, percutaneous or transjugular needle biopsy, transjugular intrahepatic portosystemic shunt creation (TIPS),

chemoembolization, and more recently percutaneous radiofrequency ablation. Hepatocellular carcinoma, for example, can be treated with percutaneous ablation for inoperable tumors or as an adjunct prior to surgical resection, with good success[2,3].

Hepatic motion secondary to respiration is a significant obstacle to precise percutaneous needle or instrument placement. Real-time ultrasound (US), computed tomography (CT), and magnetic resonance imaging (MRI), while useful for interventional guidance, have significant drawbacks that prevent them from becoming complete solutions for procedural guidance. CT fluoroscopy is becoming more popular, although the potentially increased radiation dose to the patient and operator may limit the application of this technology. The application of computer assisted surgery, including frameless stereotaxy and image guidance, may enhance the degree of precision obtainable by overcoming some of the limitations inherent in US, CT and MRI. The purpose of this paper is to summarize the reported characteristics of hepatic respiratory motion and deformation. Approaches to quantifying and correcting for this movement will be considered with the intention of providing a framework for further development and application of hepatic computer assisted surgery in patient care.

PERCUTANEOUS APPROACHES TO THE LIVER

Applications, Requirements, and Obstacles

Computer assisted, image-guided approaches to diagnosis and treatment of liver disorders are already widely used with good success. Current image-guided hepatic diagnostic procedures include percutaneous biopsy[4] of intrahepatic masses presumed to be tumors, and internal/external biliary drainage for benign and malignant biliary duct obstruction. Additionally, conventional hepatic arteriography is performed both for diagnostic purposes including hepatic transplantation evaluation and for therapeutic goals such as in hepatic trauma management.

Current percutaneous therapeutic applications include tumor ablation[3], cryotherapy[5,6] and brachytherapy[7], tumor embolization[8], and delivery of gene therapy vectors[9]. Percutaneous procedures in the liver typically require a relatively high degree of accuracy, although this degree of accuracy has not been definitively quantified. Accuracy may have different significance for individual applications. For example, in ablative procedures, placement of the radiofrequency or cryoprobe in the tumor center must be achieved with consideration of the exact zone of ablation relative to tumor margins and adjacent vital structures[10,11]. In biopsy procedures, accurate needle placement at the tumor margin, rather than in the necrotic center, increases the diagnostic yield. Finally, accurate percutaneous needle placement in intrahepatic biliary ducts typically requires an accuracy of several millimeters over the needle trajectory course of several centimeters. Requirements for accuracy will expand as targets for therapy such as micrometastases become smaller – a current trend in cancer treatment and gene therapy. However, achieving the required precision in minimally invasive procedures is complicated for moveable, deformable organs such as the liver.

A more precise definition of accuracy will be required in the future for these novel therapeutic procedures including ablations, anti-angiogenesis, and gene therapy. Current non-real-time guidance modalities such as CT will be inadequate, while real-time modalities such as US typically require considerable operator skill and coordination, potentially limiting widespread availability of new interventions. The potential exists for a significant role for a non-real-time image-based guidance system that does not employ ionizing radiation.

Ultrasound, CT, and MRI Guidance

Ultrasound offers the distinct advantage of real-time imaging capability without using ionizing radiation. Ultrasound (US), however, is an inherently non-coordinate technology that does not lend itself to stereotactic localization of tissue[12]. While US does provide a visual display of the operative field, it is limited to a two-dimensional display in most common applications[13]. Even in the form of 3-D US, it cannot convey the precise coordinate location of tissue and instruments which is required to achieve high levels of precision. Stereotactic image-guided systems based on US such as UltraGuide® have been introduced, but are not yet in widespread use and have other technical limitations related to needle bending[14]. Other weaknesses of US include high inter-operator variability, inability to penetrate gas-filled overlying colon, limited resolving power, and image obliteration which occurs after an ablative procedure[13, 15].

The use of MRI, either as an adjunct to or a replacement for US, has been explored as a possible remedy to these limitations[16]. Static MRI and CT images are routinely used for pre-operative planning. Both CT and MRI provide excellent visualization of target tissue detail. Concurrent CT or MRI images help identify suitable approaches to the intended target. However, successful needle or instrument placement under CT/MRI image guidance is a repetitive needle repositioning exercise. The needle is gradually advanced and/or re-directed while its position is re-assessed with a new static image until the desired needle position is obtained. The primary disadvantages of this process of "advance and check" are the additional time required for re-imaging and the accuracy limitations introduced by respiratory or patient motion. Needle placement for interventions also requires a high degree of operator skill[17]. CT fluoroscopy is a recently introduced imaging modality, which combines the anatomic resolution of CT with the real-time imaging capabilities of fluoroscopy. One drawback is that CT fluoroscopic imaging may expose both the patient and the interventionalist to increased doses of ionizing radiation[18, 19].

Regardless of the imaging modality employed, percutaneous interventions in the liver using this advance and check technique for needle or instrument placement share complication risks. The risk increases with the number of needle passes undertaken. Hemobillia, intraperitoneal hemorrhage, and hemothorax have been reported[2]. Complications also include bile duct injury[20, 21] and seeding of needle tract with tumor in ablative procedures[21-24]. The ideal method of intraoperative guidance would provide precise path planning, tissue visualization, and real-time guidance as aids for a single successful puncture effort. Successful interventions could therefore be potentially completed with a substantially reduced complication rate.

Frameless Stereotactic Guidance

The possibility of extending the technique of frameless stereotaxy to the liver is fairly novel but has been explored by Herline[13, 15]. Frameless stereotactic instrument guidance has been very successful in brain and spine interventions[25]. Discussions of the required degree of accuracy typically state 5 mm as the needed margin[26]. In addition, frameless stereotactic neurosurgery has reduced inter-operator variability and decreased ancillary trauma by eliminating the need for multiple needle passes.

Liver motion secondary to respiration remains a substantial barrier to implementing frameless stereotaxy for hepatic applications. The stereotactic techniques developed for neurosurgical applications use pre-operatively acquired CT or MRI images, which are mapped to the surgical field using image registration. During the procedure, the position of the instruments and tissues can be displayed and updated on the reference images in real-time. This requires that the target tissue remain motionless in order for the registered image to be valid for instrument guidance[25]. Unfortunately, the liver does not meet this requirement.

ASSESSMENTS OF HEPATIC RESPIRATORY MOTION: REVIEW

Adequate characterization of hepatic motion due to respiration is an essential first step in the development of computer assisted surgical guidance systems[13]. This understanding is necessary to determine the motion parameters of these systems and to select the optimal portion of the respiratory cycle for manipulating instruments. However, limited quantitative information is available to date[27]. In order to identify appropriate studies for this review, a database search was undertaken using the National Library of Medicine's Pubmed under the search terms: "liver motion", "hepatic motion", and "respiration." Appropriate conjunctive and disjunctive modifiers were used to narrow the search. Relevant studies, including those that measure liver or diaphragmatic motion, were reviewed. Earlier studies cited in these works, but not found in Medline, were identified and assessed. The body of literature assessing hepatic respiratory motion is not large. Therefore, all of the identified studies that quantify liver motion are discussed herein.

Of the existing reports, several describe efforts to reduce image artifacts generated by organ motion or to improve the targeting of neoplasms for radiotherapy[28-31]. Other studies of liver motion have used scintigraphy[32, 33], US[27, 34], CT [34] or MRI[35] for measurement. One study additionally reports maximum respiratory-related hepatic velocity and acceleration[27]. Other reports focus on tracking the movement of the center of an isolated spherical liver tumor during the respiratory cycle using high speed MRI[36, 37]. Finally, another group employed the registration of serial MRI images to evaluate the motion and deformation of the liver [38].

While new ultrafast CT and shortened MRI image acquisition times have made it possible to reduce the impact of liver motion on image acquisition, hepatic respiratory motion continues to be critical in radiotherapy for liver cancers[39]. Researchers have focused on ways to compensate for tumor motion so that as much normal parenchyma as

possible can be spared. Recently, one research group has assessed hepatic motion secondary to respiration in both human subjects and a porcine model specifically to assist in the development of a frameless stereotactic surgical system[13].

Considered together, these reports show liver movement to be complex, with cranio-caudal, lateral, and anterior-posterior motion in addition to movement due to deformation of the tissue. They also demonstrate that there is wide variation between individuals in the degree and direction of liver movement. Table 1 summarizes the results of nine published studies of hepatic motion in human subjects.

Study/Date	Number of Subjects	Cranio-Caudal (mm)		Anterior-Posterior (mm)	Lateral (mm)	Modality
		Quiet Inspiration	Deep Inspiration			
Weiss (1972)[32]						
(using scintigraphy)	12	11 ± 3	12-75			Scintigraphy
(using fluoroscopy)	25	13 ± 5				Fluoroscopy
Harauz (1979)[33]	51	14				Scintigraphy
Suramo (1984)[34]	50	25	55			US
Korin (1992)[35]	15	13	39	2.5		MRI
Davies (1994)[27]	9	10 ± 8	37 ± 8			US
Herline (1999)[13]	2	10.8 ± 2.5				Optical Tracking
Shimizu (1999)[37]	1	21		8	9	MRI
Shimizu (2000)[36]	6	10.6 ± 7.0		4.6 ± 1.6	5.2 ± 1.8	MRI
Rohlfing (2001)[38]	4	12-26		1-12	1-3	MRI

Table 1. Hepatic motion secondary to respiration in nine human studies

Cranio-Caudal Translation

As indicated in Table 1, all the studies agree that cranio-caudal motion is the most significant, with translation ranging from 10 to 26 mm in quiet respiration. The MRI study by Korin suggested that clinically significant liver motion could be approximated effectively by cranio-caudal movement alone, completely neglecting other axes[35]. This conclusion was sustained by the US studies of Davies the following year[27]. While this approximation would simplify the modeling and tracking of hepatic motion, more recent studies suggest that translations along the other axes, as well as motion due to deformation, are significant and cannot be neglected.

Anterior-Posterior and Lateral Translation

Measurements of movement in both anterior-posterior and lateral axes vary markedly with the assessment technique used, and there has been disagreement in the literature about the significance of these components of motion. Davies[27] and Korin[35] initially reported minimal motion in both the medial-lateral and anterior-posterior axes. The more recent evaluations by Herline[13] (using optical tracking), Shimizu[36, 37], and Rohlfing[38] (both by MRI), however, indicate that there is significant translation in both of these other axes. Shimizu observed solid tumor movement within the liver throughout the respiratory cycle and reported average movement of 8 mm anterior-posterior and 9 mm lateral[37] with similar results in a follow-up study[36]. Rohlfing et al., in their analysis of liver motion in a single patient by serial registration of MRI images, also report significant movement in the anterior-posterior and lateral directions, as shown in Table 1[38]. This difference between early and later evaluations in the reported significance of liver motion perpendicular to the cranio-caudal plane is due to differences in detection techniques and standards for evaluation. Korin[35] and Davies[27] evaluated the motion of liver margins in MRI and US images. The later studies followed the motion of single (in the case of tumor tracking)[39] or multiple[13, 38] points within the liver volume. This distinction is significant, because measurement of movement about hepatic margins would intrinsically underestimate motion due to deformation inherent in a non-rigid tissue such as the liver[38]. In addition, tracking of points within the liver volume yields results more directly relevant to the goal of tracking intrahepatic targets for interventional guidance. Based upon these considerations, it is clear that lateral and anterior-posterior translation is significant, particularly when tracking discrete targets within liver tissue.

Movement Secondary to Tissue Deformation

The liver is a non-rigid organ with a thin, flexible capsule that does not prevent deformation. Korin, et al., determined that the deformation of the liver during the respiratory cycle appeared to be insignificant according to their MRI line scan technique, estimating deformation to be less than 3 mm[35]. However, the analysis by Rohlfing[38] of hepatic motion by intensity-based free form deformation registration finds significant movement due to deformation. Because the liver is non-regular in shape and somewhat non-uniform in composition (due to the location of vascular structures and ligamentous tissue), the degree of deformation varies markedly within the organ. The registration technique used by Rohlfing[38] is a particularly sensitive way to evaluate point-by-point changes in location throughout the respiratory cycle, and to compare rigid assumptions of movement with the actual changes that occur. He reports that tissue deformation of the liver with respiration is substantial. When point-by point measurements of locations within the liver are tracked throughout the respiratory cycle, they differ from the predictions made by models that assume rigid motion between 2 and 19 mm, with an average of 6 mm across the tissue. Mis-registration was found to be most pronounced at the superior and inferior margins of the liver[38]. Other researchers estimated the error introduced by assuming rigid liver motion to be on average 3 mm[16].

Motion with Respect to Surrounding Tissue

The liver does not have a fixed relationship to the skin surface or surrounding organs during the respiratory cycle, further complicating motion characterization. Two investigators address this issue in an attempt to evaluate respiratory gating protocols,

which assume that the liver re-occupies the same position at identical moments in the respiratory cycle. Suramo determined that the liver attains the same position in only 18% of gated CT and US exposures. Twenty percent of views yielded "markedly different" liver positions (outside the CT slice, or greater than 4 mm displacement) despite identical timing of exposure by a form of respiratory gating[34]. Suramo concluded that any procedure that cannot be completed within one breath hold would be affected by this inaccuracy. Shimizu evaluated the position of hepatic tumors with respect to the overlying skin surface for possible radiotherapy treatment volume reduction by respiratory gating. Shimizu reported that the position of the tumor contours was not constant with respect to the skin surface at peak exhalation or inhalation in each respiratory cycle. This finding contradicts the previous assumption in respiration-gated radiotherapy that the position of the tumor is constant at the exhalation peak[36].

CORRECTION FOR HEPATIC RESPIRATORY MOTION

The liver moves during inspiration, surgical manipulation, and when the patient changes position to any degree. Suramo describes the liver as the "most moveable (abdominal) organ in both normal respiration and standardized breathing"[34]. It seems clear from the literature that hepatic motion consists of translation in every axis as well as movement due to deformation of the tissue itself. Accurate targeting of the moving liver therefore requires a system that can correct or account for a very complex range of movement.

Frameless stereotactic guidance for moving organs requires that the target be tracked and registered with pre-operatively acquired images. This can be accomplished in several ways. Breath holding and gating techniques attempt to time specific procedures to coincide with a fixed point in the respiratory cycle, when the liver is assumed to be motionless and therefore in registration with the pre-operative images. Modeling techniques track the motion of the liver over several cycles, and then construct a predictive model of motion based on this information. Other strategies track the liver in real-time, updating the guidance information with the current organ position. Several variations of these approaches have been reported in the literature as described below.

Gating Techniques

"Respiratory gating" is an approach that permits the approximation of a motionless liver by operating on the tissue intermittently, only at identical points in the respiratory cycle. It is even possible to register the tissue to pre-operatively obtained images also taken at the specified lung volume. End-exhalation is the point most often chosen because it represents the longest natural pause in the cycle[28]. Gating techniques to compensate for liver motion have been utilized in radiotherapy and artifact correction in MRI and CT images with some success[30, 31, 40]. Tissue motion gating for radiotherapy can potentially permit delivery of an optimal radiation dose to the tumor while minimizing exposure of adjacent healthy tissue[28-30].

Respiratory gating techniques for surgical guidance require that identical moments in successive respiratory cycles can be isolated to serve as a "trigger" for image acquisition and three-dimensional space registration. A mass, biliary duct, or hepatic vessel could

then be consistently targeted for intervention. This assumes that the liver re-occupies the same position at equivalent moments within the cycle. Measures of hepatic respiratory motion indicate however that the liver does not reliably assume the same position at equivalent lung volumes or identical moments in the respiratory cycle[34]. As a result, "breath-hold" and gating techniques may be inadequate for precise guidance of hepatic interventions without real-time imaging assistance.

Modeling Approaches

Modeling of liver motion to predict the location of a target from previously acquired images is another approach that has been explored. However, if the movement varies between cycles, prediction of that variability to sufficient precision represents an unsolved technical problem. Modeling therefore cannot provide sufficient precision for prospective use, although it has been used retrospectively for motion correction with some success[38].

Real-time Liver Tracking

Real-time liver tracking strategies for procedure guidance obviate the requirement for a motionless liver by using computer correction. This strategy tracks the target tissue within the liver along with the surgical instruments, updating these positions in real-time on guidance images. Herline, et al. report using a combination surface and point-based registration technique to register pre-operative images to intraoperative liver motion in human subjects to quantify hepatic movement (see Table 1). They then expand upon that work by using this image registration technique for stereotactic guidance in a porcine model[15]. In this study, a digitized liver surface, along with discrete surface and internal liver points (e.g., edge of the falciform ligament, portal vein bifurcation) were used in the registration. Tracking was provided by an Optotrak (Northern Digital Inc., Ontario, Canada) optical tracking system. The reported error using this combined technique was 2.9 mm for the entire surface and 2.8 mm for embedded targets. This work shows that stereotactic tracking of a moving liver is feasible with a high degree of accuracy during open surgical procedures. Obtaining this degree of accuracy without surgically exposing the liver for surface registration still needs to be investigated for minimally invasive approaches. It is also important to stress that, while this assessment of liver motion is consistent with values reported in other studies, Herline et al. use measurements obtained in an open surgical setting.

Schweikard investigated methods to compensate for hepatic tumor motion secondary to respiration for robotic radiosurgery[39]. The achievement of the desired surgical margins during radiosurgery often results in a higher than desired radiation dose to adjacent normal tissues. Schweikard was able to track the motion of a hepatic tumor and use this information to guide a robotically-controlled therapeutic source, thereby reducing the treated tissue volume, as well as the damage to normal tissue. Schweikard determined the location of the moving tumor by combining optical tracking of the patient's skin with synchronized X-ray imaging of internal markers, which were continuously updated during treatment to provide the motion compensation. This technique provides an example of real-time liver tracking achieved without surgical liver exposure. The same

technique could potentially be implemented for other minimally invasive interventions in the liver and other deformable organs.

Magnetic Tracking Technology

Magnetic tracking technology has been previously employed for real-time intra-abdominal organ tracking without surgical exposure. Solomon et al. have demonstrated the feasibility of at least three percutaneous interventional procedures using real-time magnetic tracking registered with cross-sectional images[41-43]. They performed a transjugular intrahepatic portosystemic shunt (TIPS), transbronchial needle aspiration in swine, and placed an inferior vena cava filter using this technology. Other investigators used magnetic tracking in electro-anatomical mapping of the heart thereby obviating the need for fluoroscopy[44]. These examples demonstrate the versatility and applicability of this integrated technology in multiple organ systems. In the TIPS procedure performed by Solomon et al., the actual position of the needle instrument was registered with pre-operative images, allowing the operator to successfully puncture the portal vein in transhepatic fashion without visualizing the target with a real-time imaging modality[41].

Our research group at Georgetown has been developing a percutaneous needle placement paradigm using magnetic tracking of the respiratory related motion of the liver registered with pre-operatively acquired CT images[45]. We therefore developed a liver respiratory motion simulator to test the feasibility of direct percutaneous puncture of an intrahepatic vessel whose position during the respiratory cycle is extrapolated from the position of an intravascular fiducial within the liver[46]. Banovac et al. demonstrated the anatomic feasibility of percutaneous anterior transhepatic simultaneous portal-hepatic vein punctures by retrospective image analysis[47]. This serves as a basis for further work in this new approach to the TIPS procedure.

Using active liver motion tracking based on the AURORA™ magnetic localization system (Northern Digital, Inc., Ontario, Canada) and a small percutaneously placed needle fiducial, the feasibility of transhepatic portal-hepatic vein puncture has been shown[48]. This approach may be simpler to perform with magnetic tracking assistance and a new needle placement algorithm than the traditional transjugular approach. Additionally, the accuracy of percutaneous needle placement for purposes of liver lesion biopsy or thermal ablation has also been demonstrated in a respiring liver phantom[49]. Although animal and human studies must confirm this early work, magnetic tracking appears promising as a modality for liver localization and tracking. Moreover, magnetic tracking may improve organ localization in general and lead to development of new surgical navigation methods for procedures on other internal organs.

CONCLUSION

Nine published studies of respiratory-associated hepatic motion were reviewed with the goal of defining the limitations and potential applications for image-guided systems in percutaneous liver interventions. The significant variation in these studies was discussed, and techniques for correcting for hepatic respiratory motion were described.

However, in current clinical practice, catheter and needle-based interventions in the liver are currently performed with high success and relatively low complication rates. Therefore, what improvement in outcome can be expected from the use of frameless stereotaxy in minimally invasive hepatic interventions?

First, magnetic tracking may play a significant role as an adjunct guidance system for percutaneous intrahepatic procedures where traditional real-time imaging guidance is not feasible, e.g., lack of an adequate acoustical window precludes adequate US imaging, or where patients cannot cooperate with respiratory instructions for "breath hold" approaches. The technical feasibility and radiation doses absorbed by patients and operators with CT fluoroscopy must be elucidated before this technology becomes widespread. Second, magnetic guidance may help improve the skills of practitioners who otherwise would have limited experience performing these procedures. Third, with the aid of magnetic tracking systems, experienced practitioners may enjoy shorter procedure times, thus reducing hospital costs associated morbidity. Finally, the possibilities exist for the future integration of this technology to gene delivery, antineoplastic, or anti-angiogenesis therapies.

ACKNOWLEDGEMENTS

This work was funded by U.S. Army grant DAMD17-99-1-9022. The content of this manuscript does not necessarily reflect the position or policy of the U.S. Government.

REFERENCES

1. Papatheofanis FJ. The impact of minimally invasive surgery. *Technology Economics Review.* 1997;10:66-68.
2. Livraghi T, Goldberg SN, Lazzaroni S, Meloni F, Solbiati L, Gazelle GS. Small hepatocellular carcinoma: treatment with radio-frequency ablation versus ethanol injection. *Radiology.* 1999;210:655-661.
3. McGhana JP, Dodd GD. Radiofrequency ablation of the liver: current status. *AJR Am J Roentgenol.* 2001;176:3-16.
4. Mayoral W, Lewis JH. Percutaneous liver biopsy: what is the current approach? Results of a questionnaire survey. *Dig Dis Sci.* 2001;46:118-127.
5. Ribeiro A, Nagorney DM, Gores GJ. Localized hepatocellular carcinoma: therapeutic options. *Curr Gastroenterol Rep.* 2000;2:72-81.
6. Crews KA, Kuhn JA, McCarty TM, Fisher TL, Goldstein RM, Preskitt JT. Cryosurgical ablation of hepatic tumors. *Am J Surg.* 1997;174:614-617; discussion 617-618.
7. Gunven P, Gorsetman J, Ohlsen H, Ruden BI, Lundell G, Skoog L. Six-year recurrence free survival after intraluminal iridium-192 therapy of human bilobar biliary papillomatosis. A case report. *Cancer.* 2000;89:69-73.
8. Roche A. Therapy of HCC--TACE for liver tumor. *Hepatogastroenterology.* 2001;48:3-7.
9. Afford SC, Young LS. Gene therapy for hepatocellular carcinoma-teaching old dogs new tricks. *Hepatology.* 2001;34:207-209.

10. Rhim H, Dodd GD, 3rd. Radiofrequency thermal ablation of liver tumors. *J Clin Ultrasound.* 1999;27:221-229.
11. de Baere T, Elias D, Dromain C, Din MG, Kuoch V, Ducreux M, Boige V, Lassau N, Marteau V, Lasser P, Roche A. Radiofrequency ablation of 100 hepatic metastases with a mean follow-up of more than 1 year. *AJR Am J Roentgenol.* 2000;175:1619-1625.
12. Cleary K, Anderson J, Brazaitis M, Devey G, DiGioia A, Freedman M, Gronemeyer D, Lathan C, Lemke H, Long D, Mun SK, Taylor R. Final report of the technical requirements for image-guided spine procedures Workshop, April 17-20, 1999, Ellicott City, Maryland, USA. *Comput Aided Surg.* 2000;5:180-215.
13. Herline AJ, Stefansic JD, Debelak JP, Hartmann SL, Pinson CW, Galloway RL, Chapman WC. Image-guided surgery: preliminary feasibility studies of frameless stereotactic liver surgery. *Arch Surg.* 1999;134:644-649; discussion 649-650.
14. Howard MH, Nelson RC, Paulson EK, Kliewer MA, Sheafor DH. An electronic device for needle placement during sonographically guided percutaneous intervention. *Radiology.* 2001;218:905-911.
15. Herline AJ, Herring JL, Stefansic JD, Chapman WC, Galloway RL, Dawant BM. Surface registration for use in interactive, image-guided liver surgery. *Comput Aided Surg.* 2000;5:11-17.
16. Carrillo A, Duerk JL, Lewin JS, Wilson DL. Semiautomatic 3-D image registration as applied to interventional MRI liver cancer treatment. *IEEE Trans Med Imaging.* 2000;19:175-185.
17. Liang HL, Yang CF, Pan HB, Lai KH, Cheng JS, Lo GH, Chen CK, Lai PH. Small hepatocellular carcinoma: safety and efficacy of single high-dose percutaneous acetic acid injection for treatment. *Radiology.* 2000;214:769-774.
18. Nawfel RD, Judy PF, Silverman SG, Hooton S, Tuncali K, Adams DF. Patient and personnel exposure during CT fluoroscopy-guided interventional procedures. *Radiology.* 2000;216:180-184.
19. Nickoloff EL, Khandji A, Dutta A. Radiation doses during CT fluoroscopy. *Health Phys.* 2000;79:675-681.
20. Paymani M, Zajko AB, Campbell WL. Bile leakage as a complication of liver biopsy in liver transplants. *Abdom Imaging.* 1993;18:258-260.
21. Ishii H, Okada S, Okusaka T, Yoshimori M, Nakasuka H, Shimada K, Yamasaki S, Nakanishi Y, Sakamoto M. Needle tract implantation of hepatocellular carcinoma after percutaneous ethanol injection. *Cancer.* 1998;82:1638-1642.
22. Kim SH, Lim HK, Lee WJ, Cho JM, Jang HJ. Needle-tract implantation in hepatocellular carcinoma: frequency and CT findings after biopsy with a 19.5-gauge automated biopsy gun. *Abdom Imaging.* 2000;25:246-250.
23. Takamori R, Wong LL, Dang C, Wong L. Needle-tract implantation from hepatocellular cancer: is needle biopsy of the liver always necessary? *Liver Transpl.* 2000;6:67-72.
24. Smith EH. Complications of percutaneous abdominal fine-needle biopsy. Review. *Radiology.* 1991;178:253-258.
25. Maciunas RJ. Interactive Image -Guided Neurosurgery. In: Barrow DL, ed. *Neurosurgical Topics*: American Association of Neurological Surgeons; 1993

26. Bucholz RD, Ho HW, Rubin JP. Variables affecting the accuracy of stereotactic localization using computerized tomography. *J Neurosurg.* 1993;79:667-673.
27. Davies SC, Hill AL, Holmes RB, Halliwell M, Jackson PC. Ultrasound quantitation of respiratory organ motion in the upper abdomen. *Br J Radiol.* 1994;67:1096-1102.
28. Ritchie CJ, Hsieh J, Gard MF, Godwin JD, Kim Y, Crawford CR. Predictive respiratory gating: a new method to reduce motion artifacts on CT scans. *Radiology.* 1994;190:847-852.
29. Minohara S, Kanai T, Endo M, Noda K, Kanazawa M. Respiratory gated irradiation system for heavy-ion radiotherapy. *Int J Radiat Oncol Biol Phys.* 2000;47:1097-1103.
30. Kubo HD, Hill BC. Respiration gated radiotherapy treatment: a technical study. *Phys Med Biol.* 1996;41:83-91.
31. Kubo HD, Len PM, Minohara S, Mostafavi H. Breathing-synchronized radiotherapy program at the University of California Davis Cancer Center. *Med Phys.* 2000;27:346-353.
32. Weiss PH, Baker JM, Potchen EJ. Assessment of hepatic respiratory excursion. *J Nucl Med.* 1972;13:758-759.
33. Harauz G, Bronskill MJ. Comparison of the liver's respiratory motion in the supine and upright positions: concise communication. *J Nucl Med.* 1979;20:733-735.
34. Suramo I, Paivansalo M, Myllyla V. Cranio-caudal movements of the liver, pancreas and kidneys in respiration. *Acta Radiol Diagn.* 1984;25:129-131.
35. Korin HW, Ehman RL, Riederer SJ, Felmlee JP, Grimm RC. Respiratory kinematics of the upper abdominal organs: A quantitative study. *Magnetic Resonance in Medicine.* 1992;23:172-178.
36. Shimizu S, Shirato H, Aoyama H, Hashimoto S, Nishioka T, Yamazaki A, Kagei K, Miyasaka K. High-speed magnetic resonance imaging for four-dimensional treatment planning of conformal radiotherapy of moving body tumors. *Int J Radiat Oncol Biol Phys.* 2000;48:471-474.
37. Shimizu S, Shirato H, Xo B, Kagei K, Nishioka T, Hashimoto S, Tsuchiya K, Aoyama H, Miyasaka K. Three-dimensional movement of a liver tumor detected by high-speed magnetic resonance imaging. *Radiother Oncol.* 1999;50:367-370.
38. Rohlfing T, Maurer CR, O'Dell WG, Zhong J. Modeling liver motion and deformation during the respiratory cycle using intensity-based free-form registration of gated MR images. *SPIE Medical Imaging.* 2001.
39. Schweikard A, Glosser G, Bodduluri M, Murphy MJ, Adler JR. Robotic motion compensation for respiratory movement during radiosurgery. *Comput Aided Surg.* 2000;5:263-277.
40. Mori M, Murata K, Takahashi M, Shimoyama K, Ota T, Morita R, Sakamoto T. Accurate contiguous sections without breath-holding on chest CT: value of respiratory gating and ultrafast CT. *AJR Am J Roentgenol.* 1994;162:1057-1062.
41. Solomon SB, Magee C, Acker DE, Venbrux AC. TIPS placement in swine, guided by electromagnetic real-time needle tip localization displayed on previously acquired 3-D CT. *Cardiovasc Intervent Radiol.* 1999;22:411-414.

42. Solomon SB, Magee CA, Acker DE, Venbrux AC. Experimental nonfluoroscopic placement of inferior vena cava filters: use of an electromagnetic navigation system with previous CT data. *J Vasc Interv Radiol.* 1999;10:92-95.
43. Solomon SB, White P, Jr., Acker DE, Strandberg J, Venbrux AC. Real-time bronchoscope tip localization enables three-dimensional CT image guidance for transbronchial needle aspiration in swine. *Chest.* 1998;114:1405-1410.
44. Gepstein L, Hayam G, Ben-Haim SA. A novel method for nonfluoroscopic catheter-based electroanatomical mapping of the heart. In vitro and in vivo accuracy results. *Circulation.* 1997;95:1611-1622.
45. Cleary K, Banovac F, Levy E, Tanaka D. Development of a liver respiratory motion simulator to investigate magnetic tracking for abdominal interventions. *SPIE*, San Diego, 2002; 4681: 25-29
46. Banovac F, Cleary K, Levy EB, Lindisch D, Onda S. Design and construction of a liver phantom for CT imaging and interventions that simulates liver motion seen during respiration. *Radiologic Society of North America*, Chicago, IL, 2001; 221 (P): 689
47. Banovac F, Levy EB, Lindisch D, Onda S, Clifford M. Feasibility of a single puncture percutaneous transabdominal access for creation of TIPS. *Surgical and Radiologic Anatomy.* In print.
48. Levy EB, Cleary K, Banovac F, Glossop N, Tanaka D, Xu S, Lindisch D. Implementation of a magnetic tracking system for accurate puncture needle guidance. *Poster presented at the 27th Annual Scientific Meeting of the Society of Cardiovascular & Interventional Radiology*, Baltimore, MD, 2002;
49. Banovac F, Glossop N, Lindisch D, Tanaka D, Levy E, Cleary K. Liver tumor biopsy in a respiring phantom with the assistance of a novel electromagnetic navigation device. *5th International Conference on Medical Image Computing and Computer Assisted Intervention*, Tokyo, Japan, Sept. 2002; Accepted as a poster and for publication in the proceedings.

10.2.6 Levy 2002a: Evaluation of a Magnetic ...

Reprint begins on the next page and is 6 pages.

CARS 2002 – H.U. Lemke, M.W. Vannier; K. Inamura, A.G. Farman, K. Doi & J.H.C. Reiber (Editors)

Evaluation of a Magnetic Tracking-Guided Needle Placement System Featuring Respiratory Gating in an In Vitro Liver Model

Elliot B. Levy[a], Kevin Cleary[b], Filip Banovac[a], Daigo Tanaka[b], Sheng Xu[c], David Lindisch[b], Neil Glossop[d]

[a]Department of Radiology, Georgetown University Hospital/MedStar Health, 3800 Reservoir Road, Washington, DC, USA

[b]Imaging Science and Information Systems (ISIS) Center, Department of Radiology, Georgetown University Medical Center, Washington, DC, USA

[c]NSF-funded Center for Computer Integrated Surgical Systems andTechnologies, Johns Hopkins University, Baltimore, MD, USA

[d]Traxtal Technologies LLC, Bellaire, TX, USA

Abstract

This paper presents our preliminary experience validating a needle guidance algorithm featuring magnetic tracking and respiratory gating for accurate needle placement in the liver using a specially designed phantom. Experimental results suggest that our implementation can facilitate accurate needle placement in this phantom during simulated respiratory-related liver motion.

Keywords: magnetic tracking, needle placement, liver

1. Introduction

Accurate placement of fine needles within the liver for biopsy or catheterization purposes may be accomplished using CT, MRI, or ultrasound guidance. Respirations commonly must be suspended for accurate CT-or MRI-guided needle placement. In vascular procedures such as TIPS, shunt creation between portal and hepatic veins is most often accomplished without direct real-time guidance, although planar and 3-D ultrasound and MRI guidance has been reported. Recently an interactive image guidance system featuring magnetic tracking coupled to previously acquired 3-D CT images was used to display the real-time position of the intrahepatic puncture needle during TIPS in an animal model [1]. This system featured respiratory gating consisting of a magnetic sensor placed on the animal's abdomen, allowing updating of the needle position only during a designated portion of the respiratory cycle. This algorithm required the placement of 10-20 magnetic markers on the animal's skin to permit image registration. The system accuracy was reported to be 3mm.

In this paper we report our preliminary experience validating a guidance algorithm for accurate needle placement in the liver in a uniquely designed phantom. When coupled with a magnetic tracking system, this prototype features real-time monitoring of respiratory-related target organ motion. For the purpose of phantom design, we assume that hepatic respiratory motion occurs in the craniocaudal direction only and that the liver itself is not deformed by diaphragmatic motion. The respiratory excursion of the liver has been measured as 10mm in previous reports [2, 3]. Furthermore, Davies et.al. [3] initially described upper abdominal respiratory motion by assuming that respiratory motion velocity was either constant or zero. They measured the average dwell time

(zero organ velocity) during end-expiration which lasted an average of 1.4 seconds during a mean respiratory cycle time of 4.4 seconds in their group of nine volunteers. The end-expiratory dwell time of the liver was confirmed subsequently by direct measurement of the maximum velocity and peak acceleration values by direct M-mode ultrasound scans obtained at 0.25s intervals.

Our strategy for needle placement and manipulation is patterned after the stepwise conventional "freehand" procedure for static image-guided biopsies. Preoperative images of the target are reviewed for path planning purposes. A suitable skin puncture site is chosen from which a needle trajectory unobstructed by interposed viscera can be demonstrated. The angle of trajectory and necessary depth of puncture are determined. Freehand puncture is initiated, guided exclusively by the operator's perception of the desired trajectory. Respirations must be typically suspended during needle movements to prevent undesired organ motion during needle puncture. Needle position is confirmed at the conclusion of the needle drive process by obtaining static images of the target.

For magnetic tracking-guided needle punctures, puncture site and trajectory planning are determined with the assistance of a graphical user interface (GUI) and preoperatively obtained CT dataset. In our model, resting respirations continue throughout the procedure, and needle advancement is performed only when the GUI indicates that respiratory-related organ motion has ceased during the approximately 1.4 sec end-expiratory phase pause. The system tracks the motion of the fixed catheter-based fiducial to determine the timing of the pause in respiratory-related organ motion. Unlike static image-guided procedures, the specifically designed GUI displays 1) the depth of the needle tip relative to the desired depth in graphical fashion, and 2) the position of the needle tip registered with the preoperatively obtained CT dataset. The needle procedure can therefore be terminated by the operator based upon the real-time information and guidance provided by the GUI.

2. Methodology

An abdominal torso phantom (Anatomical Chart Co., Skokie, II.) was modified by removing the ventral abdominal wall and placing a servomotor-driven platform mount in the "paraspinal" area upon which a foam liver phantom has been secured. The liver phantom contains target thin-walled "vascular structures" created by the removal of barium-coated plastic drinking straws placed within the foam mixture prior to final casting. The resulting air-filled tubes measure approximately 5mm in diameter. The phantom is moderately more firm than the human liver with respect to the tactile sense during needle puncture. The servomotor control system produces linear platform motion which simulates the respiratory motion of the liver. The tracking system consists of a small pyramidal magnetic field generator (Aurora™ Electromagnetic Tracking System, Northern Digital Inc., Toronto, Canada), a system control unit, and one or more sensor interface units. In our implementation we use two magnetically tracked sensors: a catheter and a needle. Both sensors are based on a single embedded 0.9 mm diameter coil. The catheter-based fiducial was placed through the simulated intrahepatic inferior vena cava and into a simulated hepatic vein and fixed in position with a small amount of adhesive. All motion of the liver phantom is therefore tracked by the embedded catheter-based fiducial. The remaining fiducials are calibrated flat skin markers (multi-modality radiographics markers, IZI Medical, Baltimore, MD) which can be readily identified on axial CT images of the torso. The tracked puncture needle is a modified 18 gauge trocar needle with the coil fiducial placed in the stylet (Traxtal Technologies, Bellaire, TX).

For each series of puncture experiments, a total of four skin fiducials were placed on the anterior costal margins. The phantom was placed in a Siemens CT scanner and contiguous 1mm images of the liver obtained. The CT DICOM dataset was transferred to a Windows NT workstation where the axial images were displayed and reviewed in a single window on the GUI. The target vessels

were selected and a linear puncture needle trajectory highlighted. The magnetic field generator was placed next to the torso. The registration process was done using the external and catheter-based fiducials. The skin fiducials were identified on the CT images and automatic segmentation was performed to identify the isocenter of each fiducial. The tracked needle was then placed on each fiducial sequentially, thereby recording the position in magnetic space. The catheter-based fiducial was registered in the end-expiratory phase position by identifying the tip of the catheter containing the coil fiducial on the respective CT image. In all experiments, the registration error (root mean square) measured 1-2 millimeters. The skin entry site was determined by placing the tracked needle on the "skin" of the torso, guided in real-time fashion in a third window which displayed the position of the needle tip relative to the previously determined needle trajectory. The correct needle "depth" was compared to the termination target position, and needle advancement ceased when the system graphically indicated the desired needle depth.

3. Results

In initial tests, simultaneous needle puncture of two vessels was performed in the stationary liver phantom to simulate the key step in the specifically modified TIPS procedure [4]. Needle placement was performed by hand by experienced (E.L.) and less experienced (F.B.) operators. Orthogonal biplane fluoroscopic images of the liver phantom were then obtained which confirmed successful puncture of both targets by the single needle pass (Figure 1—note that all figures are on the last page of the paper).

In a second liver phantom, a single vessel served as a target, and guided needle punctures were performed by a single operator (E.L.) on ten occasions during simulated respiratory motion. The respiratory motion ranged from a frequency of 12-40/minute and an excursion distance of 1-2 centimeters. Orthogonal biplane digital images were obtained for each needle pass to confirm successful target puncture (Figure 2). A "guidewire test" was then performed consisting of an attempt to pass a standard angiographic 0.035 inch guidewire through the needle into the targeted "vessel" (Figure 3). The time required to successfully puncture the vessel target after placing the needle tip on the skin was recorded for each needle pass. A picture of the interventional suite and experimental set-up is shown in Figure 4.

For needle passes performed during respiratory excursions, success was defined as 1) determination of the needle tip position within the vessel lumen by orthogonal digital images, and 2) successful passage of the guidewire without needle manipulation. For the 10 attempted passes; 8 passes were completely successful. In the remaining two passes, orthogonal biplane images demonstrated the needle tip within the target vessel but in an eccentric position, although withdrawal of the needle tip by 1 millimeter or rotation of the needle was required to allow successful passage of the guidewire. Needle puncture attempts averaged 28.6 sec (standard deviation 34.1 sec), with a prolonged attempt lasting 105 seconds caused by significant needle deflection within the phantom attributed to incorrect insertion of the stylet within the trocar. Needle misalignment was immediately recognized in this case, and needle redirection resulted in a successful puncture.

In all instances, the GUI provided a user-friendly, concise, and stepwise program for needle trajectory planning and needle placement. The rapid needle position update rate provided by the tracking system and interface allows for the real-time display of the position of the needle alignment and depth parameters. The intravascular, fixed catheter-based fiducial permits direct tracking of the respiratory related organ motion for real-time needle placement.

4. Discussion

Potential limitations for widespread implementation of these techniques were revealed in the course of the study. First, the presence of the CT gantry motion and biplane image intensifiers

results in distortion of the magnetic field as reflected by increased registration errors. This problem was addressed in the current study by performing the magnetic tracking-guided needle punctures at a distance of at least two feet from the image intensifiers and x-ray sources. Second, in addition to the visual cues guiding needle movement provided by the GUI, the operator can be influenced by the sound of the servomotor initiating a subsequent respiratory cycle. Third, the reported method for respiratory gating would require selective hepatic vein catheterization. The requirement for this minimally invasive procedure may initially limit the implementation of this functionality to other similar, minimally invasive procedures such as TIPS.

Needles can be accurately placed for diagnostic and interventional procedures using static image-guided methods such as conventional CT and real-time guidance including conventional and CT-fluoroscopy and ultrasound. Real-time guidance offers the advantage of concurrent monitoring of the needle position and immediate determination of successful achievement of the intended goal. As a real-time guidance modality, ultrasound is limited by the availability of a satisfactory acoustical window, while CT imaging and particularly CT fluoroscopy is associated with exposure to significant ionizing radiation. Needle placement accuracy is determined by the registration error, stability of the magnetic field, and the operator's dexterity and judgement. Real-time imaging increases the efficacy of the puncture procedure by allowing the operator to distinguish successful and errant attempts and make necessary adjustments.

Magnetic tracking including registration of conventional image space and magnetic space potentially offers the guidance advantages of real-time imaging without the additional radiation exposure. The range of available targets is limited primarily by the resolution of the modality used to acquire the preoperative images. Intravascular or intraductal interventions may be more amenable to magnetic tracking guidance as other real-time imaging modalities may not be applicable or available, and absolute positional accuracy is probably not as significant for successful guidewire introduction into vessels or ducts. Guidance accuracy is usually defined relative to the target *size*, i.e., by the diameter of the vessel or duct, distance from the needle tip to the target, and by the resolution of the imaging modality itself. However, in the case of ducts and vessels, the bevel of the needle and the incident puncture angle may significantly affect the outcome as well.

5. Conclusion

A novel magnetic-based needle guidance system featuring respiratory gating has been successfully tested using a specifically designed phantom. This preliminary effort has highlighted two important obstacles which must be overcome before such a system could be widely implemented in clinical practice. First, observed magnetic field distortion by image intensifiers, C-arms, and the CT gantry in the standard Interventional Radiology or CT suite may significantly degrade the accuracy of the system. Second, the catheter-based fiducial must be retrievable yet fixed within a hepatic vein until successful vessel puncture and introduction of a guidewire has been achieved without causing vessel thrombosis.

The ability to conduct accurate needle placement within targeted hepatic structures during resting respirations offers several advantages. First, patients who are too ill to cooperate with respiratory instructions or who are mechanically ventilated could be successfully approached. Second, the number of needle passes necessary to achieve successful vessel puncture in TIPS could be reduced, thereby reducing the complication rate. The data show that the implemented magnetic tracking system can facilitate accurate needle placement in the phantom during simulated respiratory-related organ motion.

Acknowledgements

The design and construction of the phantom and the software was supported in part by an Academic Transition Award from the Cardiovascular and Interventional Radiology Research and Education Foundation (CIRREF). Portions of this work were also funded by U.S. Army grant DAMD17-99-1-9022. The content of this manuscript does not necessarily reflect the position or policy of the U.S. Government. Thanks are due to Northern Digital Inc. for the loan of the AURORA magnetic tracking system.

References

1. Solomon SB, Magee C, Acker DE, Venbrux AC. "TIPS Placement in Swine, Guided by Electromagnetic Real-Time Needle Tip Localization Displayed on Previously Acquired 3-D CT." *Cardiovasc Intervent Radiol*, **22**: 411-414, 1999.
2. Herline A, Stefansic J, Debelak J, et.al. "Image Guided Surgery: Preliminary Feasibility Studies of Frameless Stereotactic Liver Surgery." *Arch Surg*, **34**: 644-650, 1999.
3. Davies S, Hill A, Holmes R, et.al. "Ultrasound Quantitation of Respiratory Organ Motion in the Upper Abdomen." *Brit J. Radiology*, **67**: 1096-1102, 1994.
4. Banovac, F., Levy, E., Lindisch, D., et al. "Feasibility of Percutaneous Transabdominal Portosystemic Shunt Creation." Accepted for publication in *Surgical and Radiologic Anatomy*, January, 2002.

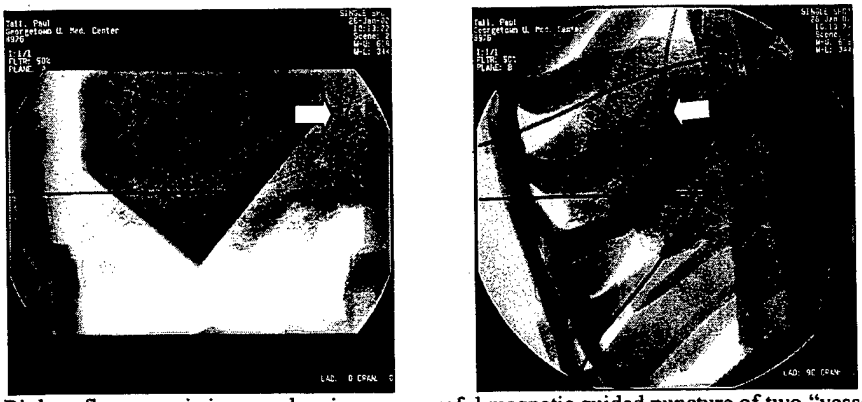

Figure 1: Biplane fluoroscopic images showing a successful magnetic guided puncture of two "vessels" in the liver phantom. The white arrows indicate the tip of the fixed catheter-based fiducial.

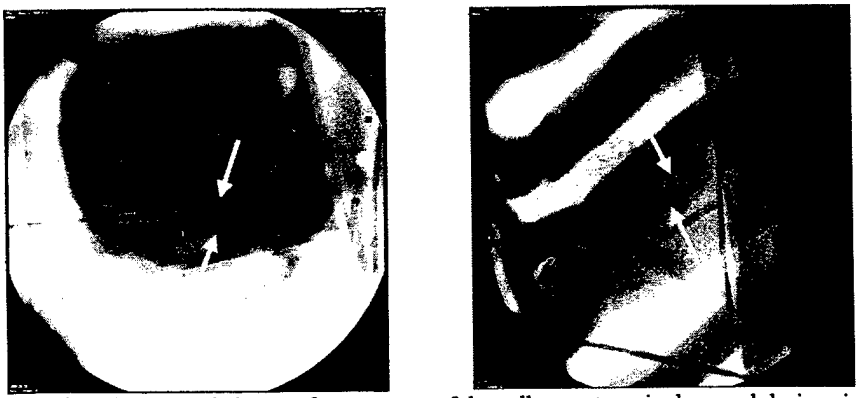

Figure 2: Biplane fluoroscopic images from a successful needle pass to a single vessel during simulated respiratory excursion of 1 cm at a frequency of 24 cycles per minute. The white arrows indicate the "vessel" walls.

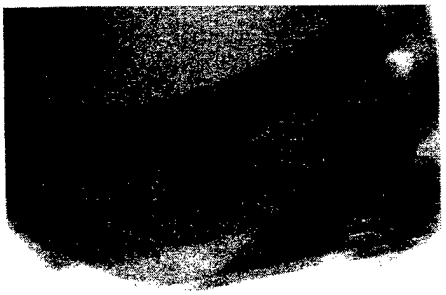

Figure 3: Guidewire test. A/P image showing 0.035 inch diagnostic guidewire inserted through needle into "vessel"

Figure 4: System testing in interventional suite

10.2.7 Mocanu 2003: Fluoroscopy Servoing

Reprint begins on the next page and is 5 pages.

To be presented at SPIE Medical Imaging 2003 and published in the proceedings

Fluoroscopy Servoing using Translation/Rotation Decoupling in an A/P View

Mihai Mocanu[a], Alexandru Patriciu[b,c], Dan Stoianovici[b,c], Dumitru Mazilu[b], David Lindisch[d], Gabriela Corral[d,e], Lucian Gruionu[b], Kevin Cleary*[d]

[a]Department of Software Engineering, University of Craiova, Romania
[b]URobotics Laboratory, Brady Urological Institute, Johns Hopkins Medical Institutions, Baltimore, Maryland, USA
[c]Mechanical Engineering Department, Johns Hopkins University, Baltimore, Maryland, USA
[d]Imaging Science and Information Systems (ISIS) Center, Department of Radiology, Georgetown University, Washington, DC, USA
[e]Biomedical Engineering Department, The Catholic University of America, Washington, DC, USA

ABSTRACT

This paper presents a fluoroscopy servoing algorithm for automatic alignment of a needle using a medical robot during interventional procedures. The goal of this work is to provide physicians with assistance in needle alignment during minimally invasive procedures under fluoroscopy imaging. This may also help reduce radiation exposure for the physician and provide more accurate targeting of internal anatomy. The paper presents the overall concept and describes our implementation along with the initial laboratory results and studies in the interventional suite. The algorithm is based on a single anterior/posterior fluoroscopic image. Future work will be aimed at demonstrating the clinical feasibility of the method.

Keywords: fluoroscopy servoing, medical robotics, spinal interventions

1. INTRODUCTION

Minimally invasive spinal procedures, such as nerve and facet blocks for pain relief, are becoming increasingly common. Our research groups at Georgetown University and Johns Hopkins have been collaborating over the past several years to adapt a needle driver robot to assist the physician in precision placement of instruments in the spine. Needle alignment during these procedures can be time consuming, particularly for inexperienced physicians or physicians who do not do these procedures on a regular basis. To assist the physician in aligning the needle using a robotic device, a few researchers have recently introduced the concept of fluoroscopy servoing. This paper describes our work in this area and presents our preliminary results.

The paper is organized as follows. In Section 2, Methods, we provide some background material on spinal interventions and the use of a robot in these procedures. This is followed by a brief review of previous work in fluoroscopy servoing and an introduction to the concept. Our implementation is then described. Our initial results are then presented in Section 3, followed by conclusions.

*cleary@georgetown.edu; phone (202) 687-8253, fax (202) 784-3479, www.visualization.georgetown.edu, Imaging Science and Information Systems (ISIS) Center, Department of Radiology, 2115 Wisconsin Avenue, Suite 603, Washington, DC, 20007.

2. METHODS

2.1 Interventional Spinal Procedures and Medical Robotics

Intra-operative fluoroscopy is the preferred imaging modality in most interventional radiology procedures. A typical spine intervention is shown in Figure 1. The patient lies prone on the table and the physician uses the fluoroscopy images to guide the needle to the target anatomy. These procedures are all done free-hand and are greatly dependent on the skill of the physician in manipulating the needle. The physician first identifies the skin entry point and then the target, thus defining the desired needle trajectory. The physician then aligns the needle by hand and partially inserts it towards the target. The physician proceeds with further insertion of the needle, checking the position of the needle by re-scanning as necessary. The main problem is that the physician has limitations in accuracy when initially lining up the needle and then staying on course. Additionally, when the physician releases the needle, the needle can drift or tilt away from the desired path.

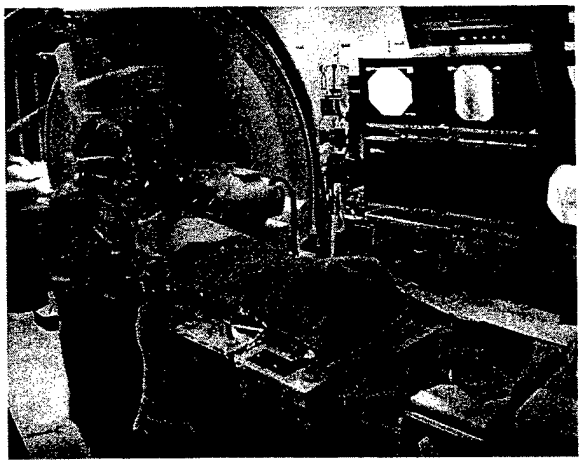

Figure 1: Typical interventional spine procedure at Georgetown and bi-plane fluoroscopy system

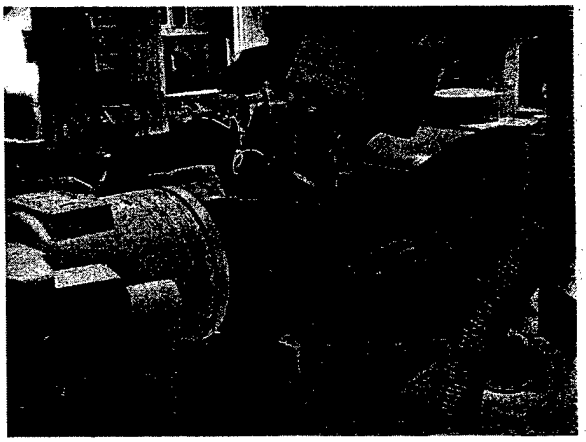

Figure 2: Robotically assisted spine intervention using joystick control

To assist the physician in this process, several research groups have proposed using a robotic device or mechanical guide to hold and manipulate the needle. At Georgetown University, we have adopted the PAKY/RCM robot developed in the Urology Robotics Laboratory at Johns Hopkins Medical Institutions for precision placement of needles in interventional spine procedures such as nerve or facet blocks [1]. A picture of a robotically assisted nerve block from an ongoing clinical trial is shown in Figure 2.

A typical spinal interventional procedure using the robot proceeds as follows:

1. The patient is positioned on the operating table and the lesion is identified on the fluoroscopy image.
2. The robot is mounted on the fluoroscopy table over the patient.
3. The passive arm is unlocked and the needle tip is placed a short distance (a few centimeters) from the skin entry point.
4. The robot is set to translational mode (XYZ stage enabled) using the touch screen and the joystick is used to move the tip of the needle to the skin entry point.
5. The robot is then set to needle orientation mode (only RCM enabled) and the joystick is used to orient the needle toward the target point using A/P fluoroscopy.
6. Finally, the robot is set to needle drive mode (PAKY needle driver enabled) and the joystick is used to drive the needle to the target point using lateral fluoroscopy.

2.2 Fluoroscopy Servoing

Once a robotic approach is taken, a natural extension is to provide automatic alignment of the needle toward the target (step 5 in the scenario described above). The term fluoroscopy servoing is taken to mean the alignment of a needle using

feedback from fluoroscopy imaging. Hence, it is an extension of the term servo control, which denotes feedback control of a motor or mechanism. Fluoroscopy servoing also draws on some ideas from the more general field of visual servoing, which is a well-established method in the field of industrial robotics.

The general concept is shown in Figure 3. The key components of the system are the C-arm (fluoroscopy system), the needle, and the robot. Additional components which are not shown here include the robot control computer and a frame grabber card (Matrox Meteor II PCI model) for digitizing the video signal from the C-arm.

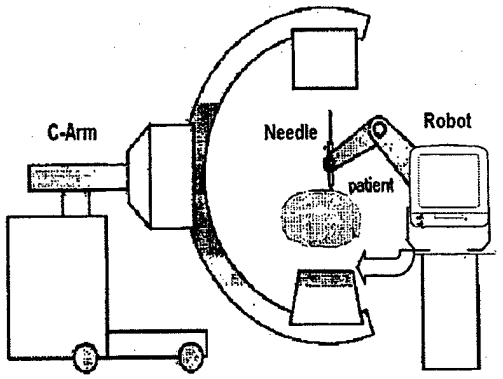

Figure 3: Schematic showing C-arm, patient, needle, and robot (courtesy of Engineering Research Center for Computer Integrated Surgical Systems and Technology, Johns Hopkins University)

The literature on fluoroscopy servoing is sparse as the first attempts to apply this concept have been relatively recent. Loser and Navab developed a two degree of freedom mechanism for automatic alignment of a needle using CT fluoroscopy [2, 3]. They performed a series of experiments with 2 mm metal balls (mean targeting error was about 0.4 mm) and pig organs (mean error about 1.6 mm). Patriciu and colleagues developed a targeting method based on portable fluoroscopy for an earlier version of the PAKY/RCM robot [4]. This method was based on two different fluoroscopy views, with the best precision obtained when the two views were orthogonal. Experimental tests with a 2 mm ball gave a targeting error not greater than 0.5 mm. The clinical feasibility of the method for percutaneous renal access was also demonstrated.

2.3 Our Implementation of Fluoroscopy Servoing

Based on the traditional fluoroscopy scenario described in Section 2.1 and the previous work of Patriciu et al., we developed an algorithm for semi-automatic needle targeting which is relatively independent of C-Arm orientation, as long as an accurate A/P view of both the lesion and needle tip is provided.

To facilitate the automatic detection of the needle in the image, a small black ball is placed at end of the needle opposite from the needle tip, thus providing a well-discriminated signature. A single A/P fluoroscopy image must be initially acquired using the frame grabber and displayed on the computer screen as shown in Figure 4. A pattern-matching algorithm running on the video acquisition board is used to rapidly locate the ball marker in the image. All calculations are performed in a fixed reference frame centered at the needle tip and oriented according to the initial position of the robot. The principle of operation is represented schematically in Figure 5. This figure shows the needle at different positions indicating the phases of the alignment process.

The physician selects the target point in the image using the computer mouse, and must also select the tip of the needle and the ball attached to the needle. By continually frame-grabbing fluoroscopy images, the computer can then automatically move the robot and orient the needle toward the target without operator assistance. First, the needle tip which is initially at P0 (left side of Figure 5) is moved to the fulcrum point F using the translational stage of the robot. Then, the distal end of the needle at P1 is displaced toward P2 on a cone and rotated on the cone to find a third point P3 (or P3'). The point P3, together with P1 and F, defines a servo plane in which the final movement towards P4 will be accomplished to align the needle toward the target T in three dimensions.

The key idea in our approach is to use the natural decoupling of motion found in the manual needle insertion procedure as described in Section 2.1. Therefore, as an aid to the physician in aligning the needle, we use the translational stage of the robot to automatically move the needle tip until it is superimposed on the lesion in the A/P view. Next, we use the rotational stage of the robot to automatically orient the needle about a fulcrum point located at the needle tip until the entire needle is superimposed with the lesion in the same A/P view.

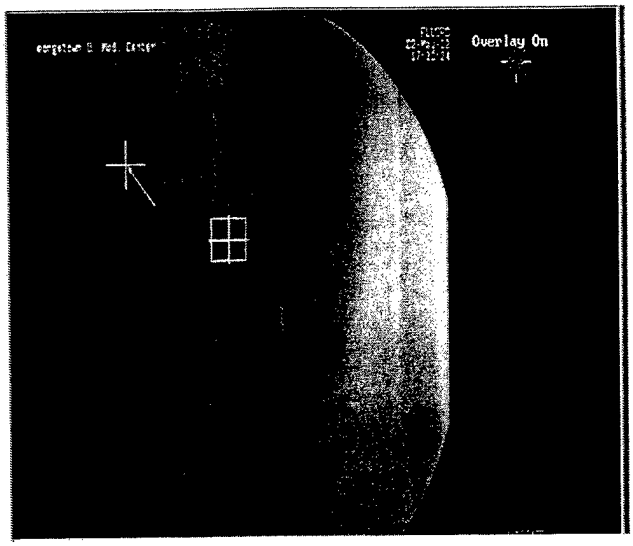

Figure 4: Fluoroscopy image in the A/P view, showing needle and radiodense sphere on its end

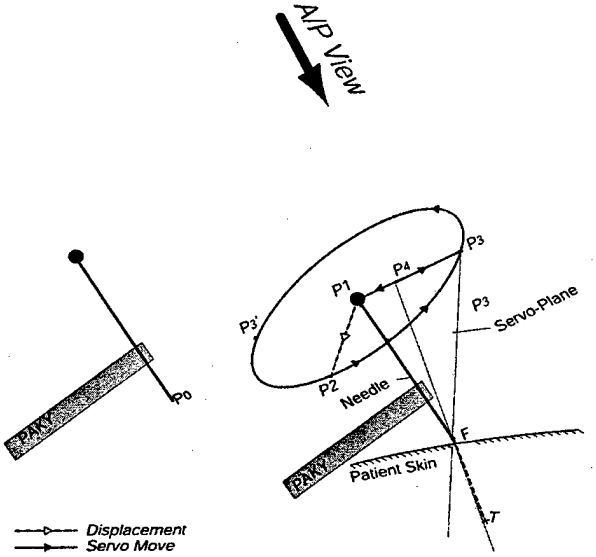

Figure 5: Fluoroscopy servoing algorithm (left side: initial position, right side: orientation steps)

Our fluoroscopy servoing system was implemented using a multi-layered software architecture. The three main layers were defined so that new team members can build on the existing code:

- Base layer: proprietary, vendor-specific software for individual hardware components
  - MEI DSP-series motion control library version 2.5.9
  - Matrox imaging library (MIL) version 6.1
  - Watchdog timer card control library
- Middle layer: in-house C/C++ based libraries including the URoboticsLib for motion control of the robot, which was built on top of the MEI library and designed and tested as a portable API using object oriented methodologies (Visual Modeler UML tool for design and Visual C++ for implementation)
- Top layer: application layer building on the other layers described here

3. RESULTS

3.1 Pre-clinical Validation

Initial testing of the algorithm was done using a video camera mounted in a positioning stand. A white background and a black needle, with a spherical ball at the distant end, were used for achieving proper contrast. Another 2 mm spherical ball represented the target. Repeated tests gave an accuracy of less than 1 mm, providing the positioning plane was near the vicinity of the insertion point. The user interface and an example frame-grabbed image is shown in Figure 6.

3.2 Preliminary Testing in the Interventional Suite

To investigate the feasibility of this technique in the interventional suite, an initial set of tests were done using an abdominal interventional phantom (CIRS Inc., Norfolk, Virginia) and a watermelon. The fluoroscopy system is a Siemens Neurostar bi-plane system and only the A/P plane was used in these experiments. The frame grabber card is connected to the video output of the monitor through a co-axial cable. Testing confirmed that the frame grabber was capable of capturing the fluoroscopy video signal in real-time and displaying it on the monitor. The experiments showed that the robot was capable of reasonably accurate targeting of an internal BB (small metal ball) placed in a watermelon as shown in Figure 7.

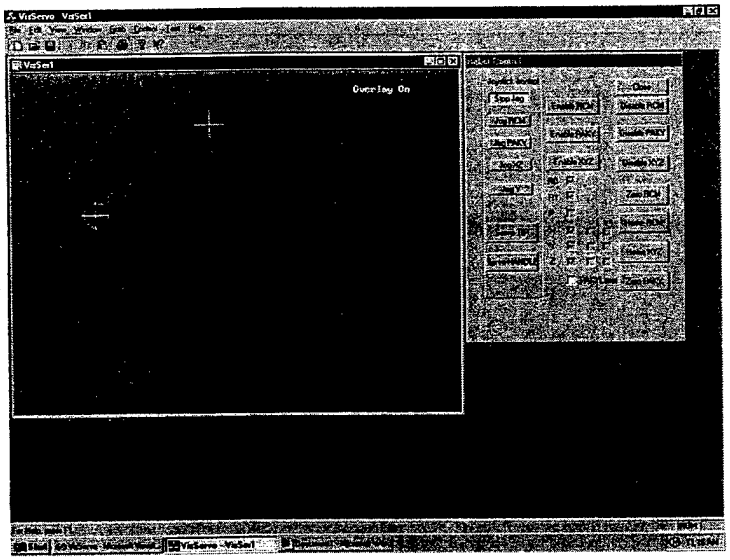

Figure 6: The user interface, showing needle in the image and robot control panel in the screen right side

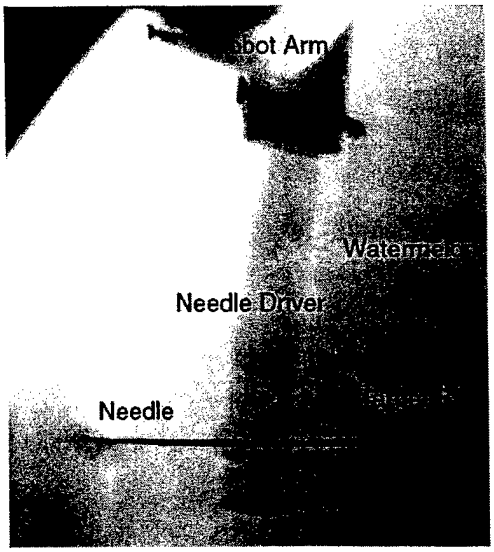

Figure 7: Watermelon phantom study (goal is to hit the target BB with the needle)

4. CONCLUSIONS

This paper presented our work in progress on developing fluoroscopy servoing for interventional spinal procedures using a recently developed medical robot. Preliminary results using a video camera and an initial test in the interventional suite were given. The advantage of this method is that it requires just a single A/P fluoroscopy view to orient the needle. However, the utility of the method in the clinical environment has yet to be demonstrated and this will be the topic of future work.

ACKNOWLEDGMENTS

This work was funded by U.S. Army grant DAMD17-99-1-9022. The content of this manuscript does not necessarily reflect the position or policy of the U.S. Government. The authors would also like to acknowledge useful discussions on fluoroscopy servoing with Nassir Navab, PhD, from Siemens Research Laboratories.

REFERENCES

[1] K. Cleary, D. Stoianovici, A. Patriciu, D. Mazilu, D. Lindisch, and V. Watson, "Robotically assisted nerve and facet blocks: a cadaveric study," *Acad Radiol*, vol. 9, pp. 821-5, 2002.

[2] M. H. Loser, N. Navab, B. Bascle, and R. H. Taylor, "Visual servoing for automatic and uncalibrated percutaneous procedures," in *Medical Imaging 2000: Image Display and Visualization*, vol. 3976, *Proceedings of SPIE*, S. K. Mun, Ed. San Diego, CA: SPIE, 2000, pp. 270-281.

[3] M. H. Loser, N. Navab, "A new robotic system for visually controlled percutaneous interventions under CT fluoroscopy," Medical Image Computing and Computer Assisted Intervention - MICCAI 2000, pp. 887-896.

[4] A. Patriciu, D. Stoianovici, L. L. Whitcomb, T. Jarrett, D. Mazilu, A. Stanimir, I. Iordachita, J. Anderson, R. Taylor, and L. R. Kavoussi, "Motion-Based Robotic Instrument Targeting under C-Arm Fluoroscopy," Medical Image Computing and Computer Assisted Intervention - MICCAI 2000, pp. 988-998.

10.2.8 Xu 2003: Registration and Tracking

Reprint begins on the next page and is 7 pages.

Registration and Tracking of a Needle Placement Robot for CT-Guided Spinal Procedures

Sheng Xu, M.S., Kevin Cleary, Ph.D., *Member, IEEE,* Dan Stoianovici, Ph.D., and Gabor Fichtinger, Ph.D.

***Abstract*—Computed tomography (CT) guided needle placement is a widely accepted practice in the medical field. The efficacy of these procedures is related to the accuracy of needle placement. Current free-hand techniques have limitations in accuracy, particularly when targeting small or deeply situated anatomy. In response to these problems and as a testbed for future developments, we propose a robotically assisted needle placement system consisting of a mobile CT scanner, a needle insertion robot, and an optical localizer. This paper presents the overall systems concept and concentrates on the registration and tracking of the robot and patient. Accuracy results using an abdominal phantom are also presented.**

***Index Terms*—image guidance, medical imaging, medical robotics, needle placement, registration, tracking**

I. Introduction and Background

A. Clinical Significance

RECENT advances in medical imaging have propelled minimally invasive image-guided biopsy and local therapies into public attention [1]. Intra-operative radiological imaging has become more accurate, faster, more affordable, and safer to both patients and physicians. Computed tomography (CT) provides good tissue differentiation and has proven to be a useful image guidance modality for percutaneous (through the skin) drainage [2], biopsy [3], and neurological pain management [4]. Spinal disorders are the fastest growing musculoskeletal subspecialty and it is estimated that over 70% of our population experiences significant low-back pain at some point their lives. CT-guided nerve blocks and facet joint injections have proven to be safe and effective methods to alleviate pain [4].

Currently, percutaneous placement of needles into the spine is performed freehand. Based on CT or fluoroscopy, the physician identifies the skin entry point and the target, thus defining the desired needle trajectory. The physician then aligns the needle by hand and partially inserts it towards the target. The physician proceeds with further insertion of the needle, checking the position of the needle by re-scanning as necessary. The main problem is that the physician has limitations in accuracy when initially lining up the needle and then staying on course. Additionally, when the physician releases the needle, the needle can drift or tilt away from the desired path. In response to these problems, we propose integrating intra-operative CT imaging with a medical robot for precision placement of the needle.

The workflow of the current manual procedure is practically identical to the steps followed by our robotic system. This parallelism offers a unique opportunity for gradual transition from a manual procedure to a fully robotic intervention. While experienced physicians can complete these procedures without difficulty, there is a need for precise and consistent aiming and delivery of the needle. The longevity of pain relief is thought to be associated with the spatial accuracy of needle placement. We also believe our system can serve as a testbed for the precision robotically guided needle placement systems of the future.

B. Prior Technical Developments

The history of medical robotics dates back to 1985, when Kwoh applied a PUMA robot to orient a needle for biopsy of the brain [5]. Other early work with needle placement robots was also focused on intra-cranial neurosurgery [6]-[8]. Since

Manuscript received June 14, 2002. The work was supported by the following organizations: (1) U.S. Army grant DAMD17-99-1-9022, (2) National Science Foundation under the Engineering Research Center grant #EEC 9731478, (3) Whiting School of Engineering and Brady Urological Institute of the Johns Hopkins University.

S. Xu is with the Engineering Research Center, Johns Hopkins University, Baltimore, MD 21218, MD USA (phone: 410-516-4318; fax:410-516-5553; email:sheng@cs.jhu.edu)

K. Cleary is with the Image Science and Information Systems (ISIS) Center, Department of Radiology, Georgetown University Medical Center, Washington, DC 20007 USA (email: cleary@georgetown.edu)

D. Stoianovici is with the James Buchanan Brady Urological Institute, Johns Hopkins Medical Institutions, Baltimore, MD21224 USA (email: dss@jhu.edu)

G. Fichtinger is with the Engineering Research Center, Johns Hopkins University, Baltimore, MD 21218, MD USA (email: gabor@cs.jhu.edu)

A company named Image Guide has been formed to commercialize the robot used in this work. Under a licensing agreement between Image Guide and the Johns Hopkins University, Dr. Stoianovici is entitled to a share of royalty received by the University on sales of the robot presented in this article. Dr. Stoianovici and the University own stock of Image Guide, Inc, which is subject to certain restrictions under University policy. The terms of this arrangement are being managed by the Johns Hopkins University in accordance with its conflict of interest policies. Dr. Cleary is a consultant to Image Guide and is on the scientific advisory board of the company.

then, however, many other clinical applications for needle placement robots have now been proposed, including abdominal interventional procedures. Perhaps the most widely used commercial system for abdominal procedures is the AESOP robot from Computer Motion, which is an endoscopic camera holder that can be voice activated [9]. Taylor pioneered the application of the remote center of motion (RCM) concept for needle placement, which provides rotational motion around a fixed fulcrum point in space. Taylor developed the first such robot for manipulation of laparoscopic instruments [10]. Loser presented a lightweight 5-bar RCM linkage for needle insertion [11] that was guided by visual servoing in a CT fluoroscopy scanner. Stoianovici developed a two degrees-of-freedom (DOF) RCM robot with a radiolucent needle driver for percutaneous renal access under fluoroscopic guidance [12], [13]. Taylor and Stoianovici also adapted the RCM module for microsurgical augmentation [14].

In addition to these hardware developments, many of these researchers and others have attempted to integrate the robotic system with the guiding imaging modality. Yanof [15] integrated an industrial robot arm for needle placement with a CT scanner and completed swine animal studies. Masamune [16] integrated Stoianovici's RCM-PAKY robot and Susil's stereotactic registration method [17] for needle insertion inside a CT scanner. Fichtinger adapted this system for transperineal access to the prostate under intra-operative CT guidance [18]. This system also implemented a simple variant of the "point-and-click needle placement" paradigm, where the target point was selected in an intra-operative image on a computer screen and a spatially registered autonomous robot moved onto the target and entered the needle, without requiring physical intervention from the physician.

C. Contribution of this Paper

The system presented here employs a full 6-DOF robot described in a related paper by Stoianovici [19]. This is in contrast to most previous percutaneous needle placement systems that utilized only 3-DOF robots.

In their research, Masamune, Susil, and Fichtinger all applied image based registration inside a CT scanner. However, the target was assumed to be stationary between the time of registration and complete insertion of the needle, an assumption that may not hold true in many real-life situations. To solve this problem, we added a real-time localization device (Polaris, Northern Digital, Waterloo, Canada) to the overall system. This localization device provides continuous measurement of the relative location of the robot and patient and allows us to compensate for any relative motion between the robot and the target. Real-time tracking of surgical instruments and imaging devices has been applied routinely in image-guided surgery (IGS) systems for navigation purposes. In the spine, pioneering work has been done by Nolte in Bern [20] and Lavallee in Grenoble [21]. The motion of the lumbar spine in the prone position during pedicle screw placement in open surgery has been studied by Glossop and Hu [22]. Several aspects of our tracking method are directly inspired by these systems, including the use of optical tracking and the assumption that the vertebral body behaves as a rigid body.

The novel aspects of our work are the following: (1) automated registration between the target and CT images based on an embedded fiducial device, (2) real-time tracking of the robot and patient, (3) the potential for real-time compensation for displacement of the target due to respiratory motion or patient movement.

II. System Components

A. Clinical Workflow

The main system components are shown in Fig. 1: CT scanner, needle insertion robot, and Polaris localizer. The intra-operative scenario for robotically assisted biopsy or therapy is as follows:

1. The patient is positioned on the table
2. The robot is mounted and calibrated
3. The patient is scanned
4. CT scans are sent to the physician's workstation
5. The physician selects the entry and target locations
6. The robot moves the needle to the entry point
7. The robot orients the needle to the target point
8. The robot inserts the needle to the predefined depth
9. Another CT scan is done for verification
10. The physician injects the therapeutic agent or takes the biopsy sample
11. The robot retracts the needle

The physician supervises each step at the control computer. In order to increase safety, the system halts the execution after each step and waits for confirmation from the physician. In essence, we implemented the "point-and-click needle placement" paradigm, where the physician selects the entry and target points on a computer screen, and an autonomous robot executes the needle placement under the supervision of the physician.

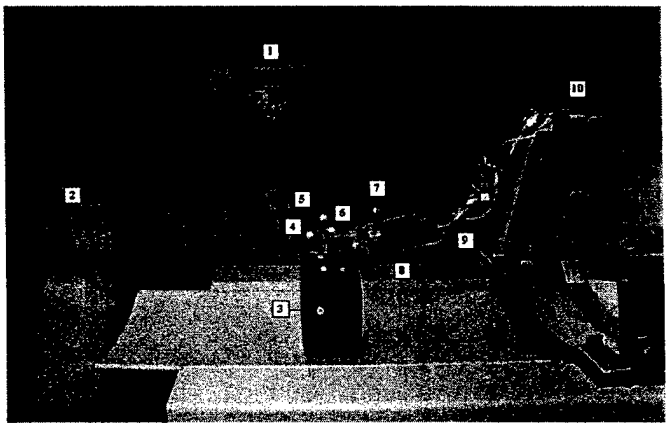

Fig. 1. System components: (1) Polaris (2) CT Gantry (3) Abdominal Phantom (4) Fiducial Carrier (5) Needle (6) Needle Driver (7) Robot Tracker (8) RCM (9) Passive Arm (10) Cartesian Bridge

B. *Planning and Monitoring Software*

The system was tested using a mobile CT scanner (Tomoscan, Philips Medical Systems, Eindhoven, Netherlands) and an abdominal interventional phantom (CIRS Inc., Norfolk, Virginia). The images are transferred from the CT scanner to the robot control computer over an Ethernet connection using the DICOM protocol. The planning and control software is based on 3D Slicer [23], which is a free open-source software package for visualization, registration, and quantification of medical data. Development of the 3D Slicer is an ongoing collaboration between the MIT Artificial Intelligence Lab and the Surgical Planning Lab at Brigham & Women's Hospital, with sustained contribution from the CISST Center in Baltimore.

For this project, the 3D Slicer was modified to provide the following capabilities: (1) path planning interface for the user to select the skin entry point and target point, which can be on different axial slices; (2) control and monitoring of the robot; and (3) control and display for the Polaris localizer. The software was developed using Tcl/Tk and the Visualization Toolkit (VTK).

C. *Needle Placement Robot and Control Software*

Manual needle punctures usually include three decoupled motions as follows. First, the tip of the needle is moved from its current location to the skin entry point. This is a three-dimensional Cartesian motion. Second, the needle is oriented by pivoting around the skin entry point. This motion involves two independent rotations. Finally, one-directional translation is necessary to insert the needle into the body through the skin. Therefore, needle placement requires 3+2+1=6 degrees of freedom.

The kinematic arrangement described in the preceding paragraph is realized in the robotic system used here. The robot contains a 3-DOF Cartesian motion stage, which is mounted over the CT table and bridges the patient. This stage is connected to a 7-DOF adjustable unencoded passive arm, which is used for gross positioning of the needle drive stage. The needle drive stage consists of a 2-DOF remote center of motion component for orientation and a 1-DOF friction-transmission for insertion of the needle. A complete description of the robot can be found in the companion paper by Stoianovici [19].

The control electronics for the robot are housed entirely within a single industrial PC chassis. An 8-axis ISA-DSP card from Motion Engineering is used for motion control. Safety features include current monitoring and a watchdog timer. The software used to control the robot is the modular robot control library (MRC), which has been developed at the Johns Hopkins University. The MRC library is a set of portable C++ classes for distributed and modular robot control, which provides Cartesian level control for serial manipulators. The library also includes classes for kinematics, joint level control, command and command table management, sensor and peripheral support, and networking support via remote procedure calls. MRC can be used in a client/server configuration and this was done in the experiments presented here. The robot server was run on the same computer that controls the robot and the client software was realized as a custom module built in the 3D Slicer package.

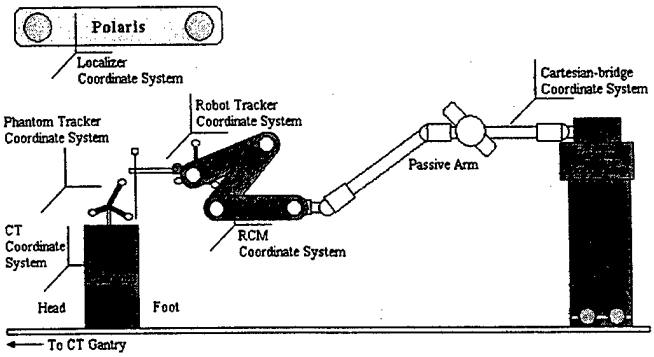

Fig. 2. Coordinate systems

III. Coordinate Transformations and Robot Movement

In our system, the key to accurate needle placement is the precise real-time computation of the coordinate transformations between the robot, patient, and imager. The optical localizing device is used to track patient motion in real-time and to register the robot to the coordinate system of the CT scanner and patient.

Five coordinate systems are used as shown in Fig. 2:

1. **Polaris coordinate system**
2. **CT coordinate system**
3. **Robot-tracker coordinate system** is defined by a rigid fiducial carrier ("robot-tracker" herein), which is mounted on the last link of the robot
4. **Cartesian-bridge coordinate system** defines the Cartesian motion stage of the robot
5. **RCM coordinate system** defines the rotational stage of the robot

Since the Polaris coordinate system is the only stationary coordinate system in our setup, every other coordinate system is transformed into the Polaris coordinate system either directly or through other coordinate systems. The needle placement task, as described in the previous section, requires that the robot first move the needle to the skin entry point and then orient the needle before driving the needle to the target.

A. *Movement to Skin Entry Point*

To move the robot to the skin entry point, the Cartesian motion stage of the robot must be registered with the CT coordinate system in which the patient's anatomy is described. This is done in several steps as follows.

1) Automated Registration of CT to Polaris. For this step, we need a common set of points in both coordinate systems. We attached a rigid plastic fiducial carrier (PassTrax, Traxtal Technologies, Toronto, Canada) to the vertebral body of an abdominal phantom. This carrier contains three retro-reflective spheres (seen by the Polaris) and nine 0.8 mm radiodense microspheres (Tilly Medical, Lund, Sweden) placed in a

known and precise arrangement. Using this fiducial carrier, the computer can automatically determine the position of the nine microspheres in both the Polaris and CT coordinate systems. We then used Arun's singular value decomposition (SVD) technique [24] to determine the transformation matrix between the Polaris and CT coordinate systems. The entry and target points can therefore be transformed from the CT to the Polaris coordinate system.

2) Registration of Needle Tip to Polaris. The initial position of the needle tip is set at the RCM using a laser light embedded in the last link of the robot. To register it to the Polaris, a single passive marker was placed on the needle during the pre-procedure phase as shown in Fig. 3. Using the RCM stage, a full 360° fulcrum motion was executed, while the Polaris was tracking the marker on the needle. Then the needle was retracted by some arbitrary distance and the same fulcrum motion was repeated. The needle defined a cone that now could be reconstructed from the recorded two trajectories of the marker on the needle. The tip of the cone yielded the RCM point in Polaris space.

3) Registration of Cartesian Bridge to Polaris. The movement of the needle to the skin entry point is achieved by using the Cartesian motion stage of the robot. The rotational transformation between the Cartesian motion stage and the Polaris is computed using the robot tracker since the combination of the robot tracker and Cartesian motion stage can be considered a rigid body for pure translations. The Cartesian motion stage was moved to the eight vertices of its maximum workspace, and positional data was simultaneously recorded in the coordinate systems of the Cartesian bridge and Polaris tracker. Similarly to step 1, the rotation matrix between the coordinate systems was then determined using the SVD.

4) Needle Movement. The desired needle movement is from the initial position of the needle tip to the entry point, both of which have been determined above in the Polaris coordinate system. Using the rotational transformation from the Polaris to Cartesian motion stage, the desired movement of the Cartesian motion stage is obtained.

B. Orientation of Needle

To orient the needle along the desired path in CT space, the RCM motion stage of the robot must be registered with the CT coordinate system, which is achieved through the following steps.

1) Path Vector in Polaris Space. This is computed in Step 1 of Section A.

2)Registration of Needle Orientation to Polaris. Similar to Step 2 of Section A, a single passive marker was placed on the needle during the pre-procedure phase and the RCM stage was set to its home orientation. The needle was driven up and down without changing the orientation of the robot, while the Polaris continuously recorded the passive marker position. Finally, the orientation of the needle was calculated using 3D line fitting.

Since the robot tracker is secured to the needle driver, both the needle orientation and the initial position of the needle tip are constant in the robot tracker coordinate system. Therefore, they can be saved as system constants after the registration is performed for the first time. Their corresponding orientation and position in the Polaris coordinate system can be calculated using the transformation between robot tracker and Polaris.

3) Registration of RCM stage to Polaris. The rotational transformation between the RCM stage and Polaris is determined using the robot-tracker. Using the orientation of the robot-tracker before and after a rotation about a single RCM joint, the rotation axis of each joint can be calculated directly in the Polaris coordinate system [25]. The rotation matrix between RCM and Polaris is therefore obtained after both RCM axes are determined.

4) Needle Orientation. Using the results from above, both the initial needle orientation and the desired path vector are transformed to the RCM coordinate system. The inverse kinematics of the RCM are then applied to orient the needle to the path.

C. Track and Compensate Patient Motion

This feature is one of the novel aspects of the system. When the Slicer application is running, a loop is being executed in the background. Inside the loop, the following steps are executed:

1. Read the location of the phantom tracker using the Polaris. Since the phantom tracker is rigidly attached to the spine through a post, its motion is considered identical to the patient's motion.
2. Register CT images to the Polaris with the new posture of the patient obtained in step 1.
3. Update the path vector (the entry point and the target point) in the Polaris coordinate system with the new transformation obtained in step 2.
4. Move the needle tip to the updated skin entry point and align the needle with the updated path vector.

In the second step, since the patient's motion has no effect on the positions of micro-spheres in the CT space, the image-processing part described in section III-A is not repeated. This saves a large amount of CPU time and makes real-time tracking and compensation possible. Our current update rate does not allow for real-time performance, because the control software was not designed to accommodate fast motion. Our

Fig. 3. Needle with a passive marker on its tip

accomplishment is making real-time performance possible from the perspective of positional updates.

IV. Experimental Results

In engineering validation of a device for interventional procedures, the software and hardware elements of the system need to be validated in idealized experiments when no contact is made with a human body, as well as in experiments when actual needle insertion takes place. Extensive experiments were done to determine the predictable portion of the system accuracy on both surface and aerial targets. An abdominal phantom with both surface and internal fiducials was CT scanned with 1.0 mm slice thickness and 0.742 mm pixel size. The passive arm was positioned in an arbitrary position. The phantom was moved into the robot's workspace within the field of view of the Polaris localizer, and then validation procedures began.

A. *Translation Accuracy*

This task was to determine the accuracy of guiding the needle tip to the entry point. It was accomplished using the special needle with a single passive marker on its tip. According to the manufacturer, the root-mean-square (RMS) error of the Polaris when tracking a single passive marker is 0.35 mm. After registration, a sample entry point was identified in the CT image. This entry point was selected in air above the phantom to avoid a potential collision between the passive marker and the phantom. The Cartesian stage was commanded to move the needle tip from its current position to the entry point. The position of the passive marker was recorded and then transformed back to the CT coordinate system. The error between the original entry point and the transformed needle tip was then calculated in the CT coordinate system. We tested 20 different entry points without re-registering the robot. The average translational distance of the needle tip to the entry point was 31.22 mm. The mean positioning error was 0.52 mm, with a standard deviation of 0.15 mm. The maximum translation was 45.29 mm with an error 0.42 mm.

The procedure followed in this experiment and the following experiment B was to identify the input (desired path) in CT space, measure the output (needle position or orientation) in Polaris space, and compare the difference between input and output in CT space. Since both the forward and inverse transformations between CT and Polaris are involved in the measurements, the results do not reflect the accuracy of CT-Polaris registration. This accuracy was determined by two factors: (a) the intrinsic 0.35 mm RMS error of the Polaris and (b) the error of image-based detection of microspheres in the fiducial carrier, which was evaluated by the Fiducial Registration Error (FRE) formula [26], yielding 0.26 mm for nine microspheres.

B. *Orientation Accuracy*

As in task A, we placed a single passive marker on the needle tip on its tip to evaluate the alignment of the needle with the desired path vector. After the path vector was identified in the CT images, the system automatically aligned the needle with this vector. To check the result, the needle was then driven up and down, and the position of the passive marker was recorded continuously by the Polaris. Using 3D line fitting, the needle vector in the Polaris coordinate system was then obtained. The needle vector was transformed back to the CT coordinate system and compared with the desired path vector. The error between the two vectors was calculated. We selected 20 arbitrary angles while keeping the phantom fixed. The mean error was 0.70 degrees, with a standard deviation of 0.42 degrees.

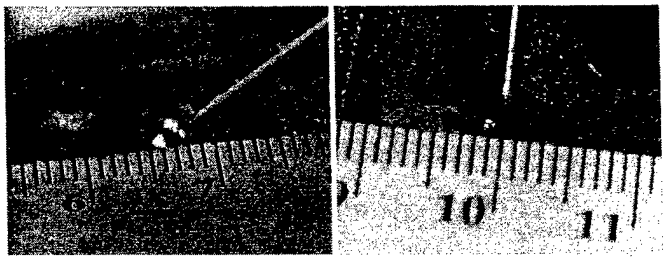

Fig. 4. Orthogonal views of needle touching a fiducial (ruler unit 1mm)

C. *Overall System Accuracy*

The system accuracy test was carried out statically and dynamically using a digital camera to verify the results. We applied 1.0 mm diameter lead balls on the phantom surface as target points for the robot. The entry point was selected in the air above the phantom and the target point was one of the lead balls. In the static test, after the registration step, the robot was commanded to move the needle tip to an entry point and align the needle with the desired path. The needle was then driven to the target point. Two orthogonal pictures were taken with the digital camera and a ruler in the field of view as shown in Fig. 4. We repeat the experiment five times with the same target point but from different entry points. The average distance between the target point and the needle tip was 1.00 mm, with a standard deviation of 0.26 mm. The dynamic test was almost the same as the static test except that every time the phantom was moved to an arbitrary new position and re-registered. We repeated the dynamic test six times. The average error was 1.66 mm, with a standard deviation of 0.38 mm. In both tests, the insertion angles were uniformly selected in the robot's workspace. The needle tip translation ranged from 17.0 mm to 47.4 mm. The insertion depth ranged from 34.8 mm to 60.1 mm.

To test the system on an internal target point, we also implanted a fiducial as the target point at a clinically representative location inside the phantom. When using sub-surface targets, tissue-needle interaction forces may affect the results. These effects include the tangential slippage upon penetrating the entry surface, the deflection of the needle, the target displacement, and the slippage of the needle in the friction transmission. Since the phantom is made from foam and rubber and the perispinal targets are usually relatively superficial, we believe most of these effects are small. Slippage of the needle was monitored by visually observing a depth marker placed on the needle before insertion. When slippage was detected, we drove the needle further directly from the operator's console using the marker as a depth encoder. Fig. 5 shows a confirmatory CT image with the

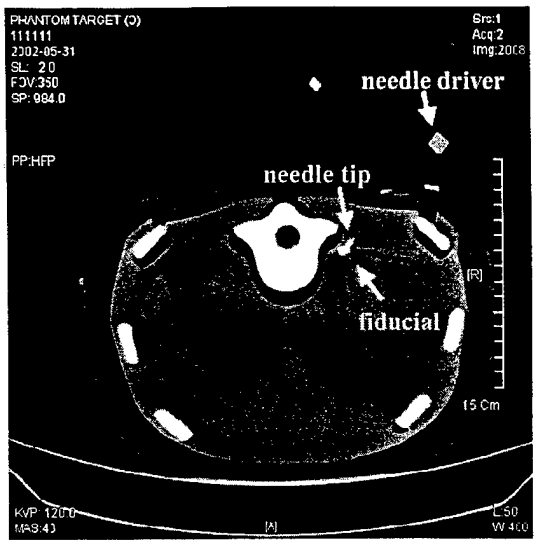

Fig. 5. Accuracy test and internal fiducial

needle directly touching the implanted fiducial. The planned path to the metal ball was on an oblique plane, passing through twelve axial 1 mm CT slices.

V. Discussion

The system presented here was intended to demonstrate the concept of simultaneous registration of the needle placement robot and the patient's anatomy and the potential for real-time compensation of intraoperative motion. The phantom studies here showed that the system is highly accurate. While the phantom experiments validated the overall concept, several weaknesses were identified that need to be addressed.

First, the robot was rather sluggish in following the motion of the phantom. It took about one second to re-adjust the position and orientation of the needle when the phantom was moved. As noted before, however, the software used here has not been optimized for real-time performance. In fact, the needle placement robot is not usually intended to perform rapid motions, in order to reduce the potential for injury to the patient.

Second, the system did not achieve a sufficiently large working volume, mainly due to interference between the relatively large tracking fiducials and the end-effector of the robot. We could not reach all clinically significant locations in the phantom, especially in oblique angles. The dimensions of the fiducial carriers need to be reduced and relocated both on the robot and the patient to alleviate this interference problem. The fiducial carrier and associated locking pin attached to the spinous process is rather large and more invasive than desired in the clinical setting.

The experiments also reinforced our previous observations that needle-tissue interaction may be a significant source of error in needle placement. Ideally, the needle should be perpendicular to the skin surface during initial insertion to avoid slippage and minimize needle deflection during penetration. Inhomogeneities in subcutaneous tissue can cause additional errors. A penetrating needle can induce deformation and displacement of soft tissue targets. Spinning the needle during advancement could reduce tissue resistance, thereby reducing deformation and displacement of the target tissue. The authors and colleagues have developed several prototypes of a spinning needle injector for this purpose [14], [27].

The current needle driver uses a friction transmission, which has a limited exertion force. If the resistance of the tissue is greater than the maximum transmission force, the needle will slip and stop short of the target. We experienced occasional slippage of the needle in the phantom experiments. The spinning needle injector mentioned above may also help alleviate this problem.

Before human trials can be considered, a detailed safety evaluation of the entire system, including the robot, the end-effector, and the control software must be performed. The current end-effector cannot automatically release the needle if excessive force or movement is detected. This is a potential safety problem if the control system cannot rapidly detected and compensate for involuntary movement of the patient.

In conclusion, this paper showed the feasibility of the overall concept and demonstrated reasonable accuracy in phantom trials. Several weaknesses were identified that need to be resolved before an automated needle placement robot system can be proposed for human trials.

Acknowledgment

The authors gratefully acknowledge the longstanding support and advice of Louis R. Kavoussi, MD (Brady Urological Institute) and Russell H. Taylor, PhD (Engineering Research Center), both at the Johns Hopkins University. We also thank David Lindisch, RT, for his assistance with the experiments at Georgetown University.

References

[1] R. K. Jain, "The next frontier of molecular medicine: Delivery of therapeutics," Nature Medicine, vol. 4, pp. 655-657, 1997.

[2] D. M. Yousem, M. J. Sack and K. A. Scanlan, "Biopsy of parapharyngeal space lesions," Radiology, vol. 193, pp. 619-622, 1994.

[3] M. J. Sack, R. S. Weber, G. S. Weinstein, A. A. Chalian, H. L. Nisenbaum and D. M. Yousem, "Image-guided fine-needle aspiration of the head and neck: five years' experience," Archives of Otolaryngology - - Head & Neck Surgery, vol. 124, no. 10, pp. 1155-1161, 1998.

[4] A. Gangi, J. L. Dietemann, R. Mortazavi, D. Pfleger, C. Kauff and C. Roy, "CT-guided interventional procedures for pain management in the lumbosacral spine," Radiographics, vol. 18, no. 3, pp. 621-633, 1998.

[5] Y. S. Kwoh, J. Hou, E.A. Jonckeere and S.Hayati, "A robot with improved absolute positioning accuracy for CT guided stereotactic brain surgery," IEEE Trans. Biomed. Eng., vol. 35, no. 2, pp. 153-160, Feb. 1988.

[6] J.M. Darke, M. Joy, A. Goldenberg, et. al. "Computer and robotic assisted resection of brain tumors," Proc. 5th Int. Conf. on Advanced Robotics, pp. 888-892, 1991.

[7] D. Glauser, H. Fankhauser, M. Epitaux, J. L. Hefti, and A. Jaccottet, "Neurosurgical robot Minerva: first results and current developments," J. Image Guid. Surg., vol. 1, no. 5, pp. 266-272, 1995.

[8] K. Masamune, L. H. Ji, M. Suzuki, T. Dohi, H. Iseki, K. Takakura. "A Newly Developed Stereotactic Robot with Detachable Drive for Neurosurgery," Lecture Notes in Computer Science, Proc. of MICCAI'98, pp. 215-222, 1998.

[9] Surgical robotics, "Evaluation of the Computer Motion AESOP 3000 robotic endoscope holder," Health Devices, vol. 31, no. 7, pp. 256-268. July 2002.

[10] R. H. Taylor, J. Funda, B. Eldridge, K. Gruben, D. LaRose, S. Gomory, M. Talamini, L. Kavoussi, J. Anderson, "A Telerobotic Assistant for Laparoscopic Surgery," IEEE EMBS Magazine Special Issue on Robotics in Surgery, pp. 279-291, 1995.

[11] M. Loser and N. Navab, "A new robotic system for visually controlled percutaneous interventions under CT Fluoroscopy," MICCAI 2000, Lecture Notes in Computer Science, Springer Verlag, vol. 1935, pp 887-896, 2000.

[12] D. Stoianovici, J. A. Cadeddu, R. D. Demaree, H. A. Basile, R. H. Taylor, L. L. Whitcomb, W. N. Sharpe, L. R. Kavoussi, "An Efficient Needle Injection Technique and Radiological Guidance Method for Percutaneous Procedures," Lecture Notes in Computer Science, CVRMed-MRCAS, Springer-Verlag, vol. 1205, pp. 295-298, 1997.

[13] D. Stoianovici, L. L. Whitcomb, J. H. Anderson, R. H. Taylor, and L. R. Kavoussi, "A Modular Surgical Robotic System for Image-Guided Percutaneous Procedures," Int. Conf. Medical Image Computing and Computer-Assisted Intervention (MICCAI), Springer-Verlag, vol. 1496, pp. 404-410, 1998.

[14] R. H. Taylor, P. Jensen, L. Whitcomb, A. Barnes, R. Kumar, D. Stoianovici, P. Gupta, Z. Wang, E. deJuan, and L. Kavoussi, "A Steady-Hand Robotic System for Microsurgical Augmentation," International Journal of Robotics Research, vol. 18, no. 12, pp. 1201-1210, Dec. 1999.

[15] J. Yanof, J. Haaga, P. Klahr, C. Bauer, D. Nakamoto, A. Chaturvedi, and R. Bruce, "CT-integrated robot for interventional procedures: Preliminary experiment and computer-human interfaces," Computer Aided Surgery vol. 6, pp. 352-359, 2001.

[16] K, Masamune, G. Fichtinger, A. Patriciu, R. C. Susil, R. H. Taylor, L. R. Kavoussi, J. H. Anderson, I. Sakuma, T. Dohi, and D. Stoianovici, "System for robotically assisted percutaneous procedures with computed tomography guidance," Computer Aided Surgery, vol. 6, no. 6, pp. 370-383, 2001.

[17] R. C. Susil, J. H. Anderson, R. H. Taylor, "A Single Image Registration Method for CT-Guided Interventions," Lecture Notes in Computer Science, MICCAI'99, Springer-Verlag, vol. 1679, pp. 798-808, 1999.

[18] G. Fichtinger, T. L. DeWeese, A. Patriciu, A. Tanacs, D. Mazilu, J. H. Anderson, K. Masamune, R. H. Taylor, and D. Stoianovici, "System for robotically assisted prostate biopsy and therapy with intraoperative CT guidance," Acad. Radiol., vol. 9, no. 1, pp. 60-74, Jan. 2002.

[19] D. Stoianovici, K. Cleary, D. Mazilu, A. Patriciu, A. Stanimir, N. Craciunoiu, V. Watson and L. Kavoussi, "AcuBot: A Robotic System for Radiological Interventions," submitted for publication, this special issue.

[20] L. P. Nolte, M. A. Slomczykowski, U. Berlemann, M. J. Strauss, R. Hofstetter, D. Schlenzka, T. Laine, and T. Lund, "A new approach to computer-aided spine surgery: fluoroscopy-based surgical navigation," Eur Spine J. 9 Suppl 1:S78-88, Feb. 2000.

[21] S. Lavallee, P. Sautot, J. Troccaz, P. Cinquin and P. Merloz, "Computer-assisted spine surgery: a technique for accurate transpedicular screw fixation using CT data and a 3-D optical localizer," J Image Guid Surg. vol. 1, no. 1, pp. 65-73, 1995.

[22] N. Glossop and R. Hu, "Assessment of vertebral body motion during spine surgery" Spine, vol. 22, no. 8, pp. 903-909, Apr. 1997.

[23] D. T. Gering, A. Nabavi, R. Kikinis, N. Hata, L. J. O'Donnell, W. E. Grimson, F. A. Jolesz, P. M. Black, and W. M. Wells, "An integrated visualization system for surgical planning and guidance using image fusion and an open MR," Journal of Magnetic Resonance Imaging, vol. 13, no. 6, pp. 967-975, June 2001.

[24] K. S. Arun, T. S. Huang, and S. D. Blostein. "Least-square fitting of two 3d point sets," IEEE Trans. Pattern Anal. Machine Intell., vol. 9, no. 5, pp. 698-700, Sept. 1987.

[25] M.W. Spong and M. Vidyasagar, "Robot Dynamics and Control", Hardcover, John Wiley & Sons, 1989, pp. 43.

[26] J. M. Fitzpatrick, J.B. West and C. R. Jr. Maurer, "Predicting error in rigid-body point-based registration," IEEE Trans. Medical Imaging, vol. 17, no. 5, pp. 694-702, Oct. 1998.

[27] Stoianovici et al. "Controllable Motorized Device for Percutaneous Needle Placement in Soft Tissue Target and Methods and Systems Related Thereto" (DM: 3752) US Application 09/943,751 filed 08/30/2001; PCT Application US01/27228 filed 08/30/2001.

Sheng Xu received the B.S. degree from Zhejiang University, Hangzhou, China, in 1995, and the M.S. degree from Tsinghua University, Beijing, China, in 1998, both in Biomedical Engineering. Currently, he is a Ph.D. candidate in the Computer Science department of the Johns Hopkins University. His research interest is medical image processing and medical robotics.

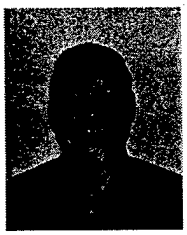

Kevin Cleary earned BS (1982) and MS (1983) degrees in Mechanical Engineering from Duke University and the PhD degree in Mechanical Engineering from the University of Texas System at Austin (1990).

Dr. Cleary was an NSF-sponsored postdoctoral fellow at the Mechanical Engineering Laboratory in Tsukuba, Japan. He then joined the Hughes STX Corporation as a robotics engineer at NASA's Goddard Space Flight Center. In 1996, he moved to Georgetown University where he began his current career as a medical researcher. For the past several years, Dr. Cleary has led a group of researchers in technology developments for minimally invasive procedures, including medical robotics and magnetic tracking of instruments.

Dan Stoianovici received a M.S. degree from the University of Craiova, Romania in 1990 and a Ph.D. degree from Southern Methodist University, Dallas, Texas in 1996, both in the field of Mechanical Engineering. His specialty is Surgical Robotics, in particular Robot Design. In 1996 he joined the research group at the Johns Hopkins School of Medicine where he is Assistant Professor of Urology and Director of the URobotics Program. Dr. Stoianovici has a joint appointment in the Mechanical Engineering Department at JHU where he teaches Computer Aided Design. His research is focused on the design and manufacturing of surgical robotics: surgical instrumentation and devices, image-guided robots, and remote surgery systems. His bibliography includes numerous articles, presentations, and twelve patens of invention of which eight have been licensed by industry..

Gabor Fichtinger earned BS (1986) and MS (1988) degrees in electrical engineering and the PhD (1990) degree in computer science from the Technical University of Budapest, Hungary.

After completing a post-doctoral fellowship at the University Texas System at Austin, he became a senior clinical engineer and research faculty at the George Washington University Medical Center, where he developed radiotherapy and neurosurgery planning systems for over a dozen treatment modalities. He joined the Johns Hopkins University in 1999. His primary research interest is robotically assisted image-guided needle placement, with special regard to prostate, spine and liver procedures. Dr. Fichtinger leads the "Percutaneous Therapy and Biopsy" research at the NSF-funded Engineering Research Center for Computer Integrated Surgical Systems and Technology.

10.3 Posters

Copies of the seven posters produced during this reporting period are reproduced in this section.

10.3.1 Banovac 2002a: Liver Tumor Biopsy

Poster is reproduced on the next page. Presented at the MICCAI conference in September 2002 in Tokyo, Japan.

Liver Tumor Biopsy in a Respiring Phantom with the Assistance of a Novel Electromagnetic Navigation Device

Filip Banovac, MD[1]
Neil Glossop, PhD[1]
David Lindisch, RT[1]
Daigo Tanaka, MA[1]
Elliot Levy, MD[2]
Sheng Xu, MS[1]
Kevin Cleary, PhD[1]

[1] Imaging Science and Information Systems (ISIS) Center, Department of Radiology, Georgetown University Medical Center, Washington, DC, USA
[2] Georgetown University Hospital, Washington, DC, USA
[3] Frontal Technologies, LLC, Fairfax and Bellaire, TX, USA
[4] NSF Engineering Research Center for Computer-Integrated Surgical Systems and Technology, Johns Hopkins University, Baltimore, MD, USA

Georgetown University Hospital
MedStar Health

PURPOSE

The purpose of this study was to evaluate the usefulness of magnetic tracking and image guidance for precision biopsy of simulated lesions in a moving liver phantom. This study was based on a liver respiratory motion simulator developed by our group and the AURORA™ magnetic tracking system under development by Northern Digital Inc., Ontario, Canada.

INTRODUCTION

Image-guided systems for intervention in the thorax and abdomen have not been developed, in part because of problems related to organ motion induced by respiration. The internal organs are not rigid nor directly accessible and therefore difficult to track and register for purposes of image guidance. This is in contrast to intracranial and musculoskeletal interventions where image-guided systems based on bony landmarks have been developed by many researchers and commercial systems are available.

SYSTEM COMPONENTS

To evaluate magnetic tracking for minimally invasive abdominal interventions, we have developed a liver respiratory motion simulator (Figure 1). The simulator consists of a dummy torso, a synthetic liver model, a motion platform, a graphical user interface, the AURORA magnetic tracking system, and a magnetically tracked needle as previously described [1, 2].

Liver Phantom

A human torso model containing a liver phantom was modified from our previously described prototype [2]. The liver phantom (Figure 2) was made from a two part flexible foam (FlexFoam III, Smooth-On, Easton, PA) which was cast from a custom made mold. The foam material was cured to approximately simulate liver tissue resistance to needle puncture. Two elliptical tumors (maximum diameters of 3.1 and 2.2 cm) containing radio-opaque CT contrast were incorporated into the liver model prior to curing to serve as tumor targets. The liver was attached to a linear motion platform at the base of the torso's right abdomen (Figure 3).

Figure 2: Liver Model

The platform can be programmed to simulate physiologic cranio-caudal motion of the liver with options for respiratory rate control, breath depth, and breath pause (breath hold). A rib cage and single layer latex skin material (Limbs and Things, Bristol, UK) were added for aesthetic and physical reality.

Figure 3: A foam liver model (white) mounted on a linear platform inside the torso model.

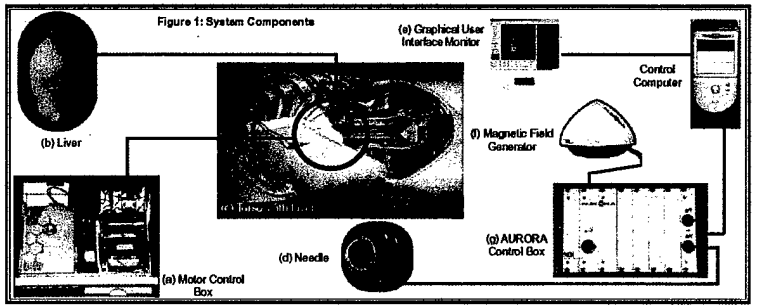

Figure 1: System Components

Magnetic Tracking Device and Sensors

A prototype of a new magnetic field based tracking system, the AURORA, was used in the experiments. The system consists of a control unit, sensor interface device, and field generator as shown in Figure 4.

The AURORA uses cylindrically shaped sensors that are extremely small (0.9 mm in diameter and 8 mm in length). This enables the sensors to be embedded into surgical instruments. We used two magnetically tracked instruments in these experiments: 1) A prototype 5-French catheter with an embedded sensor coil provided by Northern Digital Inc.; and 2) A needle/probe combination (MagTrax) as shown in Figure 5.

The MagTrax (Trantal Technologies, Bellaire, Texas) needle/probe consists of a 15 cm stylette with a magnetic sensor at its tip and an 18-gauge cannula. This instrument was used in the study to puncture the tumors.

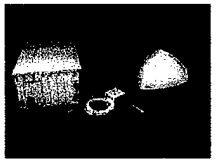

Figure 4: AURORA control unit and field generator (courtesy of Northern Digital Inc.)

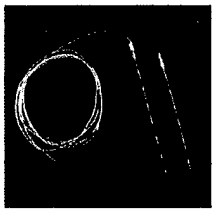

Figure 5: MagTrax needle/probe with a stylette containing a magnetic sensor in its tip and leads exiting the hub. An 18-gauge cannula is seen on the right.

Guidance System and Software

APC-based software application called ROGS (Respiring Organ Guidance System) was developed to assist the physician in performing the puncture of the liver parenchyma and needle guidance into the liver tumors. The system incorporates a graphical user interface shown in Figure 6. The ROGS software allows for the loading of serial axial CT images, pre-procedural planning to the target of interest, tracking of respiratory motion, and real-time display of the biopsy needle as it approaches the target tumor. The sequence of steps in path planning and needle placement is shown in Figure 7.

Figure 6: Graphical user interface (center window shows probe overlaid on image, respiratory tracking in upper right, targeting window in lower right).

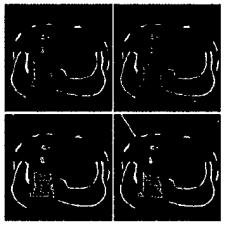

Figure 7: Target tumor on an axial image of the phantom torso is selected by the radiologist (a); subsequently, the radiologist selects the skin entry point (b) and a planned path appears on the reconstructed image; the needle/probe is placed at the skin entry point (c) using cross hairs targeting window (Fig 6, lower right); finally, the needle is driven into the tumor (d) along the planned path indicated by the dotted line.

TUMOR BIOPSY EVALUATION

A series of tumor targeting experiments were performed to test the usefulness of the system in accurately guiding a user to a target while the phantom resumes physiologic respiration. Two users (F.B. and D.L) independently performed 8 punctures each. The experimental design was divided into three stages.

Stage 1: CT Scanning and Registration

1. A magnetically tracked catheter was wedged in the hepatic vein of the liver. Several skin fiducials (multimodality markers, IZI Medical, Baltimore, Maryland) were placed on the rib cage.
2. A series of 3 mm axial slices with 1 mm axial reconstructions were obtained on CT VolumeZoom (Siemens, Erlangen, Germany) from the base of the lungs through the liver while the liver was kept in end-inspiration (simulating the breath-hold technique used in clinical practice).
3. The images were transferred to the PC using the DICOM standard.
4. The tracking catheter was left in the hepatic vein and the simulator was moved to the interventional radiology suite. The magnetic field generator was positioned near the phantom above the chest.
5. The position of the wedged catheter was read in the magnetic coordinate system. The position of the skin fiducials were read in the magnetic coordinate system by touching each fiducial with the MagTrax needle/probe.
6. The position of the catheter and fiducials was determined in CT coordinate space by prompting the user to select these same points on the CT images.
7. A least-squares fit registration algorithm was invoked to determine the transformation matrix from magnetic space to CT space.

Stage 2: Biopsy Path Planning Phase

8. Each user was allowed one practice "planning phase" and "puncture (biopsy) phase" to get familiarized with the software.
9. The user selected the target and a suitable skin entry point by scrolling through the axial images (Figure 7a and 7b) and selecting a biopsy path.
10. Simulated respirations were initiated at 12 breaths per minute with 2 cm cranio-caudal liver excursion.

Stage 3: Biopsy Phase

11. The MagTrax needle/probe was positioned on the skin entry point as determined in the "planning phase" and displayed by the software overlay.
12. A real-time display of the current liver position was displayed by the software system based on the position of the magnetically tracked catheter.
13. The MagTrax needle was tracked in real-time and the transformation matrix computed in step 7 was used to compute the overlay of the probe on the CT images which were reconstructed so to show the planned path of the needle.
14. When satisfied with the target position relative to the planned path, the user would initiate temporary cessation of respiration (simulating a 20 second breath hold in clinical practice). If the allotted time was exceeded, the phantom would continue spontaneous respirations for a minimum of 20 seconds (hyperventilation in clinical practice). Any partially inserted needle would be left in place as is frequently done during biopsy procedures.
15. Repeating step 14 the user would keep making minor adjustments to the needle until satisfied with the needle position as displayed on ROGS.
16. The time for each "planning phase" and "biopsy phase" were recorded. Multi-projection fluoroscopic images were taken at the end of each needle placement to ascertain whether the target tumor was successfully punctured.

PRELIMINARY RESULTS

The targeted tumor was successfully punctured in 14 out of 16 attempts (87.5%). This was done without any additional real-time imaging guidance such as fluoroscopy. Instead, fluoroscopy was used to confirm the final location of the needle and evaluate accuracy.

Each user missed the target tumor once. In those instances, the maximal tangential distance from the lesion to the needle was 3.98 mm. On most occasions, the user was able to reach the tumor in a single continuous puncture after the needle was positioned on the skin entry point. The planning time, needle manipulation time, and total procedure times for the 16 trials are presented in Table 1.

	Mean Planning Time (s) ± SD	Needle Manipulation Biopsy Time (s) ± SD	Total Procedure Time (s) ± SD
User 1	72 ± 35	79 ± 40	151 ± 69
User 2	61 ± 31	111 ± 41	172 ± 43
Overall	71 ± 36	93 ± 43	163 ± 67

Table 1. Planning, needle manipulation and total procedure times for ROGS assisted biopsy of tumors in a respiring liver phantom

CONCLUSIONS

The integrated navigation system for image guided procedures as described here is a paradigm for future applications in minimally invasive radiology and surgery. The system serves as a first step in validation of magnetic tracking technology as it would be applied in assisting physicians to perform minimally invasive procedures on internal organs that move during the respiratory cycle.

This demonstration conveys the use of this system in a liver model; as such it could be applied to help target small liver tumors for biopsy or ablation. The experiments were completed in the interventional suite and showed the feasibility of using the AURORA system in that environment. In the future the system could be applied to percutaneous cholangiography, percutaneous biliary drainage, and portosystemic shunt creation. It is also amenable to modifications that would expand its uses to most intra-abdominal and intrathoracic organs.

BIBLIOGRAPHY

1. Cleary, K., Banovac, F., Levy, E., Tanaka, D. *Development of a Liver Respiratory Motion Simulator to Investigate Magnetic Tracking for Abdominal Interventions.* SPIE Medical Imaging 2002. San Diego, CA. Vol. 4681.
2. Banovac, F., Cleary, K., Levy, E., Lindisch, D., Onda, S., Tanaka, D. *Design and Construction of a Liver Phantom for CT Imaging and Interventions that Simulates Liver Motion Seen During Respiration.* Radiological Society of North America 87th Scientific Assembly and Annual Meeting 2001 Chicago, IL. Vol. 221

ACKNOWLEDGMENTS

This work was funded by U.S. Army grant DAMD17-99-1-9022, an NIH National Research Service Award Fellowship (F32HL68394-01), and a CIRREF Academic Transition Award. The content of this manuscript does not necessarily reflect the position or policy of the U.S. Government. The authors would like to thank Northern Digital Inc., for the loan of the magnetic tracking system.

10.3.2 Banovac 2002b: Abdominal Interventions

Poster is reproduced on the next page. Presented at the CARS conference in June 2002 in Paris, France.

Feasibility of Image-Guided Abdominal Interventions Using a Novel Magnetic Position Sensing Device in an Interventional Radiology Suite

Filip Banovac[a]
Neil Glossop[b]
Michael Jay[a]
David Lindisch[a]
Kevin Cleary[a]

Georgetown University Hospital
MedStar Health

Purpose

The purpose of this study was to evaluate the accuracy of a new magnetic localizing system (AURORA™, Northern Digital Inc., Waterloo, Canada) (Figure 1) in the interventional radiology environment (Figure 2). The study evaluated the positional accuracy of a new needle probe (MagTrax™ Needle Probe, Traxtal Technologies, Bellaire, TX) that contains a small embedded magnetic position sensor near the tip of the needle (Figure 3). This work is part of our research effort to incorporate magnetic tracking in an image-guided system for minimally invasive abdominal interventions.

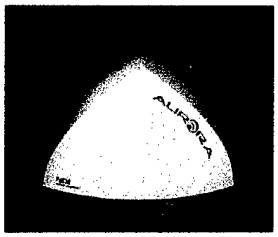

Figure 1. AURORA Magnetic Field Generator

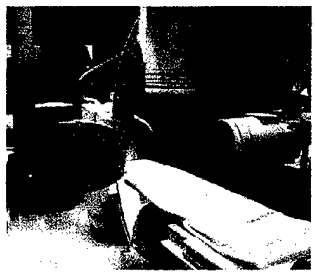

Figure 2. SIEMENSNeuroStar Interventional Suite

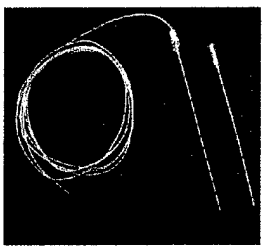

Figure 3: MagTrax needle/probe with a stylette containing a magnetic sensor in its tip and leads exiting the hub. An 18-gauge trocar is seen on the right.

Materials & Methods

A novel robot designed for interventional procedures was mounted on the fluoroscopy table in the interventional suite to serve as a needle holder and precision positioning device (Figure 4). First, the robot was used to accurately position a magnetically tracked needle at seven locations over a 100 by 40 by 40 mm volume. Second, the robot was used to position the needle on the surface of a custom made liver phantom at five different positions. The needle probe interfaces with a novel magnetic position sensing system (AURORA™) and its tip position and orientation can be displayed in real time. Distances between repositioning attempts were determined by root mean square calculations between successive points.

Equipment

A newly designed PAKY/RCM needle driver Robot was used in conjunction with a Seimens NeuroStar T.O.P Polytron for this study.

The PAKY/RCM needle driver robot consists of of a translation stage with 3 degrees of freedom (DOF), a 7 DOF passive positioning stage and a 3 DOF oreintation/driving stage. The robot is mounted on the Siemens NeuroStar table with a specially designed frame and a custom designed locking mechanism. The controls for the robot are; a touch screen monitor, joystick control, and emergency stop button (Figure 5).

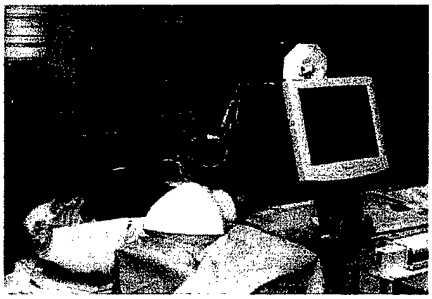

Figure 4. Robot and Magnetic Tracker in Interventional Suite

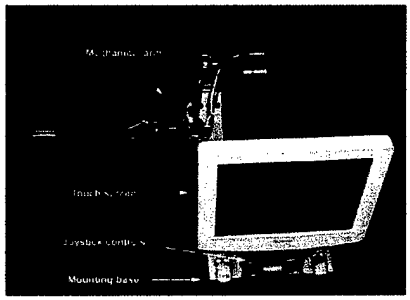

Figure 5. Robot Componets (courtesy of Dan Stoianovici, Ph.D.)

Tabulation of Data

Results

The results from the first experiment are shown in Table 1. The table shows the average magnetically measured displacement and standard deviation for each of the seven displacements. The tests were repeated seven times. The axis of motion was defined by the coordinate system of the robotic device. The results from the second experiment are shown in Table 2. The table shows the average magnetically measured displacement and standard deviation for each of the five points on the liver surface (relative to the robot coordinate system with an origin near the center of the liver phantom). The tests were repeated five times.

Conclusion

Based on this initial study, the AURORA magnetic tracking system appears accurate enough for use in the interventional radiology suite. Further studies with a larger number of data points and other studies such as cadaver tests are warranted to further investigate this technology.

Acknowledgements

This work was funded by U.S. Army grant DAMD17-99-1-9022 and NIH National Research Service Award (F32) HL68394-01. The content of this manuscript does not necessarily reflect the position or policy of the U.S. Government. We thank the Urology Robotics Laboratory at Johns Hopkins University and Dan Stoianovici, PhD who designed and manufactured the robot used in this study.

We thank Northern Digital Inc. for the loan of the Aurora magnetic tracking sytsem.

Correspondence: Kevin Cleary, PhD
Email: cleary@isis.imac.georgetown.edu; lindisch@isis.imac.georgetown.edu
Phone: (202) 784-3420; Fax: (202) 784-4896;
Website: www.isis.georgetown.edu

Table 1: Magnetically measured displacement arranged by axis of motion of the robot positioning device.

	Robot Displacement (n=7)	Magnetically determined displacement (mm)	Standard Deviation
x-axis	0 mm to 100 mm	100.45	0.40
	100 mm to 0 mm	100.46	0.58
y-axis	0 mm to 20 mm	19.88	0.10
	20 mm to -20 mm	39.28	0.02
	-20 mm to 0 mm	19.43	0.04
z-axis	0 mm to 20 mm	19.99	0.02
	20 mm to -20 mm	40.06	0.05

Table 2: Magnetically measured measurement (mm) by the AURORA magnetic position sensing system of five surface locations of the phantom liver

Displacements from middle of liver surface to: (n=5)	AURORA Displacement	Robot Displacement ± Standard Dev.
to superior segment of right lobe	35.00 ± 0.08	35.00
to inferior segment of right lobe	59.01 ± 0.13	58.08
to medial segment of left lobe	92.95 ± 1.30	93.17
to lateral segment of left lobe	61.61 ± 0.49	62.94

10.3.3 Cleary 2003b: Robotically Assisted Interventions

Poster is reproduced on the next page. Presented at the BIROW workshop in January 2003 in Bethesda, Maryland.

Robotically Assisted Interventions in the Spine and Lung

Kevin Cleary, Ph.D.[a]
Vance Watson, M.D.[a]
David Lindisch. R.T.[a]
Alexandru Patriciu. M.S.[b]
Dumitru Mazilu. Ph.D.[b]
Dan Stoianovici, Ph.D.[b]

[a] Imaging Science and Information Systems Center,
Department of Radiology, Georgetown University Medical Center, Washington, DC
[b] Robotics Laboratory, Brady Urological Institute,
Johns Hopkins Medical Institutions, Baltimore, Maryland

Abstract

Percutaneous interventions are performed by freehand passages of instruments, such as needles, from the skin surface to the anatomy of interest. The main problem with this approach is that the physician can be inaccurate in aligning the instrument and staying on course. A joystick-controlled robotic needle driver may allow the physician to more precisely target the anatomy. This poster describes our experience with a robotic needle driver in a clinical trial of nerve and facet blocks. Our plans for future research in robotically assisted lung biopsy are also given.

Materials & Methods

The robotic needle driver consists of a three degree-of-freedom (DOF) translational stage, a 2-DOF rotational stage which can orient the needle to any angle, and a 1-DOF needle drive mechanism (Figure 1). The robot is controlled using a joystick and touch screen. The interventionalist can thus manipulate the needle under x-ray fluoroscopy without direct exposure to the radiation beam. After cadaver studies using the robot to precisely position a needle in the lumbar spine were successful, a randomized clinical trial of 20 patients undergoing nerve and facet blocks was approved by the FDA and the local institutional review board. The procedure is done in the standard manner except the robot is used to position, orient, and drive the needle under physician control (Figure 2). A/P fluoroscopy (Figure 3) is used to position and orient the needle, and lateral fluoroscopy (Figure 4) is used to monitor the depth of insertion.

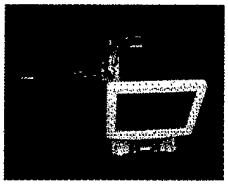

Figure 1: 6 DOF Robot

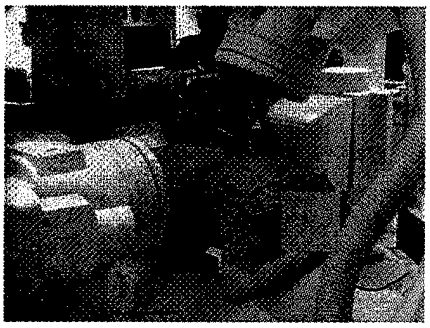

Figure 2: Clinical Trial

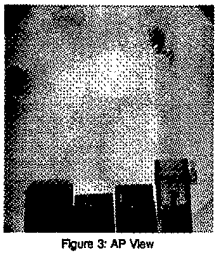

Figure 3: AP View

Figure 4: Lateral View

Contact Information:
Kevin Cleary, PhD
Email: cleary@georgetown.edu
Telephone: (202) 687-8253

Results

The study was conducted from August to December, 2002. The study was done in the interventional suite using a Siemens bi-plane fluoroscopy system. The results of the 20 patients enrolled are shown in Table 1. The standard manual technique was used on 10 patients and the robotic device was used on 10 patients. No complications were observed in the study. One of the patients in the robotics arm had to be converted to a manual procedure due to slippage of the needle driver. This conversion was done without difficulty or complications.

There were two outcome measures: 1) accuracy of needle placement (Table 2) and 2) pain relief (Table 3). Accuracy of needle placement was determined as follows. Before the interventionalist began placing the needle, both an A/P and lateral image of the patient were obtained. The interventionalist would then annotate each image with an arrow to indicate the desired target location of the needle. After the needle was placed, an A/P and lateral image was again obtained. The two sets of images were compared to determine the distance between the intended location of the needle and the actual location of the needle. Pain relief was measured using a visual-analog scale, with 0 representing no pain and 10 representing excruciating pain.

Patient	Age	Sex	Technique	Block	Level	Pain Before	Pain After	Pain 1 week	Accuracy (mm) A/P/Lat
1	70	M	Manual	Facet	L4-5	1	0	1	0.6/0.84
2	59	F	Manual	Nerve	L-5	1	0	0	0.41/0.23
3	60	M	Manual	Nerve	L-4	8	0	3	0.9/0.57
4	30	M	Manual	Nerve	L-4	9	1	2	0.89/0.91
5	55	F	Robot	Nerve	L-4	8	4	4	1.92/1.45
6	76	F	Robot	Nerve	S-1	4	3	4	0.23/0.18
7	74	F	Robot	Nerve	L-5	3	0	1	0.34/0.17
8	74	F	Robot	Nerve	L-4	4	1	2	2.00/1.44
9	60	F	Manual	Nerve	L-5	8	1	2	0.41/1.22
10	60	M	Robot	Nerve	L-4	8	0	1	0.66/0.10
11*	66	F	Robot	Facet	L-5	9	4	5	0.28/0.66
12	65	F	Manual	Facet	L-5	7	0	3	0.22/1.39
13	42	M	Manual	Facet	L-4	2	0	2	0.82/038
14	62	F	Robot	Nerve	L-4	5	1	2	0.42/1.01
15	69	M	Manual	Facet	L-4	8	3	7	0.53/0.57
16	70	M	Robot	Facet	L-3	8	2	7	0.90/0.97
17	65	F	Robot	Facet	L-3	6	0	0	0.63/0.42
18	42	M	Manual	Nerve	L-5	8	4	5	1.09/1.90
19	65	F	Manual	Facet	L-5	8	0	0	0.00/2.40
20	42	M	Robot	Nerve	L-5	8	3	7	0.75/0.55

* Patient was converted to manual procedure

Table 1: Results from 20 patients

	Robot (N=10)	Manual (N=10)
Distance From Target (mm)		
n	10	10
Mean	1.105	1.238
Median	0.845	1.135
Standard Deviation	0.764	0.528
Min, Max	0.29, 2.46	0.47, 2.40
Difference in Means (Robot - Manual)	-0.133	
One-sided Upper 95% Conf. Interval	-inf, 0.376	
Adjusted Upper 95% Conf. Interval*	-inf, 0.511	

*One-sided upper 95% confidence interval for difference in means after adjusting for the effects of age and block type (obtained using regression model).

Table 2: Accuracy of Needle Placement

	Robot (N=10)	Manual (N=10)
Pain (pre-treatment)		
n	10	10
Mean	6.3	6.0
Median	7.0	8.0
Standard Deviation	2.16	3.27
Min, Max	3, 9	1, 9
Pain (post-treatment)		
n	10	10
Mean	1.8	0.9
Median	1.5	0.0
Standard Deviation	1.62	1.45
Min, Max	0, 4	0, 4
Pain Difference (post - pre treatment)		
n	10	10
Mean	-4.5	-5.1
Median	-4.5	-6.0
Standard Deviation	1.90	2.92
Min, Max	-8, -1	-8, -1
Difference in Means (Robot - Manual)	0.6	
One-sided Upper 95% Conf. Interval	-inf, 2.53	
Adjusted Upper 95% Conf. Interval*	-inf, 2.29	

*One-sided upper 95% confidence interval for difference in means after adjusting for the effects of age and block type (obtained using regression model).

Table 3: Pain Outcome

Discussion

While there is not enough data yet for statistical significance, some general trends can be observed. The mean accuracy in the robot (1.105 mm) and manual (1.238 mm) is about the same. Therefore, it appears that the robot is capable of accurate needle placement.
As expected, the pain score post-treatment was significantly less than the pain score pre-treatment in both the robot and manual arms. In the robot arm, pain scores fell from a mean of 6.3 pre-treatment to 1.8 post-treatment. In the manual arm, pain scores fell from 6.0 pre-treatment to 0.9 post-treatment.

Future Work (Lung Biopsy)

The next clinical application that we are investigating is lung biopsy. The goal is to use the robotic system to assist the physician in accurate computed tomography (CT) fluoroscopy-guided needle biopsy of lung nodules. The use of CT for lung cancer screening is rapidly expanding. Percutaneous image-guided biopsy of the lung is a moderately difficult procedure with the potential for morbidity from pneumothorax and hemorrhage. For those nodules less than one cm in size, biopsy is more difficult, and there are a limited number of trained personnel who can perform them. We expect the increasing utilization of screening CT will result in a rapid growth in demand for imageguided percutaneous biopsy of these nodules. This project will proceed in two phases. The goal of the first phase is to demonstrate the feasibility of using a joystick-controlled robotic system to accurately hit simulated lesions in a phantom under CT fluoroscopy guidance. A prototype gripper will be developed and tested on a custom-built respiring lung phantom model. The goal of the second phase is to develop an enhanced gripper along with a path planning capability and demonstrate this approach in phantom and animal studies.

Acknowledgements

This work was funded in part by U.S. Army grants DAMD17-96-2-6004 and DAMD17-99-1-9022. The content of this poster does not necessarily reflect the position or policy of the U.S. Government. The statistics were analyzed by Byron McKinney of Beta Statistics.

10.3.4 Cleary 2002b: Cadaveric Study

Poster is reproduced on the next page. Presented at the CARS conference in June 2002 in Paris.

A Cadaveric Study of Robotically Assisted Spinal Needle Placement versus Manual Placement

Kevin Cleary, PhD[a]
Kevin Riutort, MS[b]
Vance Watson, MD[c]
Dan Stoianovici, PhD[d]

Georgetown University Medical Center, Washington, DC, USA
[a] Imaging Science and Information Systems (ISIS) Center, Department of Radiology
[b] School of Medicine
Interventional Neuroradiology, Department of Radiology
[d] Urobotics Laboratory, Brady Urological Institute
Johns Hopkins Medical Institutions, Baltimore, MD, USA

PURPOSE

To compare the ability of an experienced physician in performing perispinal nerve and facet blocks on a cadaver using a joystick-controlled robotic needle driver (Figure 1) versus manual placement of the needle.

METHODS

Using C-arm fluoroscopy and manual placement, a 22-gauge needle was placed a total of eight times into the lumbar perispinal region of an elderly male embalmed cadaver (Figure 2). This procedure was repeated using a robotic needle driver (Figure 3) for a total of sixteen needle placements. Small metal BB nipple markers 1 mm in diameter were percutaneously inserted to serve as targets near the lumbar nerve roots and facet joints. The physician then attempted to place a needle to hit the target points, both manually and using the robot. Radiographs (Figure 4) were obtained after each placement to assess the accuracy of placement while the time and number of re-adjustments required to place the needle were measured. The time was measured starting from the initial needle placement until the physician was satisfied with the final placement. A re-adjustment was defined as a withdrawal and re-orientation of the needle.

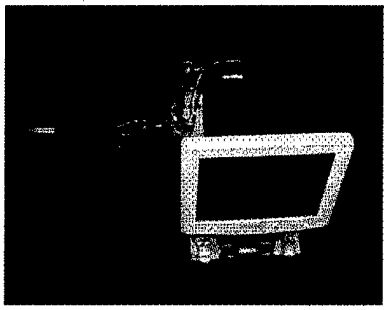

Figure 1. Robot showing touch screen, translational mechanism, and needle driver end-effector.

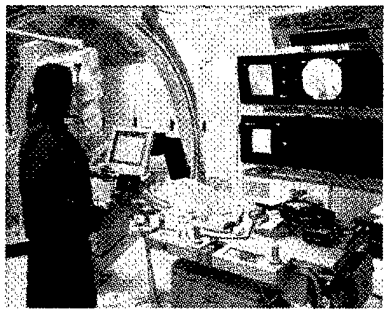

Figure 2. Physician operating joystick to control robot.

Figure 3. Close-up view of robot and cadaver.

RESULTS

Using *manual placement*, the average time for needle placement was 99.5 ± 29.9 seconds with an average of 3.50 ± 1.41 re-adjustments (n=8). Using *robotically assisted placement*, the average time for needle placement was 58.0 ± 22.4 seconds with an average of 0.38 ± 0.52 re-adjustments (n=8).

Figure 4.
Sample Fluoroscopy Images Showing Needle Placement

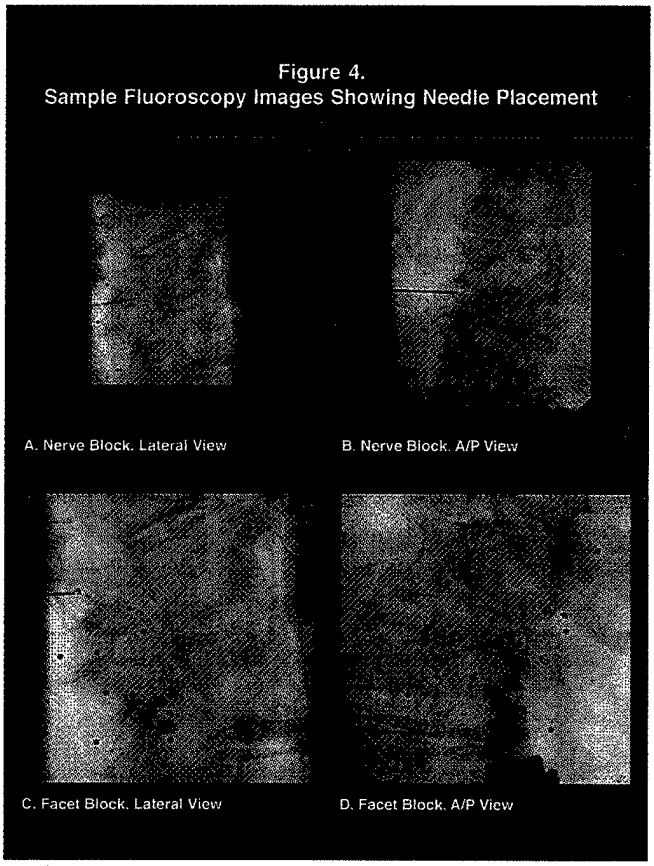

CONCLUSIONS

Using robotically assisted placement, an experienced physician can reduce the time to place a needle in the spine compared to the conventional, manual method. The reduction in time is a result of the decrease in the number of times the needle trajectory needs to be re-adjusted. Clinical studies are required to further investigate the advantages and disadvantages of this system for interventional needle procedures.

ACKNOWLEDGEMENTS

This work was funded by U.S. Army grant DAMD17-99-1-9022. The content of this manuscript does not necessarily reflect the position or policy of the U.S. Government. The robotics needle driver was designed and built by the URobotics Laboratory at Johns Hopkins Medical Institutions.

10.3.5 Cleary 2002c: Feasibility of Electromagnetic ...

Poster is reproduced on the next page. Poster made for in-house review only.

Feasibility of Electromagnetic Position Sensing in the CyberKnife Stereotactic Radiosurgery Suite

Kevin Cleary[a], Chris Gange[a], David Boyd[a], and Sonja Dieterich[a]

[a] Imaging Science and Information Systems Center, Department of Radiology, Georgetown University Medical Center, Washington, DC

Georgetown University Hospital
MedStar Health

Purpose

To examine the feasibility of using electromagnetic position sensing technology for tumor tracking in the stereotactic radiosurgery suite. The position sensing device tested uses very small coils (1 mm in diameter by 8 mm in length) that could be embedded in tumors for tracking purposes. The CyberKnife® radiosurgery system (Accuray, Sunnyvale, CA) could then move the radiation beam in real-time for more precise treatments.

Materials & Methods

An electromagnetic position sensing system (AURORA™, Northern Digital Inc., Waterloo, Canada) (Figure 1) was positioned in the CyberKnife suite within the treatment area for a typical patient (Figures 2 and 4). The sensor coil to be tracked was incorporated into an 18-gauge needle for manipulation purposes (MagTrax, Traxtal Technologies, Bellaire, TX) (Figure 3). A highly accurate robotic system designed for precision manipulation in interventional procedures was used to position the needle at ten locations within a typical treatment area (PAKY/RCM, URobotics Laboratory, Johns Hopkins, Baltimore, MD) (Figure 5). The translational position of the sensor coil at each location was recorded using the electromagnetic position sensing system. For analysis, the coordinate systems of the robot and the sensing system were aligned and the Euclidean distance between points were computed. The experiments were repeated four times.

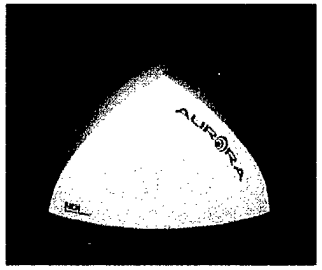

Figure 1. AURORA Magnetic Field Generator

Figure 2. Robot and Magnetic Tracker in CyberKnife Suite

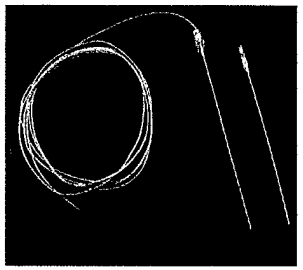

Figure 3. MagTrax needle/probe with a stylette containing a magnetic sensor in its tip and leads exiting the hub. An 18-gauge cannula is seen on the right.

Figure 4. Close-up of Robot and Magnetic Tracker

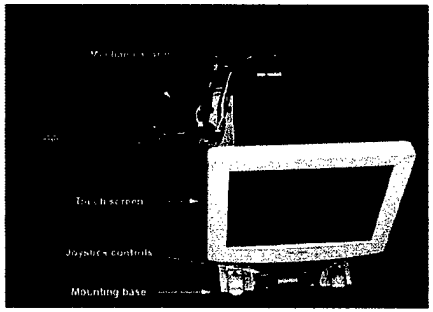

Figure 5. Robot Components (courtesy of Dan Stoianovici, Ph.D.)

Table 1. Positional Errors for Aurora Tracking System (mm)

Point	Distance RMSE	Average Distance	*HSD	Std. Dev.	Maximum	Minimum	N
5	1.09	0.93	(a)	0.65	1.75	0.24	4
7	1.61	1.61	(a)	0.09	1.68	1.50	4
1	1.87	1.85	(a)	0.32	2.29	1.58	4
2	2.34	2.32	(a)(b)	0.33	2.63	1.98	4
4	2.53	2.39	(a)(b)(c)	0.96	3.78	1.58	4
8	2.40	2.39	(a)(b)(c)	0.23	2.72	2.21	4
0	3.54	3.45	(b)(c)	0.86	3.95	1.39	8
3	3.76	3.74	(b)(c)	0.35	4.27	3.50	4
6	4.00	3.90	(c)	1.04	5.38	3.12	4
Overall	2.83	2.60		1.12	5.38	0.24	40

* Differences in mean distance between points are assessed using Tukey's Honestly Significant Difference (HSD) at alpha=0.05 level of significance. Differences between points having common letter designations do not reach this level of statistical significance.

Results

The average root mean square error, based on a total of 40 measurements, was 2.83 ± 1.12 mm.

Conclusion

It may be feasible to use electromagnetic position sensing for improved localization of tumors during stereotactic radiosurgery using the CyberKnife. Several institutions have begun treatment of lesions in internal organs such as the pancreas and lung. Movement of abdominal organs has been reported to be as much as 3 cm. Tracking these lesions in real-time using electromagnetic position sensing could result in more precise treatments. The results presented here are an initial step. Additional studies are needed to investigate other factors such as turning on the radiation beam during tracking.

Acknowledgements

This work was funded by U.S. Army grant DAMD17-99-1-9022. The content of this manuscript does not necessarily reflect the position or policy of the U.S. Government. We thank the Urology Robotics Laboratory at Johns Hopkins University and Dan Stoianovici, PhD, who designed and manufactured the robot used in this study. We thank Northern Digital Inc. for the loan of the Aurora magnetic tracking system. We thank Traxtal Technologies for supplying the MagTrax needle/probe.

Correspondence: Kevin Cleary, PhD
Email: cleary@isis.imac.georgetown.edu
Phone: (202) 784-3420; Fax: (202) 784-4896;
Website: www.isis.georgetown.edu

10.3.6 Levy 2002b: Implementation of a Magnetic Tracking ...

Poster is reproduced on the next page. Presented at the SIR Conference in April 2002 in Baltimore, Maryland.

Implementation of a Magnetic Tracking System for Accurate Puncture Needle Guidance

Elliot B. Levy, MD[1]
Kevin Cleary, PhD[2]
Filip Banovac, MD[1]
Neil Glossop, PhD[3]
Daigo Tanaka, MA[2]
Sheng Xu, MS[3]
David Lindisch, RT[2]

[1] Department of Radiology, Georgetown University Hospital-MedStar Health, Washington, DC
[2] Imaging Science and Information Systems (ISIS) Center, Washington, DC
[3] Traxtal Technologies, Houston, Texas
[4] Johns Hopkins University, Baltimore, Maryland

Acknowledgments

This work was funded by a CIRREF Academic Transition Award.

Purpose

- To facilitate intrahepatic vascular puncture such as the transjugular intrahepatic portosystemic shunt procedure (TIPS) during uninterrupted respirations.

Goals

- To design a needle guidance algorithm featuring magnetic tracking and respiratory gating for accurate needle placement in the liver.
- Modify the TIPS procedure to feature percutaneous transhepatic puncture of the portal and hepatic veins.
- Validate the algorithm using a specifically designed phantom.
- The proposed guidance system is envisioned to play a significant role in improving the accuracy and efficacy of intrahepatic portocaval shunt creation in TIPS.

Background - TIPS

- The feasibility of TIPS creation was first evaluated by Rosch, et.al. in swine in 1969 (1).
- Successful TIPS deployment may be achieved in up to 96% of patients (2), although the procedure is technically difficult.
- Typically, the most time consuming and technically challenging step in the TIPS procedure is the transhepatic puncture of the portal vein originating from the hepatic vein.
- The desired portal vein can be identified and targeted by several techniques including wedged hepatic venography using iodinated contrast or carbon dioxide, transhepatic portography, percutaneous placement of target guidewires or markers in the portal vein, and 2-D or 3-D ultrasound guidance (3,4,5). Most often, the portal vein is successfully punctured in "blind fashion" after several needle passes under fluoroscopic control.
- With a larger number of attempts, the fluoroscopy exposure time increases in addition to the likelihood of an errant transcapsular puncture.
- Recently an interactive image guidance system featuring magnetic tracking coupled to previously acquired 3-D CT images was used to display the realtime position of the intrahepatic puncture needle during TIPS in an animal model (6). This system featured respiratory gating consisting of a magnetic sensor placed on the animal's abdomen, allowing updating of the needle position only during a designated portion of the respiratory cycle. This algorithm required the placement of 10-20 magnetic markers on the animal's skin to permit image registration. The system accuracy was reported to be 3mm.

Background - Respiratory Gating

- For phantom design purposes, we assumed that hepatic respiratory motion occurs in the craniocaudal direction only and that the liver itself is not deformed by diaphragmatic motion.
- The respiratory excursion of the liver has been measured as 10mm in previous reports (7,8).
- Davies et.al. (8) measured the average dwell time (zero organ velocity) during end expiration which lasted an average of 1.4 seconds during a mean respiratory cycle time of 4.4 seconds in their group of nine volunteers.

Methods

TIPS Procedure Modification

- Simultaneous percutaneous transhepatic puncture of a portal and hepatic vein, with guidewire passage into the inferior vena cava/right atrium.
- Snare retrieval of the guidewire via the right internal jugular vein.
- Our previous retrospective review suggests that transabdominal simultaneous puncture of portal and hepatic vein branches is anatomically possible in a majority of patients (9).

Algorithm for Needle Placement

- Patterned after the stepwise conventional "freehand" procedure for static image-guided biopsies.
- Preoperative CT images of the target are reviewed for path planning purposes.
- A suitable skin puncture site is chosen from which a needle trajectory unobstructed by interposed viscera can be anticipated. The angle of trajectory and necessary depth of puncture are determined with the assistance of the magnetic tracking system.

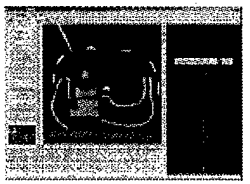

Graphical User Interface

- Needle advancement is performed only when the graphical user interface (GUI) indicates that respiratory-related organ motion has ceased during the end-expiratory phase pause (dwell time).
- Target organ motion is tracked by the catheter-based fiducial to determine the timing of the pause in respiratory-related organ motion.
- The GUI displays: 1) the depth of the needle tip relative to the desired depth in graphical fashion; and 2) the position of the needle tip registered with the preoperatively obtained CT dataset. The needle procedure can therefore be terminated by the operator based upon the real-time information and guidance provided by the GUI.

Phantom

- Modified abdominal torso phantom (Anatomical Chart Co., Skokie, Il.) with an internal servomotor-driven platform mount in the "paraspinal" area.
- A foam liver phantom containing 4-5mm dia. thin-walled "vessels" is secured to the platform mount.
- "Vessels" are created by the removal of barium-coated plastic drinking straws placed within the foam mixture prior to final casting.
- The servomotor control system produces linear platform motion which simulates the respiratory motion of the liver.

Magnetic Tracking System

- Small pyramidal magnetic field generator (AURORA™ Magnetic Tracking System, Northern Digital, Inc., Toronto, Canada).
- Four flat circular skin markers placed on the costal margins which can be readily identified on axial CT images of the torso.
- One single 0.9mm diameter coil fiducial embedded in a 5 French plastic catheter, which was placed through the simulated intrahepatic inferior vena cava or a simulated hepatic vein and fixed in position with a small amount of adhesive.
- The tracked puncture needle consists of a modified 18 gauge trocar needle with a single 0.9mm diameter coil fiducial embedded in the stylet.

Design of Experiments

- Obtain contiguous 1mm axial CT images of the liver phantom.
- Transfer CT DICOM dataset to Windows NT workstation.
- Identify and target vessels and skin entry site using Graphical User Interface (GUI).
- Activate magnetic field and register catheter-based fiducial in "end-expiratory phase."
- Skin fiducials registered by automatic segmentation to identify isocenters, after which tracking needle was sequentially placed on each fiducial.
- Determine registration error (RMS, root mean square).
- Needle angulation and depth of needle puncture determined with assistance of GUI.
- Needle advancement performed *only* during end-expiratory pause indicated by GUI.
- **Experiment #1:** Single vessel target punctured on ten occasions, with respiratory motion at 12-40/minute with excursion distance of 1-2cm.
- **Experiment #2:** In-line simultaneous puncture of two vessels during simulated respiratory motion of 12-24/minute with 1-2cm excursion.

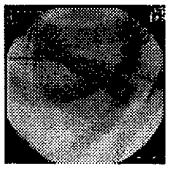

Frontal View of Phantom, Successful Two Vessel Respiratory-Gated Puncture

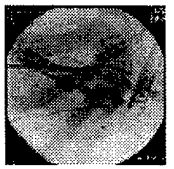

Frontal View of Phantom, Successful Two Vessel Respiratory-Gated Puncture Guidewire Test

Lateral View of Phantom in Successful Two Vessel, Respiratory-Gated Puncture

Observations and Results

- Success was defined as 1) determination of needle tip position by orthogonal digital imaging within the single vessel lumen (Experiment #1), or 2) within the lumen of the deeper vessel while the needle shaft bisected the superficial vessel lumen (Experiment #2).
- A successful "guidewire test" consisting of an attempt to pass a standard angiographic 0.035 inch guidewire through the needle (without any additional manipulation) into the targeted "vessel."
- The time required to complete the needle puncture of the target vessels after placing the needle tip on the skin was recorded for each needle pass.
- Mean error is determined by calculation to be the difference between the final position of the needle-based fiducial and the selected deep target coordinates.

Experiment #1

Total Punctures	10
Successful Punctures	8
Mean Duration of Attempts(sec)	28.6
Respiratory Rates(per minute)	12-40
Respiratory Excursion (cm)	1-2
Registration Error (RMS)(mm)	1.7
Standard Deviation	0.3

Experiment #2

Two Vessel Puncture with Respiratory Motion Gating	
Respiratory Rate (per minute)	12-24
Respiratory Excursion (cm)	1-2
Total Attempts	17
Total Successful Attempts	11
Percent Successful	65%
Mean Duration of Attempts (sec)	22.8
Standard Deviation	6.5
Mean Error (mm)	6
Standard Deviation	2.8

Comparison

	Successful Attempts	Unsuccessful Attempts
Mean Duration of Attempts (sec)	21.2	22
Standard Deviation	4.6	10
Mean Error (mm)	4.8	8.2
Standard Deviation	2.2	2.6

- Needle puncture attempts were sequential unless the GUI indicated severe alteration of the course of the needle and impending failure (n=2, Experiment #2), after which the needle was withdrawn and re-puncture attempted.
- Unsuccessful needle passes in Experiment #2 occurred partially as a result of needle tip deflection caused by improper placement of the stylet.
- Some prolongation of needle puncture duration occurred when the initial movement of the needle resulted in puncture of only the surface of the liver, after which significant needle tip displacement occurred with the subsequent respiratory cycle.
- Registration error increased dramatically (30-fold) when the magnetic field generator and fiducials were placed under the image intensifier or within the CT gantry.

Conclusions

- A novel magnetic-based needle guidance system for intrahepatic vessel puncture, e.g. TIPS, featuring respiratory gating has been tested using a specifically designed phantom, with a 65% immediate success rate.
- Potential magnetic field distortion caused by image intensifiers, C-arms, and the CT gantry in the standard Interventional Radiology or CT suite may significantly degrade the accuracy of the system.
- A retrievable catheter-based fiducial which can be temporarily fixed within a hepatic vein will be tested in an animal model in future experiments.
- Magnetic tracking including registration of conventional image space and magnetic space potentially offers the guidance advantages of realtime imaging without the additional radiation exposure.

Needle Manipulation Using Image Overlay

References

1. Rosch J, Hanafee WN, Snow H. Transjugular portal venography and radiological portacaval shunts: An experimental study. Radiology 1969;92: 1112-1114.
2. LaBerge JM, Ring EJ, Gordon RL, et.al. Creation of transjugular intrahepatic portosystemic shunt (TIPS) with the Wallstent endoprosthesis: Results in 100 patients. Radiology 1993; 187: 413-420.
3. Fontaine AB, Marschyl A, Hoffer E, et.al. Use of CT-Guided Marking of the Portal Vein in Creation of 150 Transjugular Intrahepatic Portosystemic Shunts. J Vasc Interv Radiol 1997; 8:1073-1077
4. Harman JT, Read JD, Kopecky KK, et.al. Localization of the Portal Vein for Transjugular Catheterization: Percutaneous Placement of a Metallic Marker with Real-time US Guidance. J Vasc Interv Radiol 1992; 3: 545-547.
5. Rolzenzi M, Kane RA, Takahashi J, et.al. Portal Vein: US Guided Localization Prior to Transjugular Intrahepatic Portosystemic Shunt Placement. Radiology 1995; 196: 868-870
6. Solomon SB, Magee C, Acker DE, Venbrux AC. TIPS Placement in Swine, Guided by Electromagnetic Real-Time Needle Tip Localization Displayed on Previously Acquired 3-D CT. Cardiovasc Interv Radiol 1999; 22: 411-414.
7. Minohara S, Tatsuaki K, Masahiro E, et.al. Respiratory Gated Irradiation System for Heavy-Ion Radiotherapy. . Int. J. Radiation Oncology Biol. Phys. 2000; 47: 1097-1103
8. Davies S, Hill A, Holmes R, et.al. Ultrasound Quantitation of respiratory Organ Motion in the Upper Abdomen. Brit J. Radiology 1994; 67: 1096-1102
9. Banovac F., Levy, E., Lindisch, D., et al. Feasibility of Percutaneous Transabdominal Portosystemic Shunt Creation. Accepted for publication in Surgical and Radiologic Anatomy, January, 2002

10.3.7 Watson 2002: Robotically Assisted ...

Poster is reproduced on the next page. Presented at the ASNR conference in May 2002 in Vancouver.

Robotically Assisted Perispinal Selective Nerve and Facet Blocks: Cadaveric Studies.

Vance Watson[1], MD Dave Lindisch[2], RT
Kevin Cleary[2], PhD

Georgetown University Medical Center, Washington, DC
[1] Interventional Neuroradiology, Department of Radiology
[2] Imaging Science and Information Systems (ISIS) Center, Department of Radiology

Introduction

To develop a joystick controlled robotic needle driver to perform spinal procedures, and in the initial phase evaluate the device by placing 22-gauge needles for transforaminal selective nerve blocks and facet blocks. At Georgetown University Medical Hospital, the procedure is done in an interventional suite that accomodates bi-plane fluoroscopy, angiography, and our PAKY Robot.

Materials & Methods

Technique

The lead author used bi-plane fluoroscopy and manual technique to place needles into the lumbar perispinal region of a 98 year-old female embalmed cadaver and implant metal BB markers 1 mm in diameter to serve as targets as shown in Fugure 1. Six in neural exit foramina and six at facet joints. A robotic needle driver was then used to approach as closely to the target markers as possible. Anterior-posterior and lateral radiographs were obtained after each placement to assess the accuracy of placement. A second set of experiments in a 46 year-old male embalmed cadaver was performed in a similar manner with four facet and four nerve blocks performed "free-hand" and the same by the robot. Distance from target, time to task, and number of passes were recorded and used to judge performance.

History and Indications

The first medical application of a robot occured in 1985[1], which was a simple robotic positioning device used for needle orentiation of a brain biopsy. The robot that was used for this procedure was a PUMA 560 industrial robot

Medical robotics evolution has been a slow and steady process, There are now several commericallly available.

We at Georgetown University Hospital in collaboration with the Department of Radiology research group, The Imaging Sciences and Information Systems (ISIS Center) ,ISIS Center, The Urology Robotics Laboratory of the Johns Hopkins Instutions and the Computer Intergrated Surgical Syetems and Technology (CISST) Engineering Research Center at Johns Hopkins University are focusing our efforts on minimally invasive spine procedures with emphasis on physician assist systems for precise placement of instruments.

Clinical applications can be catogized by the role that the robot plays in the clinical application,[2] or by applications.[3] The roles are (1) intern replacements, (2) telesurgical systems, (3) navigational aids, (4) precise postioning systems, and (5) precise path systems. The applications are(1) Neurosurgery, (2) Orthopedic, (3) Urology, (4) Maxillofacial surgery, (5) Radiosurgery, (6) Ophthalmology, and (7) Cardiac.

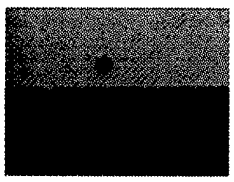

Figure 1. target BB's used in cadaver study 1mm diameter

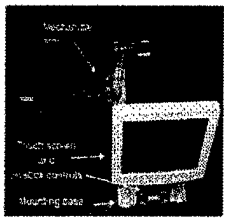

Figure 2. Robot controls

Figure 3. Cadaver study and physician operating joystick to control robot

Figure 4. Bi-plane Fluoroscopy with Robot mounted on interventional table

Equipment

A newly designed PAKY/RCM needle driver Robot[4] was used in conjunction with a Seimens NeuroStar T.O.P Polytron for this study.

The PAKY/RCM needle driver robot consists of of a translation stage with 3 degrees of freedom (DOF), a 7 DOF passive positioning stage and a 3 DOF oreintation/driving stage. the robot is mounted on the Siemens NeuroStar table with a specially designed frame. The controls for the robot are; a touch screen monitor, joystick control, and emergency stop button. Figure 2.

The robot is mounted on the interventional table using a custom-designed locking mechanism. The robot is positioned initially near the skin entry point by loosening the passive gross positioning mechanism and moving the needle driver end of the robot by hand. Once this initial position has been attained, this mechanism is locked and the robot is switched to physician control.

The Cadaver Study

The physician controls the robot by manipulating the joystick on the control panel. Different modes of operation, such as translational motion of the entire unit or rotational motion of the end-effector, can be selected. The system was intentionally designed to limit motion to one mode at a time to make it easier for the physician to understand the action of the joystick. An emergency stop button is prominently located next to the joystick as a precaution. The system may be shut down at any time using this button. The physician remains in control of the device at all times and may revert to the current manual technique at any time. The operation of the robot by the physician through a joystick is shown in Figure 3

The robot controller is housed in an industrial PC chassis and contains all the electronics and safety monitoring devices. The robot controller includes several safety features, including a watchdog timer board that is used to regularly monitor the system operation.
copy.
The robot is mounted on the interventional table using a custom-designed locking mechanism. The robot is positioned initially near the skin entry point by loosening the passive gross positioning mechanism and moving the needle driver end of the robot by hand. Once this initial position has been attained, this mechanism is locked and the robot is switched to physician control.

Once the targets were placed, the robotic device was used along with a 22 gauge needle in an attempt to position the needle to within 3 mm of the target. The typical scenario was as follows. The passive arm was unlocked and the needle tip was placed within a few centimeters of the skin entry point above the target area. The robot was then set to translational mode by selecting this mode on the touch screen. Using the joystick for control, the physician then moved the tip of the needle to the skin entry point while monitoring the position of the robot by direct vision. The robot was then set to rotational mode by selecting this mode on the touch screen. Using the joystick once again, the physician then oriented the needle to point towards the target point while monitoring the orientation using A/P fluoroscopy. When the physician was satisfied that the needle was pointing toward the target, the robot was then set to needle drive mode by selecting this mode on the touch screen. Using the joystick once again, the physician drove the needle toward the target while monitoring the needle depth and trajectory using lateral fluoroscopy.

As each needle was placed (by Dr. Watson), the corresponding A/P and lateral fluoroscopy images were saved in digital format for follow-up analysis. The level, type of block (nerve or facet), and corresponding images were recorded by Dr. Cleary, who served as an observer during the study. After the study, the images were analyzed by Mr. Lindisch and the distance from the target to the needle on both A/P and lateral fluoroscopy was recorded and confirmed by Dr. Cleary. The images were sent in the DICOM format from the Siemens Neurostar to a desktop computer running the PiView medical imaging software. Each image can then be viewed in PiView and the distance from the center of the target to the center of the needle can be measured by the software[1]. This was done for all 24 images (A/P and lateral from each of the 12 blocks). Representative results for nerve block 4 and facet block 2 are shown in Figures 5-8.

[1] It should be noted that two assumptions are made in making these measurements and calculating the distance. First, it is assumed that the measurement scale on the PiView imaging software is correct to within 10%. This scale is based on the pixel to mm value from the DICOM header in each image. This value comes from the Siemens Neurostar system and is based on a measurement plane near the isocenter of each C-arm. It is our experience that objects near the isocenter like those measured here will be within 10% of the measured values. Second, to calculate RMS values, we assume that the A/P and lateral views are orthogonal. This is a good assumption for this cadaver study.

Correspondence: Vance Watson, MD
Email: watson@isis.imac.georgetown.edu; cleary@isis.imac.georgetown.edu; lindisch@isis.imac.georgetown.edu
Phone: (202) 784-3420; Fax: (202) 784-4896; Website: www.isis.georgetown.edu

Figure 5. lateral view

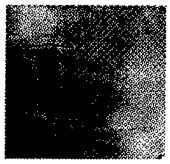

Figure 6. AP view

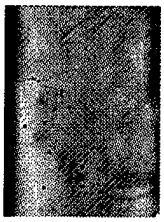

Figure 7. Lateral view

Figure 8. AP view

Results

The results of the accuracy study are given in Table 1. The average placement accuracy was 1.44 mm and the standard deviation was 0.66 mm. In most cases the physician was able to drive the needle directly toward the target. However, in some cases the needle deviated slightly and the physician needed to correct the needle path. This was done by re-orienting the needle slightly in the direction opposite the deviation. When the needle was then driven further into the body, the path would then generally move closer to the target.

Trial number	Level	Distance from target (A/P fluoroscopy) mm	Distance from target (lateral fluoroscopy) mm	Distance from target (root mean square distance) mm
Nerve 1	Right 4	1.10	1.70	2.02
Nerve 2	Right 3	0.00	1.71	1.71
Nerve 3	Right 2	0.00	0.80	0.80
Nerve 4	Left 2	1.75	1.34	2.20
Nerve 5	Left 3	2.50	0.19	2.51
Nerve 6	Left 4	1.40	0.74	1.58
Facet 1	L1-2 Left	0.26	0.29	0.39
Facet 2	L2-3 Left	0.96	1.53	1.81
Facet 3	L3-4 Left	1.49	0.19	1.50
Facet 4	L3-4 Right	0.70	0.13	0.71
Facet 5	L2-3 Right	0.80	0.00	0.80
Facet 6	L1-2 Right	0.00	1.19	1.19
Average		0.91	0.82	1.44
Standard deviation		0.79	0.65	0.66

Note: RMS distance calculated from square root of (A/P squared + lateral squared)

Table 1

Discussion

Based on the study data reported here, it is feasible to use a physician controlled robotic needle driver to accurately place needles in the nerve and facet regions of the spine. All the needles were placed without difficulty and no system failures were observed using the robot. The benefit of using the robotic needle driver are two-fold:

1) It is a steady and precise holder for the needle (the needle never deflects or sags when partially inserted as it tends to in the current manual procedure and the needle can be re-oriented and inserted in very precise increments).
2) The physician can view the location and trajectory of the needle in the body in real-time since the physician's hand is not in the path of the x-ray beam.

The next step in our research program is a clinical trial using the robot for nerve and facet blocks. Institutional review board and FDA approvals should be finalized shortly for an initial study of 20 patients.

References

1 Kwoh, Y. S. Hou, J. Jonckheere, E. A. Hayati, S. A robot with improved absolute positioning accuracy for CT guided stereotactic brain surgery. IEEE Trans Biomed Eng; 35; 2; 153-60; Feb, 1988

2 Taylor RH. Robots as surgical assistants; where we were, whither4r we are tending, and how to get there. In; Proceedings of the 6th Conference on Artificial Intelligence in Medicine Europe (AIME 97). Gemobie France, 1997. p3-11

3 Cleary, K.; Nguyen, C.State of the art in surgical robotics: Clinical applications and technology challenges. Comput Aided Surg 2001; 6; 6; 312-28

Acknowledgements

This work was funded by U.S. Army grant DAMD17-99-1-9022. The content of this manuscript does not necessarily reflect the position or policy of the U.S. Government. The Urology Robotics Laboratory at Johns Hopkins (director, Dan Stoianovici, PhD) designed and built the robot used in this study. The authors would also like to thank Martin Dym, PhD, and Lori Lincoln for supplying the cadaver.

10.4 Protocol for Skin Motion Tracking

Protocol begins on the next page and is 12 pages long.

Georgetown University Institutional Review Board Application (Protocol) for Biomedical IRB Review (AB-1)

Section One: Application Information

Principal Investigator	Kevin Cleary, Ph.D.
Department	ISIS Center, Department of Radiology
Title	Associate Professor
Phone: (202) 687-8253 **Pager:** (202) 901-2033	**Fax:** (202) 784-3479
E-mail address: cleary@georgetown.edu	
Mailing Address: Imaging Science and Information Systems (ISIS) Center, 2115 Wisconsin Avenue, NW, Suite 603, Washington, DC, 20007	

Title of Project	**Purpose of Project**
Periscopic Spine Surgery: Anatomical Motion Tracking During Radiation Treatment	The purpose of this research study is to analyze patient organ motion data collected during radiation treatment using the CyberKnife® and compare this data to skin motion detected at the same time by non-invasive optical trackers. The CyberKnife is an FDA-approved stereotactic radiosurgery system to treat tumors and lesions throughout the body. This study will serve as a first step towards our long-term goal of using skin motion to predict internal organ motion. This may lead to more precise treatment delivery for mobile target volumes.

Consultants or co-investigators	**Department or Institution**
Donald McRae, Ph.D., CyberKnife Program Director	Radiation Medicine
James Rodgers, Ph.D., Head of Radiation Physics	Radiation Medicine
Gregory Gagnon, M.D., Radiation Oncologist	Radiation Medicine
Fraser Henderson, M.D., Neurosurgeon	Neurosurgery, Radiation Medicine
Walter Jean, M.D., Neurosurgeon	Neurosurgery, Radiation Medicine
Sonja Dieterich, Ph.D., Postdoc/Study Coordinator	Radiation Medicine

Estimated duration of total project	One year (estimated start date is August 2002 and estimated completion date is August 2003)
Estimated total number of subjects (including control subjects)	100
Age range of subjects	Patients will be recruited from the existing patient population undergoing CyberKnife treatment. There are no special inclusion or exclusion criteria for this study. The typical

	age range for these patients has been from 16 to 80 years of age.
Sex of subjects	The typical distribution for these patients has been roughly equal between male and female patients.
Where will study be conducted?	Georgetown University Hospital 3800 Reservoir Road NW Department of Radiation Medicine Bles Building, Lower Level
Source of subjects	Patients will be recruited from within Georgetown University Hospital and affiliated with the CyberKnife Stereotactic Radiosurgery program of the Departments of Neurosurgery and Radiation Medicine.

Grant Support for Project	**Commercial Support for Project**
This project is being funded by a grant from the U.S. Medical Research and Material Command, grant number DAMD17-99-1-9022. The principal investigator for this grant is Dr. Cleary. The protocol and consent form will also be reviewed by the Army Human Subjects Research Review Board (HSRRB).	None.

Section Two: Additional Georgetown University Regulatory Information

1. Does this project involve the use of biohazardous materials, recombinant DNA and/or gene therapy?
   - ☐ Yes. If so, Institutional Biosafety Committee (IBC) approval must be obtained. Contact 202-687-4712 for assistance.
   - xx No.

2. Does this project include the use of radioisotopes and/or radiation-producing devices regardless of whether the use is incidental to the project?
   - ☐ Yes. If so, all protocols must be submitted to the GUH RSC along with a completed RSC-4 or RSC-5 form. The forms require information on the use of radioisotopes and radiation-producing devices and must include dose calculations. Call 202-687-4712 to obtain forms or if additional information is required.
   - xx No. (radiation will be delivered by the CyberKnife as part of the standard treatment of these patients. The CyberKnife is an FDA approved device)

3. Does this project involve the use of fetal tissue?
   - ☐ Yes
   - xx No

4. Do any investigators or co-investigators have a conflict of interest as defined in the Georgetown University Faculty Handbook?

☐ Yes. If yes, please explain.

xx No

7. Is there a current Conflict of Interest form for each investigator on file at the Office of Regulatory Affairs?

☐ Yes

xx No. If not, please fill out the form (which can be obtained in the Institutional Review Board Office and forward the original to the Office of Regulatory Affairs, and attach a copy to this application).

Section Three: Information for Protocol Review
Please answer each specific question and use additional sheets as needed. A response of "See attached protocol or grant application" is not sufficient.

4. Provide a brief historical background of the project with reference to the investigator's personal experience and to pertinent medical literature. Use additional sheets as needed.

The CyberKnife is an FDA-approved stereotactic radiosurgery system to treat tumors and lesions throughout the body. Stereotactic radiosurgery is a technique for cancer treatment where multiple beams of radiation are directed to accurately target and destroy tumors while minimizing the dose to healthy tissue. The CyberKnife became operational at Georgetown on March 12th, 2002. As of May 21st, 2002, 14 spine patients have completed treatment. A picture of the CyberKnife facility at Georgetown is shown in Figure 1. The image from the ceiling mounted diagnostic X-ray source (1) is captured by amorphous silicon image detectors (3). The linear accelerator (2) is mounted on a computer controlled robotic arm.

Traditionally, stereotactic radiosurgery has been limited to the brain using a metal head frame bolted to the skull. This frame is used for precise localization of the anatomy, which is critical for accurate treatments. The CyberKnife incorporates image guidance and a robotic positioning system to direct the multiple beams of radiation. Therefore, patients are immobilized with a mask system. The combination of robotics and image-guidance is unique to the CyberKnife and allows for the treatment of lesions not only in the head, but also throughout the body (Adler 1999).

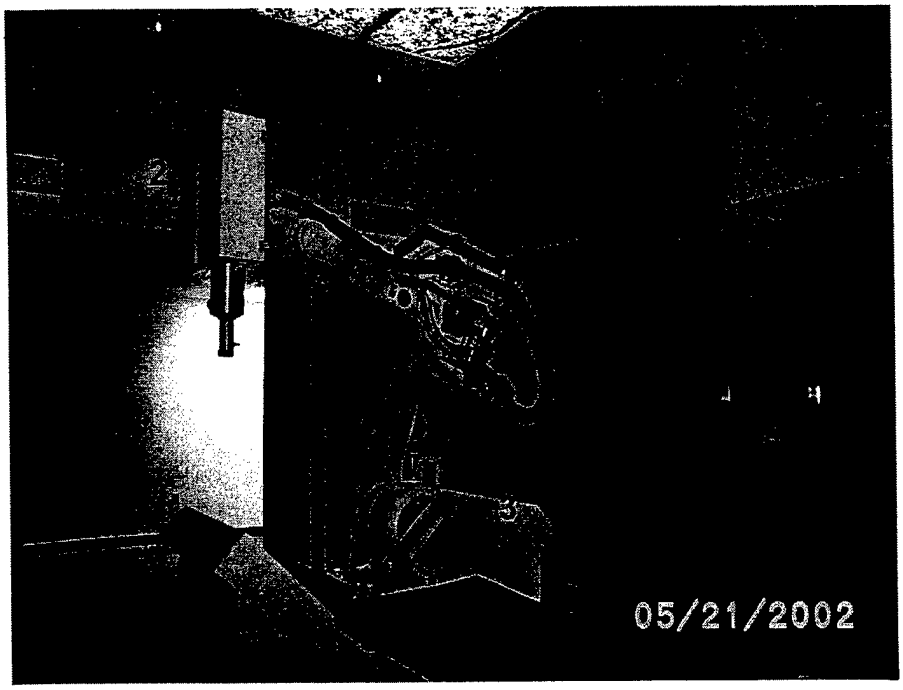

Figure 1: CyberKnife treatment facility at Georgetown (1. Ceiling mounted diagnostic X-ray sources, 2. Compact linear accelerator mounted on computer controlled robotic arm, 3. Amorphous silicon image detectors)

To accurately treat internal organs throughout the body, the issue of organ motion due to respiration must be addressed. Traditionally, breath-hold techniques have been used where the patient is asked to hold their breath and radiation is only delivered during breath-holds. However, many patients that would otherwise be candidates for CyberKnife treatment cannot tolerate breath holding. In addition, this method significantly prolongs the treatment time. One solution to this problem is to track internal organ motion and move the radiation beam in real-time to compensate for this motion. Since the linear accelerator (the device that supplies the radiation beam) of the CyberKnife is mounted on a computer-controlled robotic arm, the CyberKnife is capable of moving the radiation beam in real-time to compensate for organ motion. Therefore, the patient will be able to breathe normally during the treatment.

Accuray, the company that manufactures the CyberKnife, and Stanford Medical Center has investigated skin motion tracking as a predictor of internal organ motion. The study by Schweikard et al. (Schweikard 2000) was the first of this type. The Schweikard study is the only study of this type known to the investigators (partially because the system is new and only a few sites nationwide have this equipment). The goal of our study is to acquire additional patient data in an attempt to validate and extend the Accuray results.

This data is essential to advance the state-of-the-art of CyberKnife treatment so that respiratory motion compensation and other enhancements can be incorporated in future treatment delivery. This should lead to more precise treatments and better patient care. The data may also be useful in other minimally invasive interventions such as robotically assisted lung biopsies that are being studied by Dr. Cleary's research group.

Literature cited in this section:

Adler, J. R., Jr., M. J. Murphy, et al. (1999). "Image-guided robotic radiosurgery." Neurosurgery 44(6): 1299-306; discussion 1306-7.

Schweikard, A., G. Glosser, et al. (2000). "Robotic motion compensation for respiratory movement during radiosurgery." Comput Aided Surg 5(4): 263-77.

5. The plan of study. State the hypothesis or research question you intend to answer. Describe the research design and procedures (including standard procedures) to be used in the research. Specifically identify any experimental procedures. Provide statistical justification for the number of subjects to be studied and the degree of change expected. Describe any special equipment or unusual procedures to be used for this research project. Use additional sheets as needed.

a. Overview and Description

The long-term goal of this research study is to determine how respiratory motion tracking can be used to improve the accuracy of stereotactic radiosurgery using the CyberKnife. The initial steps toward achieving this goal proposed here is to collect data on skin motion (gathered by an optical tracking method) and attempt to correlate it to organ motion data as determined from radiographic images during CyberKnife treatment. Organ motion tracking using 120 kVp digital radiographic image pairs is a standard part of every CyberKnife treatment. During a treatment session, an x-ray image is taken every few minutes to monitor patient motion. The CyberKnife compensates for patient movement of up to one centimeter in all three translational directions. The amplitude and relative phase of skin motion versus organ motion can then be quantified and mathematically modeled. This will be useful in more precisely targeting cancer.

The skin motion tracking will be done using a commercial infrared tracking system (Polaris, Northern Digital, Ontario, Canada). The Polaris can track the motion of non-invasive hemispherical sensors, which will be temporarily attached to the skin using double-sided tape. Three to five of the sensors will be placed on the chest of the patient, at locations such as the sternum and the ribs. The sensors can be easily removed at the end of the procedure.

The non-invasive sensor is shown in Figure 2 and the optical tracking system is shown in Figure 3. The infrared tracking system emits infrared light that is reflected by these hemispheres. The reflections are detected by the infrared tracking system and used to determine the position of the sensors. This position data will be stored on a laptop computer for further analysis as described in Section C, data analysis plan.

A photograph showing how the tracking system will be positioned and how the sensors will be placed is given in Figure 4. Except for the addition of the skin markers on the patient's chest and the placement of the optical tracking system in the room, the standard treatment plan is not changed.

The Polaris tracking system has been used in a similar manner in interventional radiology cases at Georgetown by Dr. Cleary's group under another approved protocol (Periscopic Spine Surgery: Vertebral Body Motion Tracking: 01-048). This tracking system is also a standard

component of several commercial image-guided surgery systems that are FDA approved. Therefore, no problems with operating this equipment in the hospital environment are expected.

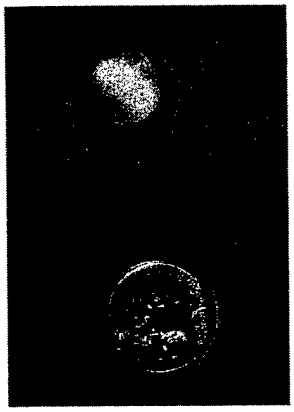

Figure 2: Non-invasive sensor compared to a dime (three to five sensors will be placed on the skin)

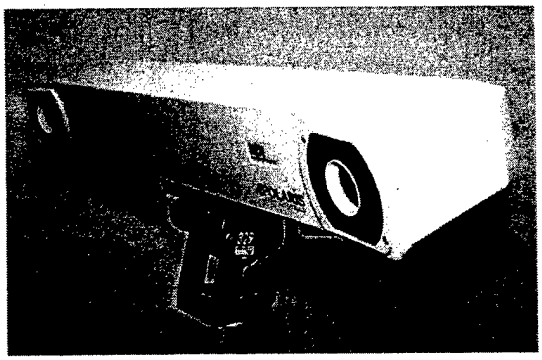

Figure 3: Infrared tracking system (placed on a tripod in the treatment room)

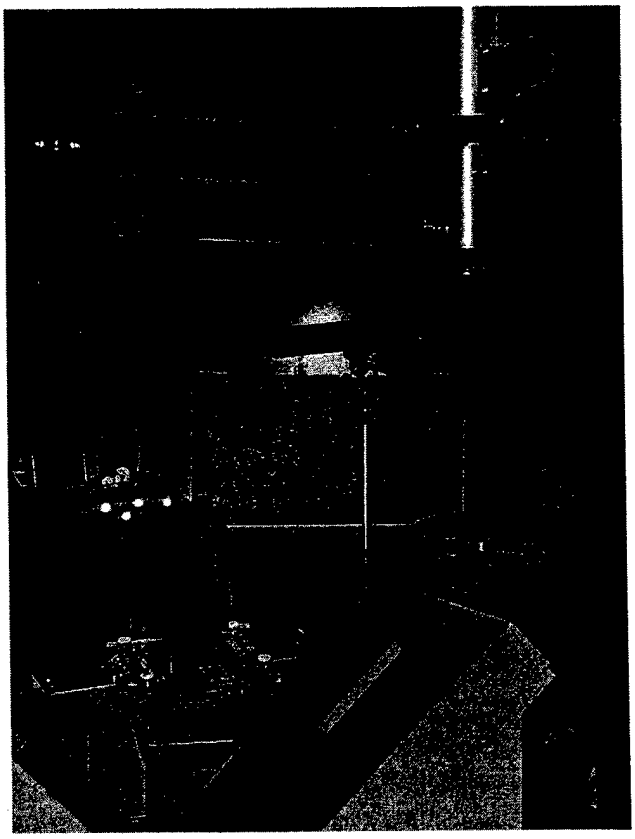

Figure 4: Patient setup for gathering infrared tracking data during CyberKnife treatment (skin sensors can be seen as bright spots on chest, the infrared tracking system is directly in front of the picture on the wall)

b. Step-by-Step Instructions

The standard Stereotactic Radiosurgery treatment procedure using the CyberKnife system consists of the following steps:

1. After consultation with the physician specialists involved, a set of radiographic markers, called fiducials, will be placed by the neurosurgeon in and around the tumor volume to be treated. These fiducials are for tracking internal organ motion.
2. A customized body cast will be made to facilitate treatment set-up.
3. CT scans will be obtained using the body cast. These CT images are essential for the planning and delivery of the CyberKnife treatment.
4. Radiation dose planning is performed using the CT images and optionally MRI or PET images. A medical physicist performs this step with input and guidance from the radiation oncologist and neurosurgeon.
5. The CyberKnife treatment is delivered in one to five treatment sessions.
6. During the treatment session, diagnostic quality radiographic images are obtained by the CyberKnife system. These images are required to locate and monitor the exact position of the target (tumor) volume prior to and during radiation treatment delivery.

Under the research protocol proposed here, the standard treatment will be followed as described in steps 1-6 above. In addition to the standard treatment, we will add two additional steps as follows:

5a. When the patient is being prepared for treatment, the Polaris infrared tracking system and a laptop computer will be set up in the CyberKnife suite. After the patient is positioned on the treatment couch, three to five non-invasive sensors will be attached to the patient's chest using double-sided tape (as shown in Figure 4 above). The CyberKnife treatment will then be delivered in the standard manner. During the treatment, the optical tracking data will be recorded on the laptop computer. These data will not contain any patient identifiable information.

6b. After the treatment is completed, the tracking data from the laptop computer will be analyzed as described in the data analysis plan. The digital radiographic images and organ motion data from the CyberKnife treatment system will also be saved and analyzed as described in the data analysis plan.

In summary, the standard CyberKnife treatment protocol will not be modified in any way. The only difference is that several non-invasive sensors will be attached to the patient's chest before the treatment. Data from the sensors will be recorded during the treatment and later analyzed to attempt to correlate skin motion with internal organ motion.

c. Justification as to the Number of Cases Required

The sample size of 100 has been chosen to ensure data collected are representative of the wide range of patients likely to present themselves for this type of treatment. Specifically, the data should include patients with a wide range of demographic characteristics, physical status, and lesion location. Since the patients will follow the standard CyberKnife treatment protocol, this data can be collected as part of the day-to-day routine in Radiation Medicine. We have dedicated

a postdoctoral researcher for this task (Sonja Dieterich) and expect to complete data collection within one year.

d. Data Analysis Plan

The following data will be recorded for each patient:

1. Age and gender of patient and date of treatment
2. Location and type of lesion
3. Set of chest motion data collected from the infrared tracking system (numerical values)
4. Set of organ motion data from the CyberKnife system (numerical values)
5. Set of radiographic images from the CyberKnife system

All chest motion data, organ motion data, and radiographic images will be time-stamped to allow the simultaneous positions of the chest motion and spine motion to be determined. Primary analyses will be performed separately for each patient and lesion. Secondary analyses will describe the variation in applicable parameters among the patient population.

External chest motion data and internal organ motion data will be plotted to assess patterns in the respective movements during treatment. Displacements of the internal markers in each coordinate direction, as well as absolute displacements, will be plotted to measure the motion range of the lesion observed during treatment. Absolute displacements will be summarized using descriptive statistics including the maximum displacement and standard deviation.

Correlation between internal and external motion will first be assessed by overlaying corresponding displacements on a single plot. Then displacement pairs will then be used to regress organ displacement on chest displacement. Deviation from the regression line will be reported using root mean squared error and maximum error. Residuals from the regression model will be evaluated for discernable patterns.

The ability of external markers to accurately predict the movement of internal markers will be evaluated as follows. A deformation model will be computed for each patient following methods described in the study by Schweikard (Schweikard 2000). Predictive accuracy will be assessed graphically, and by root mean squared error and maximum error.

Because the primary analyses will be performed individually for each patient, data analysis will be performed as data become available. The distribution of applicable parameters among the patient population will be estimated at the end of the study. For example, it will be of interest to report the distribution of maximum organ displacement during treatment, maximum predictive errors, etc. It may also be instructive to evaluate whether the value of these parameters is dependent upon recorded patient characteristics or lesion location. These assessments will be made using standard linear regression methods.

The digital radiographic images will not be used in the initial analyses, but will be saved for potential follow-up analysis.

6. Indicate what you consider to be the risks to subjects and indicate the precautions to be taken to minimize or eliminate these risks. Justify the need for a placebo control group if one is included in this study. Where appropriate, describe the data monitoring procedures that will be employed to ensure the safety of subjects. Use additional sheets as needed.

The risks and discomforts are the same as the usual risks and discomforts associated with radiation treatment. No additional risks are anticipated. This research involves the gathering of data during the procedure and analysis of this data after the procedure. The procedure itself will not change in any manner.

7. Roles and Responsibilities of the Research Team

This information was requested by the Army Human Subjects Research Review Board (HSRRB). The team members are listed in Section 1 on Page 1 of this protocol. The roles and responsibilities are:

- Kevin Cleary, Ph.D., Principal Investigator. Dr. Cleary is responsible for study design, protocol approval, coordination of the research team, and monitoring of the study.
- Donald McRae, Ph.D., Radiation Medicine Physicist. Dr. McRae is the CyberKnife program director and has overall responsibility for the physics aspects of the CyberKnife treatment. He has also been involved in the study design.
- James Rodgers, Ph.D., Radiation Medicine Physicist. Dr. Rodgers is the Director of Radiation Physics and has overall technical responsibility for the Department of Radiation Medicine. He has also been involved in the study design and will assist Dr. Cleary in monitoring of the study.
- Gregory Gagnon, M.D., Radiation Oncologist. Dr. Gagnon is responsible for the clinical aspects of the radiation treatment. He and the radiation oncology nurses will be responsible for explaining the CyberKnife treatment to the patients and administering the consent form.
- Fraser Henderson, M.D., and Walter Jean, M.D., Neurosurgeons. Dr. Henderson and Dr. Jean are responsible for patient recruitment and follow-up care.
- Sonja Dieterich, Ph.D., Postdoctoral Researcher/Study Coordinator. Dr. Dieterich will be involved in data collection and analysis and serve as the study coordinator.

Section Four: Selection of Subjects and the Informed Consent Process

8. Indicate whether this project involves any of the following subject populations?

- ☐ **Children (Children are defined by District of Columbia law as anyone under age 18.)**
- ☐ **Prisoners**
- ☐ **Pregnant women**
- ☐ **Cognitively impaired or mentally disabled subjects**
- ☐ **Economically or educationally disadvantaged subjects**

None of the subject populations listed above are involved.

Subjects must be at least 18 years old to participate in this study. If you are pregnant as determined by clinical history and laboratory test, you may not participate in this study. This exclusion is due to the procedure being performed, not the fact that data is being gathered. These procedures have the potential for damage to the fetus due to radiation exposure.

The procedures used in this study may be unsafe for an unborn baby, an infant, sperms, and eggs. If you, as a subject of study, are a woman of child bearing potential, you must agree to avoid pregnancy during your participation in this study. If you, as a subject, are a man, you must agree to not conceive a child during your participation in this study. If you do become pregnant during the study or if you father a child during the study, you should immediately notify Dr. Gagnon at (202) 784-3420. In addition, if you are already pregnant or are breast feeding, you cannot participate in this study.

Patients who are candidates for radiation therapy are asked to sign a consent form before planning for the treatment is even started. The consent form has a sentence that reads "I understand that conception/pregnancy during or immediately following radiation is not advised". This form is presented to the patients by the radiation oncologist or the radiation oncology nurses. If there are questions regarding a patient's pregnancy status, urine testing is done.

9. Describe how subjects will be recruited and how informed consent will be sought from subjects or from the subjects' legally authorized representative. If children are subjects, discuss whether their assent will be sought and how the permission of their parents will be obtained. Use additional sheets as needed.

Subjects will be recruited from within Georgetown University Hospital and affiliated with the CyberKnife Stereotactic Radiosurgery program of the Departments of Neurosurgery and Radiation Medicine. Patients who are to receive CyberKnife treatment will be asked to participate in this research study.

10. Will subjects receive any compensation for participation in cash or in kind?

- ☐ **Yes. If so, please describe amount or kind of compensation in the space below.**
- **xx No.**

Section Five: Privacy and Confidentiality of Data and Records

11. Will identifiable, private, or sensitive information be obtained about the subjects or other living individuals? Whether or not such information is obtained, describe the provisions to protect the privacy of subjects and to maintain the confidentiality of data. Use additional sheets as needed.

The data to be gathered during this study was listed in Section 5d (Data Analysis Plan) as follows:

1. Age and gender of patient and date of treatment
2. Location and type of lesion
3. Set of chest motion data collected from the infrared tracking system (numerical values)

4. Set of organ motion data from the CyberKnife system (numerical values)
5. Set of digital radiographic images from the CyberKnife system

In this data set, the only item that has patient identifiable data is item 4, the spine motion data from the CyberKnife treatment system. This data is stored in a log file on the treatment system computer. The log file includes the patient name. A software program will be used to remove this patient name from the log file before this data is stored. This program will be written using Matlab and we have written similar programs in the past so this is easy to do.

A sample log file for item 4 is shown in Figure 5. This first set of characters on each line (15:34.50.134610 for example) is the time stamp. The line where the patient name is listed is shown in the highlighted grey color. This data set is from a phantom test, so the patient name is "BLucy" (Lucy is the name of the phantom and not the name of a real patient). The software program we will write will strip out the patient name and replace it with blanks. Note that the internal motion data (the centroid of the target anatomy) is shown at the bottom of Figure 5 where the x, y, and z coordinates are given.

```
       15:34:50.134610 --> TlsImage::dumpFields: datasetName =
[redacted]

       15:34:50.135094 --> TlsImage::dumpFields: node = -999
       15:34:50.135520 --> TlsImage::dumpFields: 200 x 200
       15:34:50.135997 --> TlsImage::dumpFields: length = 40000
       15:34:50.136422 --> TlsImage::dumpFields: this is an 8-bit image
...
       15:35:15.754505 --> Node Number = 0
       15:35:15.754919 --> X Coord = -0.170186
       15:35:15.755428 --> Y Coord = -0.080065
       15:35:15.755846 --> Z Coord = 0.507890
```

Figure 5: Sample motion data from the CyberKnife system (data item 4)

The research data and related records for this project will be stored in the clinical areas in Radiation Medicine. This stored data will have no patient identifiable information. The data will be stored for up to two years after the closure of the study.

Section Six: Additional Items Required for Army Human Subjects Review

12. Informed consent process

Informed consent will be obtained for all patients participating in the study using the consent form approved by the Institutional Review Board at Georgetown University and the U.S. Army Human Subjects Research Review Board. Before the procedure is carried out, a member of the medical staff will explain the procedure including the risks and benefits and allow the patient to review the consent form as well as ask any questions the patient may have.

13. Benefits of the Research to the Subject

There is no direct benefit to any individual patient for participating in the study. The data gathered will be useful for researchers developing new stereotactic radiosurgery treatment techniques and may prove beneficial to future patients by enabling more precise treatments.

14. Modification of the Protocol
Any modifications to the protocol will be first reviewed and approved by the Georgetown Institutional Review Board (IRB) and then the Army Human Subjects Research Review Board (HSRRB) before implementation. The nature of the modification will determine the type and level of the review.

15. Indicate any proposed compensation for participation in cash or in kind.
No compensation or other payments will be made.

16. Review of Research Records
It should be noted that representatives of the U.S. Army Medical Research and Materiel Command are eligible to review research records as a part of their responsibility to protect humans subjects in research.

17. Review of Research Records
Adverse events that are both serious and unexpected will be immediately reported by telephone to the USAMRMC Deputy, Office of Regulatory Compliance and Quality (301-619-2165) (non duty hours call 301-619-2165 and send information by facsimile to 301-619-7803). A written report will follow the initial telephone call within 3 working days. Address the written report to the U.S. Army Medical Research and Materiel Command, ATTN: MCMR-RCQ, 504 Scott Street, Fort Detrick, Maryland 21702-5012. Please note on the MRMC website: Http://mrmc-www.army.mil, under Regulatory Compliance and Quality, Human Subjects Protection, the HSRRB Policy Memorandum 02-01 (27 February 2002), "Reporting of Unanticipated Problem Risks to Subjects or Others" including a reporting form in Appendix B.